CANDU FUEL BUNDLE IN A CTR BLANKET

TIME DEPENDANT STUDIES OF A 19-ELEMENT CANDU FUEL BUNDLE IN THE BLANKET OF A THERMONUCLEAR REACTOR

by

TERRY WAYNE STONE, B.Sc.

A Thesis

Submitted to the School of Graduate Studies

in Partial Fulfilment of the Requirements

for the Degree

Master of Engineering

McMaster University

1977

MASTER OF ENGINEERING (1977)
(Engineering Physics)

MCMASTER UNIVERSITY
Hamilton, Ontario.

PART A

TITLE: Time Dependent Studies of a 19-element CANDU Fuel Bundle in the Blanket of a Thermonuclear Reactor

AUTHOR: Terry Wayne Stone, B.Sc. (University of Windsor)

SUPERVISOR: Dr. S.A. Kushneriuk

NUMBER OF PAGES: viii, 93

Abstract

Effects in 19 element CANDU fuel bundles containing ThO_2 and UO_2, located in thermonuclear reactor blankets, have been examined for a variety of blanket designs. The buildup in time of nuclides derived from Th^{232} by neutron capture was studied. The essential CTR (Controlled Thermonuclear Reactor) blanket features that were examined were tritium breeding in the blanket (the fusion reaction of interest was the DT reaction resulting in the production of a 14.1 MeV neutron and a 3.5 MeV alpha particle), neutron multiplication in the blanket and the U^{233} production. Means of optimizing these features were also examined. Some conclusions concerning the use and influence of the CANDU bundle are made.

It is of interest to study the details of the buildup of U^{233} in the bundles with the view of perhaps transferring bundles directly from the CTR blanket into a core of a fission power reactor. As such, it would be necessary to convert approximately 3% of the initial thorium present to U^{233} before transferral. This report examines time steps over which this could be achieved and looks at the performance of the blanket as a whole when such changes occur. The production of unwanted radioactive isotopes is looked at with suggestions of how to minimize this production without harming the rest of the blanket's basic functions.

Procedures outlined in the preliminary report "Bench-Mark Neutronic Calculations for Fusion Reactor Designs" by S.A. Kushneriuk and P.Y. Wong form a basis for all of the calculations made in this report. Based on the findings of that report, it is expected that values presented here do reflect, to a fair degree of accuracy, conditions encountered in the CTR blankets studied.

ACKNOWLEDGEMENTS

The author wishes to thank Dr. S.A. Kushneriuk for encouragement and overall direction. Also to be thanked are P.Y. Wong and P.M. Garvey for help in tracing errors incurred with the codes.

TABLE OF CONTENTS

LIST OF FIGURES

LIST OF TABLES

INTRODUCTION

Blankets surrounding a chamber in which certain fusion reactions take place have been proposed to serve various purposes. For reactors based on DT fusion, the most important of the many blanket functions is the breeding of tritium, which does not occur naturally, in order to supply fuel for these fusion devices. To breed tritium, the material needed is lithium; i.e. for the DT fusion reactor, the raw materials needed are deuterium and lithium, the deuterium for direct use in the fusion reaction and lithium for breeding purposes. Because of the possibly great difficulties that may be encountered in the development of economical fusion reactors, to date, it has been suggested that a blanket could also be used for direct energy multiplication by having fissile fuel create thermal energy or it could be used indirectly by providing fuel bundles enriched in U^{233} for use in nuclear reactors. CTR blankets, however, face conditions which, up till now, have not been encountered in reactor devices; high fluxes of high energy neutrons have only been met to some extent in fast breeder reactors. Thus first wall heating and atom dislocation studies are very important and have not been dealt with in this report.

Studies undertaken here represent a continuation of work reported in the paper "On the Matching of Fusion Breeders to Heavy Water Reactors" by Lavergne, Robinson and Mertel (ref. 8). In it, similar methods to those used here were employed to examine the matching of D-T fusion breeders to heavy water CANDU-type reactors. Their approach to the matching differs from that taken in this report in that they examined the irradiation of Th, ThO_2 and ThC within a blanket with the intent of separating out the

U^{233} or else subsequently loading the thorium into CANDU fuel bundles. Thus, problems arose concerning the removal of the irradiated thorium from the blanket because of the large quantities of tritium present. The alternative method of irradiating an entire bundle has been discussed here so that, while problems of removing the bundle from the blanket still exist, extraction of the U^{233} or fabrication and handling of the irradiated Th or thorium compounds would be avoided.

Actual calculational methods that were used are discussed first and then different concepts of devices that would employ the fusion reactor are looked at. Projected parameters of the devices are listed so that some idea of the blanket dimensions and overall operating conditions can be formed. A brief review of materials, mainly those used here, has been included. The main body of this report goes on to use some of these projected design parameters to see how the CANDU fuel bundles would fare in a blanket environment. While much of the emphasis is on the overall fuel bundle and other material behaviour in the blanket, some geometry effects, for example the effects of imposing finiteness on an infinite cylinder calculation, and spatial effects, such as tritium breeding as a function of position in the blanket are also looked at.

COMPUTATIONAL METHODS

The transport code used for these calculations was ANISN*, a discrete ordinates code that solves for the steady state flux of simple geometrical systems (sphere, slab, cylinder). A P_3-S_4 approximation was used. That is, the scattering function $\sigma^s(v'\underset{\sim}{\Omega}' \rightarrow v\underset{\sim}{\Omega})$ can be expanded and subsequently truncated in Legendre polynomials by

$$\sigma^s(v'\underset{\sim}{\Omega}' \rightarrow v\underset{\sim}{\Omega}) = \sum_{\ell=0}^{L} \frac{2\ell+1}{4\pi} \sigma_\ell{}^s(v' \rightarrow v) P_\ell(\underset{\sim}{\Omega}' \cdot \underset{\sim}{\Omega})$$

where L in this case is 3. The subscript on S stands for the number of points in the interval (-1,+1) representing the direction cosines of various direction vectors (see Appendix I and the following section on discrete ordinates). For more complicated geometries, a Monte-Carlo code called MORSE was available but due to time limitations, it was not used in this study. The cross-section library used was ENDF/B-IV which is the most recent and up-to-date library available at this writing. The cross-section data was processed into 100 energy groups with the code SUPERTOG to obtain the group to group transfer cross sections $\Sigma_{gg'}$ which are used by ANISN. However, SUPERTOG did not process the (n,3n) reactions (probably because these are high energy reactions which until now have not contributed significantly in reactor calculations). This is important in first wall

---

* *The report "Bench-Mark Calculations for Fusion-Reactor Blankets", ref. 2, compared neutronics calculations using ANISN and the ENDF/B-IV data library with neutronics calculations done by other laboratories and with actual experimental results. It was concluded in that report that although the code ANISN could only deal with simple geometries and although the processing code SUPERTOG needed modifications (ability to handle (n,3n)), results agreed reasonably well with comparative reports.*

material considerations due to the large amount of first group flux there (see Tables 2, 3 and 4). Because of the length of time that a full 100 group calculation takes on ANISN (approx. 10 min.), the cross section collapsing option in ANISN was used to reduce the number of groups from 100 to 17 (accuracy is maintained by flux weighting the cross sections). This is particularly convenient for the time studies done here since approximately ten runs were needed for each design (only zones with Th^{232} had concentration changes. Thus, the flux shapes were relatively unchanged which meant the few group cross-sections were essentially accurate over the time ranges considered). A Watt spectrum was used to represent the neutron fission energy spectrum. The group energy ranges and integrated Watt spectra for these ranges are given in Table 1. Figures 1, 2, 3 and 4 give plots of the ENDF/B-IV cross sections for the materials of interest here. Resonance self-shielding effects and temperature effects were not included in the neutronics calculations.

For the time studies all cross sections used were the collapsed cross sections calculated by ANISN. Programs to retrieve these cross sections and to put them into a form suitable for use in the time calculation were written. Finally a program that calculated the isotope concentrations as a function of time and position in a bundle using analytical solutions of equations laid out in the Time Studies section was written. The basic scheme was to assume the initial concentration of Pa^{233}, U^{234}, and U^{233} was zero and then to run ANISN. Assuming the flux to be constant over some timestep $t_0 \rightarrow t_1$, new concentrations of these isotopes were computed up to the time t_1 and the process was repeated.

Groups (1 - 17)	Equivalent 100 Groups	Energy Range	Watt Spectrum
1	1	13.5 - 14.9 MeV	4.13×10^{-5}
2	2 - 7	7.4 - 13.5	8.27×10^{-3}
3	8 - 13	4.1 - 7.4	9.24×10^{-2}
4	14 - 19	2.2 - 4.1	2.42×10^{-1}
5	20 - 25	1.2 - 2.2	2.73×10^{-1}
6	26 - 31	0.7 - 1.2	1.92×10^{-1}
7	32 - 37	369 - 672 KeV	1.05×10^{-1}
8	38 - 43	202 - 369	5.02×10^{-2}
9	44 - 49	111 - 202	2.22×10^{-2}
10	50 - 55	25 - 111	1.44×10^{-2}
11	56 - 61	5.5 - 25	1.58×10^{-3}
12	62 - 67	1.2 - 5.5	1.68×10^{-4}
13	68 - 73	0.28 - 1.2	1.77×10^{-5}
14	74 - 79	61 - 275 eV	1.87×10^{-6}
15	80 - 89	5 - 61	2.14×10^{-7}
16	90 - 99	0.41 - 5	5.04×10^{-9}
17	100	thermal	1.18×10^{-10}

Table 1 Few group energy ranges and the Watt spectrum

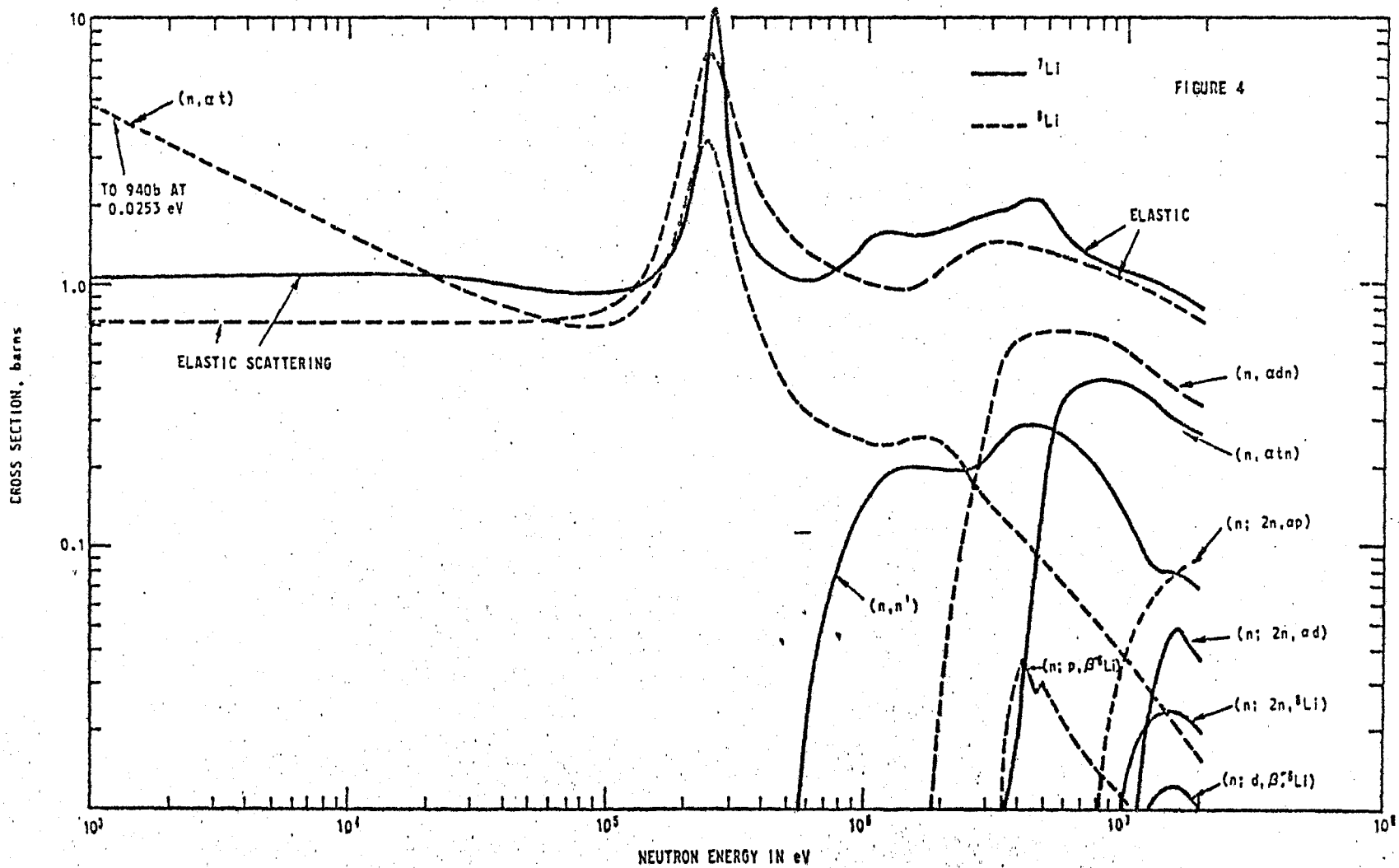

Figure 1 ENDF/B-IV cross sections for Li^6, Li^7

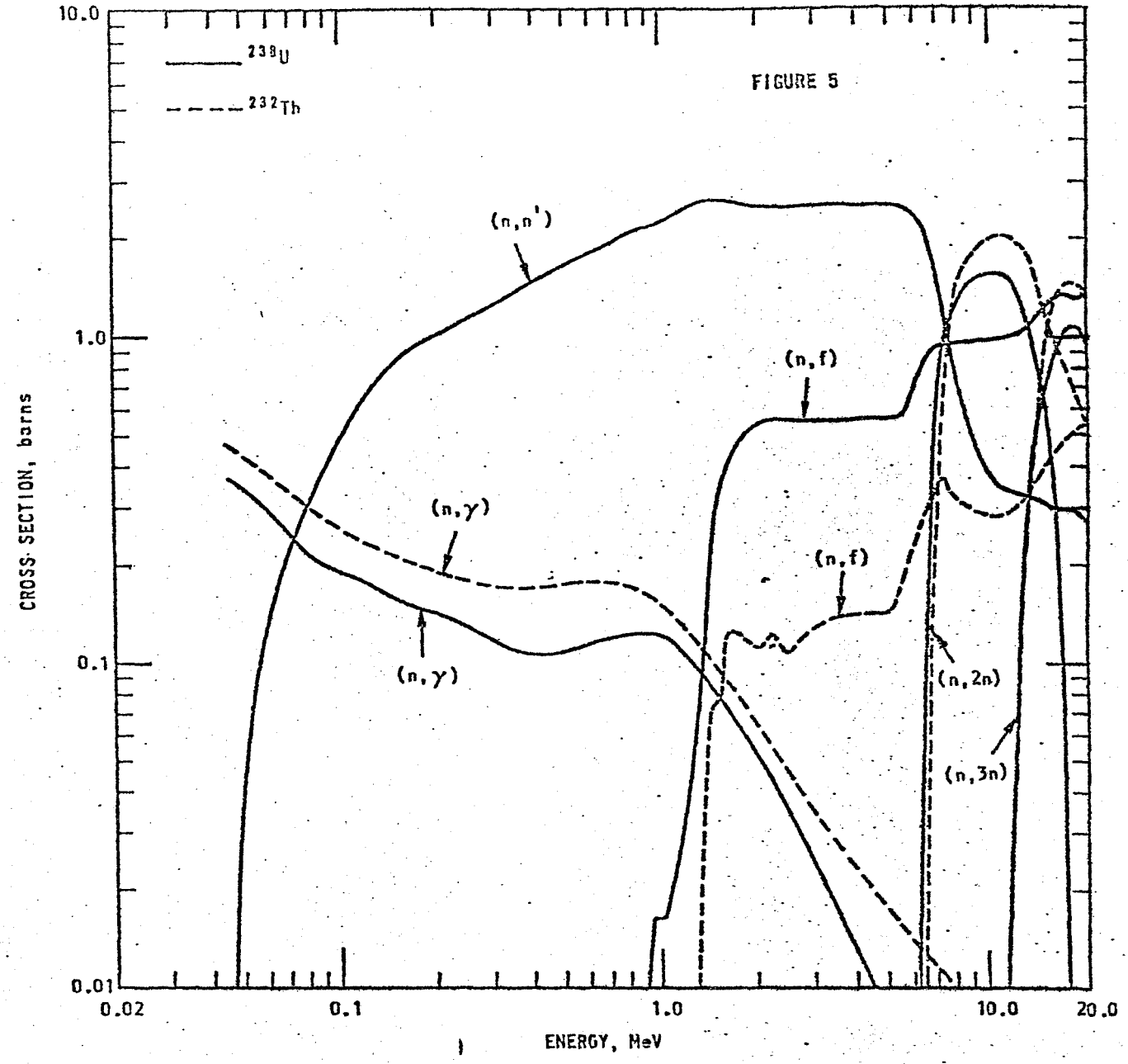

Figure 2 ENDF/B-IV cross sections for U^{238} and Th^{232}

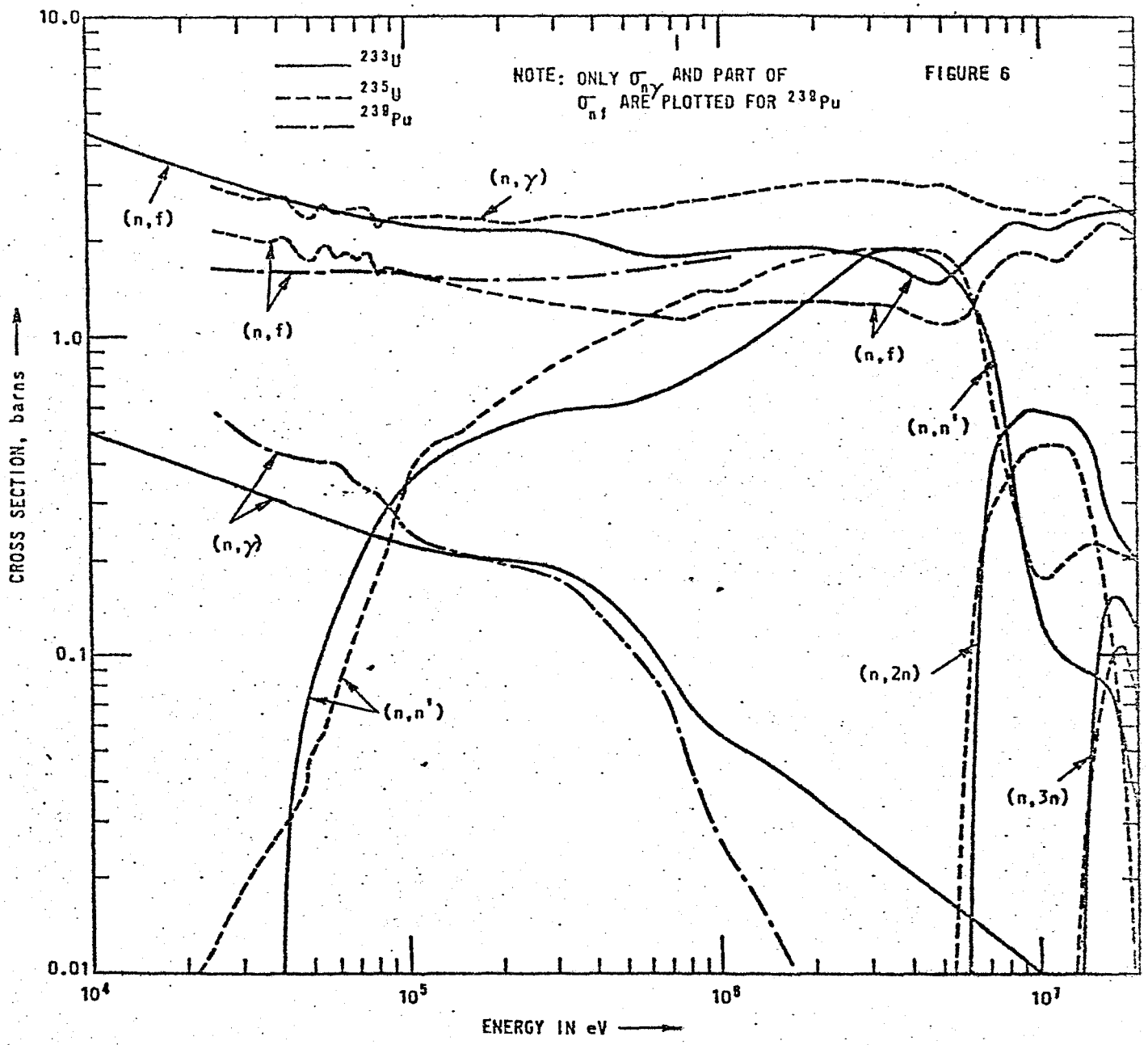

Figure 3 ENDF/B-IV cross sections for U^{233}, U^{235} and Pu^{239}

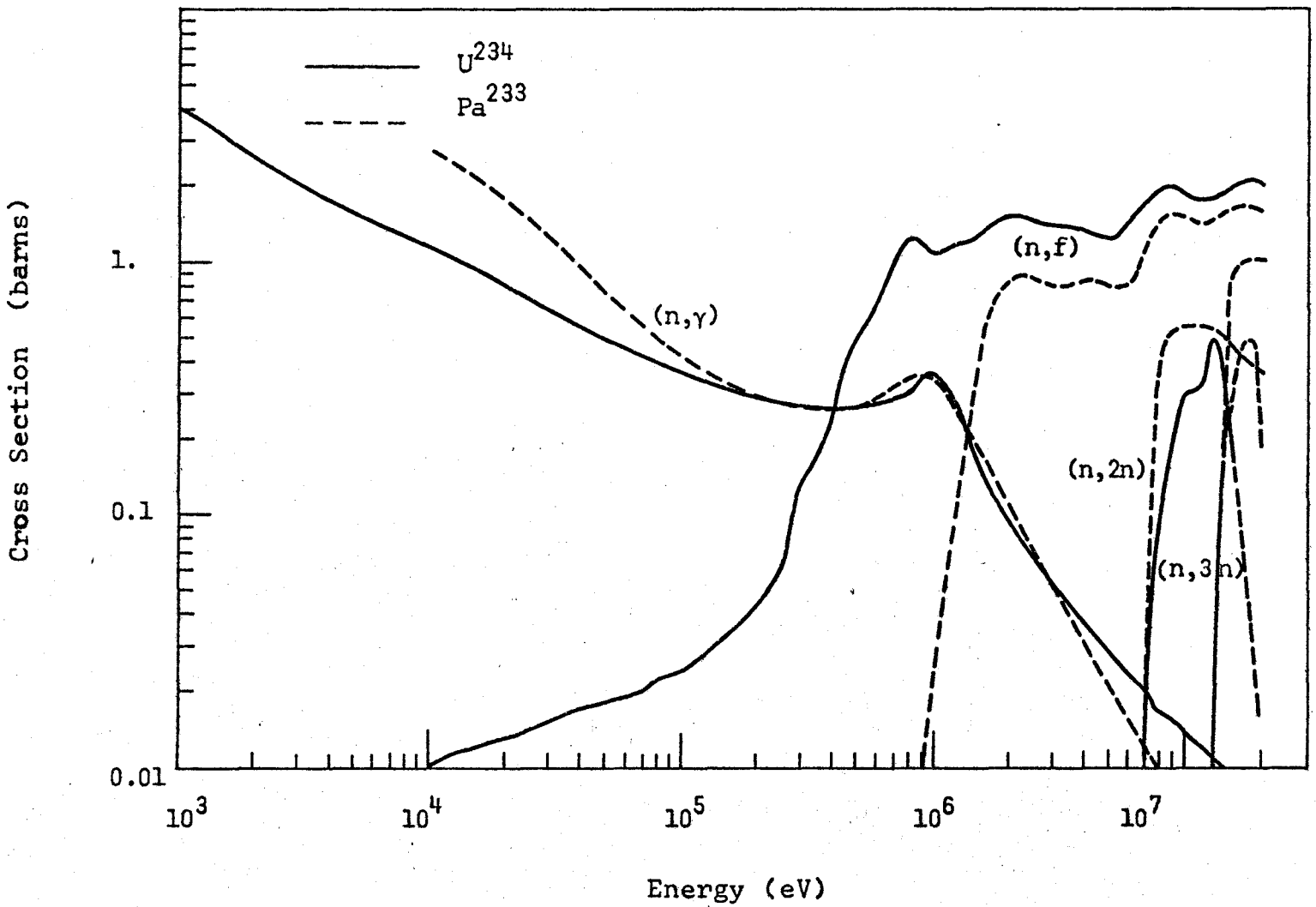

Figure 4 ENDF/B - IV cross sections for U^{234} and Pa^{233}

DISCRETE ORDINATES[8)]

As its name suggests, this method discretizes the neutron transport equation by dealing not with functions at a point but with averages of functions over energy, volume, and angular interval. As in the theory of multigroup representations of the transport equation, if $\psi(\underset{\sim}{r},v\underset{\sim}{\Omega},t)$ is the neutron flux per unit volume, per unit speed, per unit solid angle at position $\underset{\sim}{r}$ with velocity $v\underset{\sim}{\Omega}$ at time t, let $\psi_g(\underset{\sim}{r},\underset{\sim}{\Omega},t)$ be the average of ψ over the speed range $v_{g+1/2}$ to $v_{g-1/2}$. It is convenient to use the function $N_g(\underset{\sim}{r},\underset{\sim}{\Omega},t) \equiv \psi_g(\underset{\sim}{r},\underset{\sim}{\Omega},t)(v_{g-1/2} - v_{g+1/2}) = \int_{v_{g+1/2}}^{v_{g-1/2}} \psi(\underset{\sim}{r},v\underset{\sim}{\Omega},t)\,dV.$

The average of N_g over the volume of a mesh cell (denoted $V_{i+1/2,j+1/2,k+1/2}$) and over the area on the unit directional sphere denoted w_m at $t = t_s$, is

$$N_{g,s,m,i+1/2,j+1/2,k+1/2} = \frac{\int_{\Delta v}\int_{\Delta r} N_g(\underset{\sim}{r},\underset{\sim}{\Omega},t_s)\,d\Omega dV}{\int_{\Delta v}\int_{\Delta r} dr dV}.$$

In this notation, i+1/2, j+1/2, k+1/2, m and g are centred subscripts but s is not.

The transport equation can then be discretized in rectangular geometry as follows: if a coordinate system is set up as below, with μ, n, ξ the direction cosines of the unit direction vector $\underset{\sim}{\Omega}$ at $\underset{\sim}{r}$,

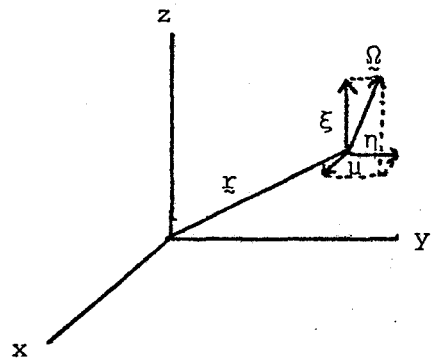

the difference in the number of neutrons in a volume cell $v_{i+1/2,j+1/2,k+1/2}$ (starting at (i,j,k)) in the direction range w_m (a finite area on the unit sphere about the point r) at times t_s and t_{s+1} is

$$w_m(N_{g,s+1,m,i+1/2,j+1/2,k+1/2} - N_{g,s,m,i+1/2,j+1/2,k+1/2})\ V_{i+1/2,j+1/2,k+1/2}/V_g.$$

Dimensions of N_g are numbers of neutrons times speed/unit volume/unit solid angle. Thus, the above expression is dimensionless. The number of neutrons crossing a cell face in the direction range w_m in time Δt is the product of the average flux at the cell surface, an average cosine of the angle between the surface normal and the neutron direction*, the angular area, the cell surface area and the time interval. If $A_{i,j+1/2,k+1/2}$ is the area of the 'i'th' surface of a finite space cell, B the area in the j'th direction and C the area in the k'th direction, the flow of neutrons into the cell is

---

* *In rectangular geometry, the volume cells are just cubes so these cosines are the direction cosines* μ, n, ξ.

$$\omega_m \mu_m A_{i,j+1/2,k+1/2} N_{g,s+1/2,m,i,j+1/2,k+1/2} \Delta t + \omega_m \eta_m B_{i+1/2;j,k+1/2}$$

$$\cdot N_{g,s+1/2,m,i+1/2,j,k+1/2} \Delta t + \omega_m \zeta_m C_{i+1/2,j+1/2,k} N_{g,s+1/2,m,i+1/2,j+1/2,K} \Delta t.$$

For the same direction, the flow of neutrons out of the cell is

$$\omega_m \mu_m A_{i+1,j+1/2,k+1/2} N_{g,s+1/2,m,i+1,j+1/2,k+1/2} \Delta t +$$

$$\omega_m \eta_m B_{i+1/2,j+1,k+1/2} N_{g,s+1/2,m,i+1/2,k+1/2} \Delta t +$$

$$\omega_m \zeta_m C_{i+1/2,j+1/2,k+1} N_{g,s+1/2,m,i+1/2,j+1/2,k+1} \Delta t$$

where, as before, the above two expressions are dimensionless.

A source of neutrons produced in the cell per unit volume, per unit direction, per unit time is denoted by $S_{g,s+1/2,m,i+1/2,j+1/2,k+1/2}$ and the number of source neutrons released in the cell is

$$\omega_m S_{g,s+1/2,m,i+1/2,j+1/2,k+1/2} V_{i+1/2,j+1/2,k+1/2} \Delta t.$$

When neutrons collide with materials with macroscopic cross sections σ, they are assumed to be removed from the cell and this number is

$$\omega_m \sigma_{g,s+1/2,i+1/2,j+1/2,k+1/2} N_{g,s+1/2,m,i+1/2,j+1/2,k+1/2} V_{i+1/2,j+1/2,k+1/2} \Delta t.$$

Equating the time rate of change of the number of neutrons in the cell to gains minus losses, the conservation equation for the cell is (after

dropping all centred subscripts)

$$(N_{s+1} - N_s)V/v\Delta t = \mu(A_i N_i - A_{i+1}N_{i+1}) + \eta(B_j N_j - B_{j+1}N_{j+1})$$

$$+ \xi(C_k N_k - C_{k+1}N_{k+1}) + SV - \sigma NV.$$

In rectangular geometry, $V = \Delta x\Delta y\Delta z$ and $A_i = \Delta y\Delta z = A_{i+1}$,

$$\frac{N_{s+1} - N_s}{V\ \Delta t} + \mu\left(\frac{N_{i+1} - N_i}{\Delta x}\right) + \eta\left(\frac{N_{j+1} - N_j}{\Delta y}\right) + \xi\left(\frac{N_{k+1} - N_k}{\Delta z}\right) + \ N = S$$

which is a finite difference approximation of

$$\frac{1}{V}\frac{\partial N}{\partial t} + \mu\frac{\partial N}{\partial x} + \eta\frac{\partial N}{\partial y} + \xi\frac{\partial N}{\partial z} + \sigma N = S,$$

the analytic form of the transport equation in rectangular geometry. However, what makes discrete ordinates different from the spherical harmonics method is the choice of angular quadrature weights (the breaking up of μ, η and ξ). The appendix gives the derivation of a commonly used set in cylindrical geometry.

CTR DESIGNS AND RELATED BLANKET PARAMETERS

At this time, there are four CTR designs being seriously investigated. These are the mirror, the theta pinch, the tokamak and the laser pellet concepts.

Reactions which will drive these fusion devices are

1. $D + T \rightarrow {}^{4}He + n$
   3.5 MeV 14.1 MeV

2. $D + D \rightarrow {}^{3}He + n$
   .82 MeV 2.45 MeV

3. $D + D \rightarrow T + H$
   1.01 MeV 3.02 MeV

4. $D + {}^{3}He \rightarrow {}^{4}He + H$.
   3.6 MeV 14.7 MeV

Reaction 1 is the fusion reaction of interest for several reasons. There is a large amount of energy produced (17.6 MeV) of which 14.1 MeV or 80% of the reaction energy is transmitted by the neutron. This makes many blanket designs feasible since the neutron can be used for energy multiplication by fast or slow fissioning (hence more versatility in materials choice), or solely for breeding tritium (the Li^{7} breeding reaction is a higher energy reaction).* Also the high energy of this neutron means versatility as regards blanket thickness as well as first wall radius. On the other hand, damage by atom displacement and radiation in the blanket are serious considerations so that fluxes might have to be limited or methods found by which this damage could be lessened.**

The four designs can further be broken into two categories, electromagnetic confinement of the plasma and inertial confinement of the plasma. Electromagnetic confinement provides magnetic pressure to keep the plasma contained. This magnetic pressure can heat the plasma to fusion temperature or this can be done by auxiliary means. Inertial confinement uses lasers to focus large amounts of energy onto small areas (see Fig. 12).

---

* *See Fig. 1 for a plot of $Li^{7}(n,n'\alpha)T$ cross section.*

** *One method of protecting the first wall is to make it porous to some coolant such as Lithium thus achieving a thin layer of material to shield agsinst pellet debris, gamma-rays and X-rays.*

THE MIRROR REACTOR

This is a magnetic confinement device. The basic design is given in Fig. 5.[4] A charged particle sees a weaker magnetic field in the ends or mirror regions. Therefore, the movement of this particle tends to be reversed as a result of the increase in field strength so the particles are essentially trapped. Because of stability requirements however, magnetic coils as shown in Fig. 5 shaped in a 'Yin-Yang' design are being investigated. As seen in this figure, the blanket geometry would be nearly spherical. Design parameters are also given in this figure.* Spherical designs examined in this report are probably too small to be used with such a design.**

THE THETA-PINCH REACTOR

Figure 6 shows a basic design of the theta-pinch (TP) configuration[4]. The current flows in the poloidal or 'theta' direction which results in a 'pinch' effect that confines and heats the plasma The fusion power density is 44 times greater, and more importantly, the fusion power output is 5 times greater than a mirror 'Yin-Yang' design. Thus, while the mirror design will probably only find applications as a small power

---

* *In these tables, 'neutron wall-loading' is the energy flux of the fusion neutrons incident on the first wall of the blanket and is a measure of the fusion neutron source strength normalized to the area of the first wall. With 14.1 MeV neutrons produced by D-T fusions, a 1 MW/m^2 neutron wall leading is equivalent to a fusion neutron source of 4.43 10^{13} $n/cm^2/sec$ at the first wall.*

** *Many of the results listed in this report are for a unit 14.1 MeV neutron point or line source. Hence, obtaining a source strength from given first wall, loading values and then doing an appropriate scaling of this reports' findings is possible.*

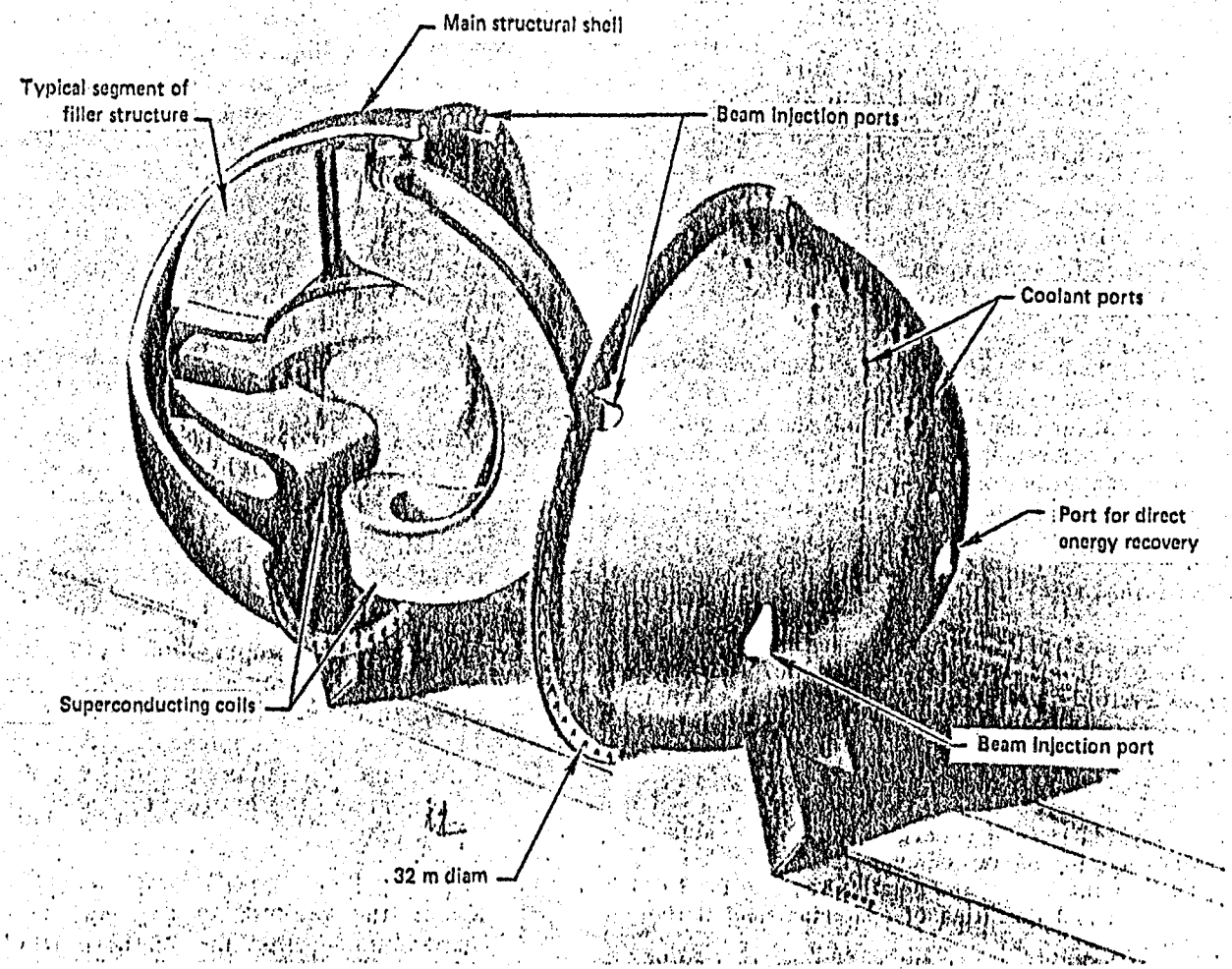

Figure 5(a) A mirror reactor model. See Fig. 5(b) for the mirror reactor confinement scheme and Table 11 for operating parameters.

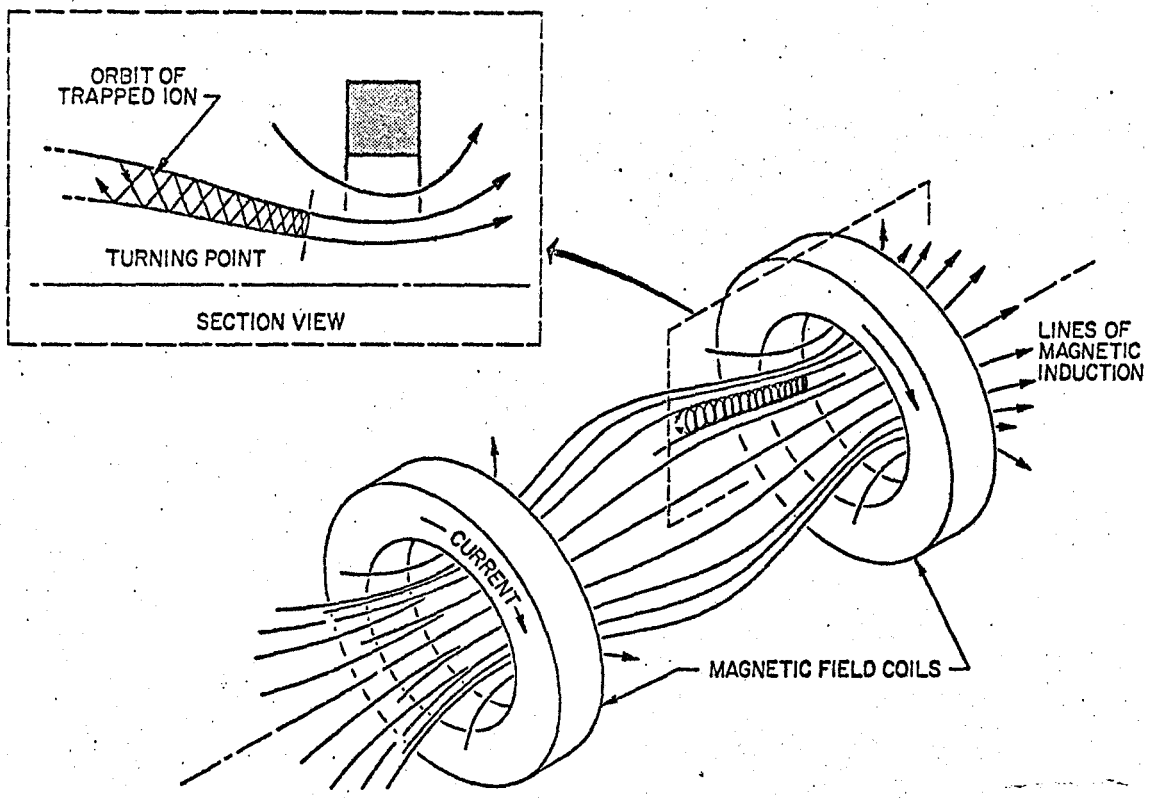

Figure 5(b) Principles of the mirror reactor confinement scheme. See Table 2 for operating parameters.

Parameter	Value
plasma volume (a)	130 m^3
ion density (b)	1.2 10^{14} / cm^3
mean ion energy (c)	610 KeV
mean electron energy	80 KeV
central field	50 kG
mirror field	150 kG
fusion power density	4.5 MW / m^3
fusion power output	590 MW
fractional burnup (d)	8 %
confinement time	3.1 s
neutron wall loading	1.6 MW / m^2
fuel feed rate (e)	5.6 10^{21} / s

(a) the volume is nearly spherical

(b) equals amounts of deuterium and tritium

(c) the mean energies of D and T are not the same; this figure is an average of the two

(d) approximately 6% of the deuterium and 10% of the tritium undergo fusion

(e) fuel is injected at the relative rate D/T = 1.6

Table 2 Operating parameters for a mirror reactor

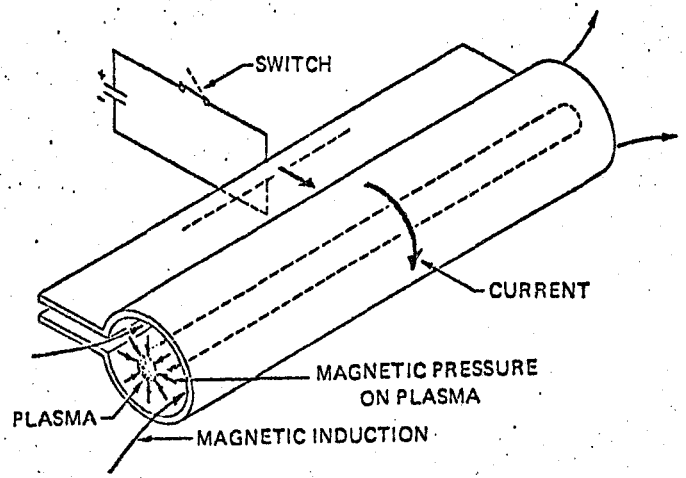

Figure 6(a) Principles of the theta-pinch confinement scheme. See Fig. 6(b) for a view of an actual design (RTPR) and Fig. 6(c) for inertial confinement designs and Tables 3 and 4 for operating parameters.

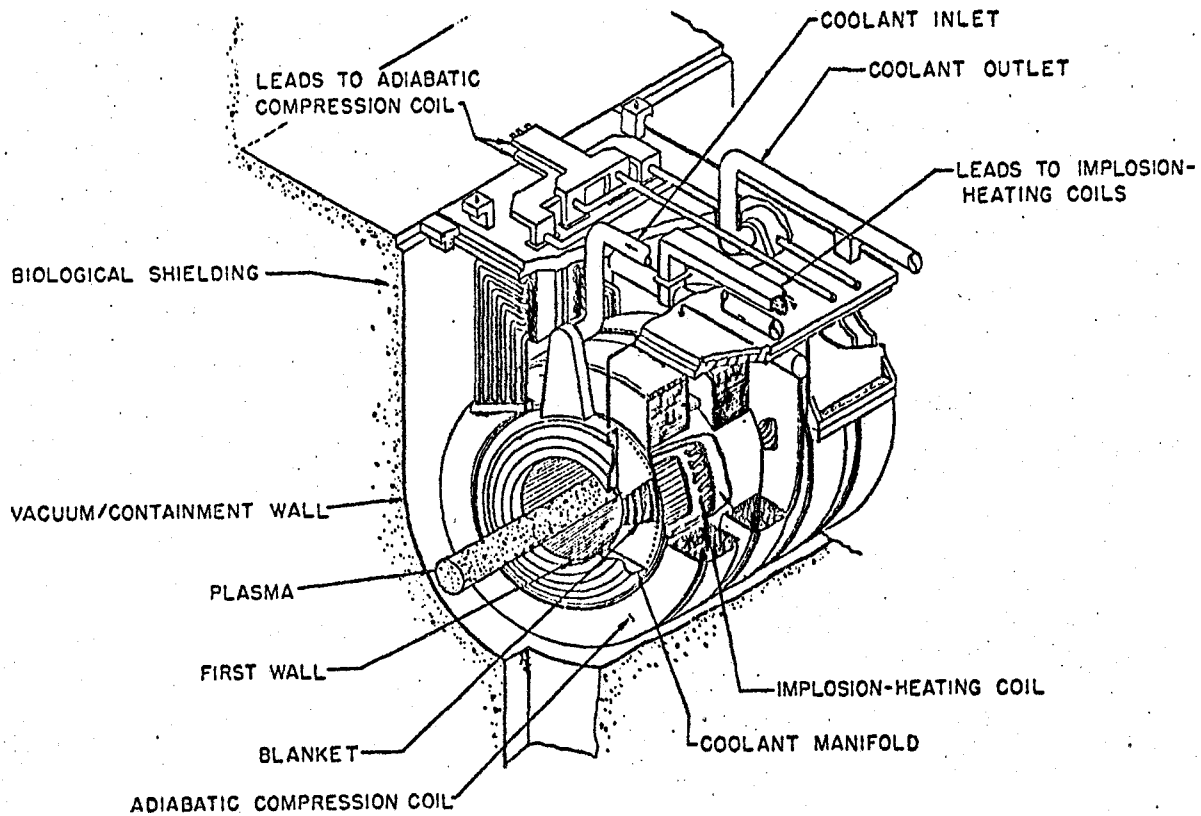

Figure 6(b) The reference theta-pinch (RTPR): cutaway view of a 2-m long module. See Fig. 6(c) for inertial confinement designs and Table 3 for theta-pinch reactor operating parameters.

Parameter	Value
radius of first wall	50 cm
plasma radius at start of burn	11.3 cm
plasma radius at end of burn	20.0 cm
major radius of torus	56 m
plasma volume at start of burn	14.1 m^3
density at start of burn (a)	2.5 10^{16} / cm^3
fractional burnup	4.8%
fusion power density (b)	200 MW / m^3
fusion power output (b)	2820 MW
neutron wall-loading (c)	2 MW / m^2

(a) the ion density consists of equal amounts of deuterium and tritium

(b) based on the plasma volume at start of burn and a 10-sec cycle time

(c) based on a first-wall radius of 50 cm and a 10-sec cycle time

Table 3 Operating parameters of the theta-pinch reactor

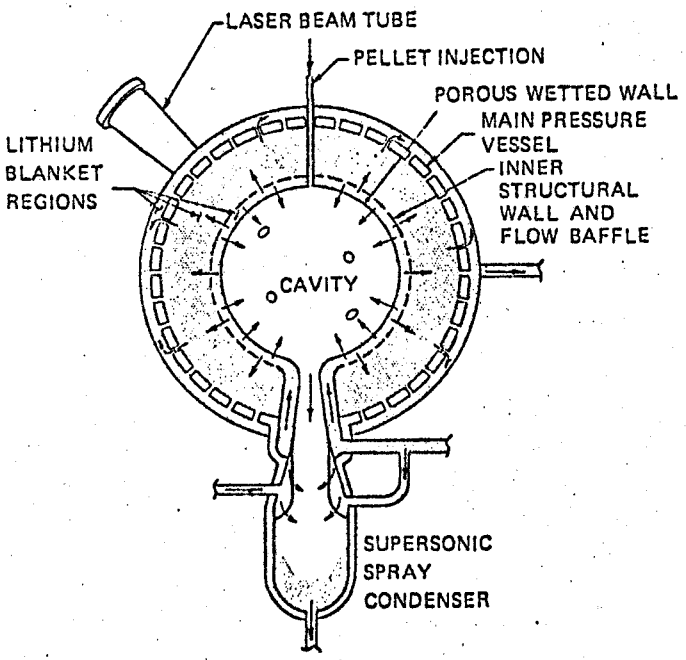

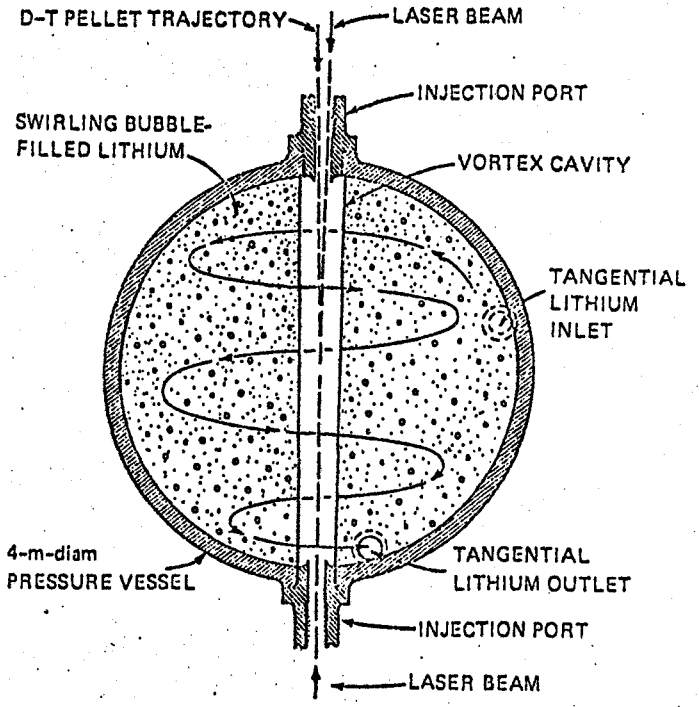

Figure 6(c) Inertial confinement designs. See Table 4 for operating parameters.

Parameter	Value
cavity radius (a)	1.7 m
laser energy (b)	1 MJ
fusion energy release	100 MJ/ microexplosion
cavity pulse rate	1.2 / s per cavity
neutron wall-loading (c)	2.6 MW / m^2
number of cavities (d)	24
fusion power output	2880 MW

(a) spherical geometry

(b) the laser energy is delivered by a CO_2 laser system with eight beams

(c) based on a cavity radius of 1.7 m, a fusion energy release of 100 MJ per pellet microexplosion and a cavity pulse rate of 1.2 shots per sec per cavity

(d) a single laser system serves all 24 cavities

Table 4 Operating parameters for a wetted-wall laser-pellet reactor

unit, the theta-pinch reactor holds promise as a large power producer. It is expected that TP reactors will be toroids and the first wall radius (see Fig. 6) suggests a blanket thickness of about 1 meter. Because of the high power densities, cycle times (the time for one heating, fusion and cooling of the plasma) of the order of ten seconds and a layer of neutral gas between the plasma and first wall are needed to decrease radiation damage of the first wall. The toroid major radius of 56 meters means large inventories of all materials. Infinite and finite cylinder studies done in this report would be applicable to this design.

THE TOKAMAK REACTOR

This, like the Theta-Pinch Reactor is a toroidal, magnetically confined scheme. An axial current, as shown in fig. 7,[4] is induced in the plasma by a changing magnetizing flux to provide a pulsed poloidal magnetic field that works together with a steady state toroidal field to confine the plasma. The axial plasma current also provides initial ohmic heating within the plasma. In addition, this plasma requires a pulsed transverse field to provide control of the position of the plasma column. Parameters for this reactor are shown in fig. 7. Note the high fusion power output. Again, infinite and finite cylinder calculations done here can be applied.

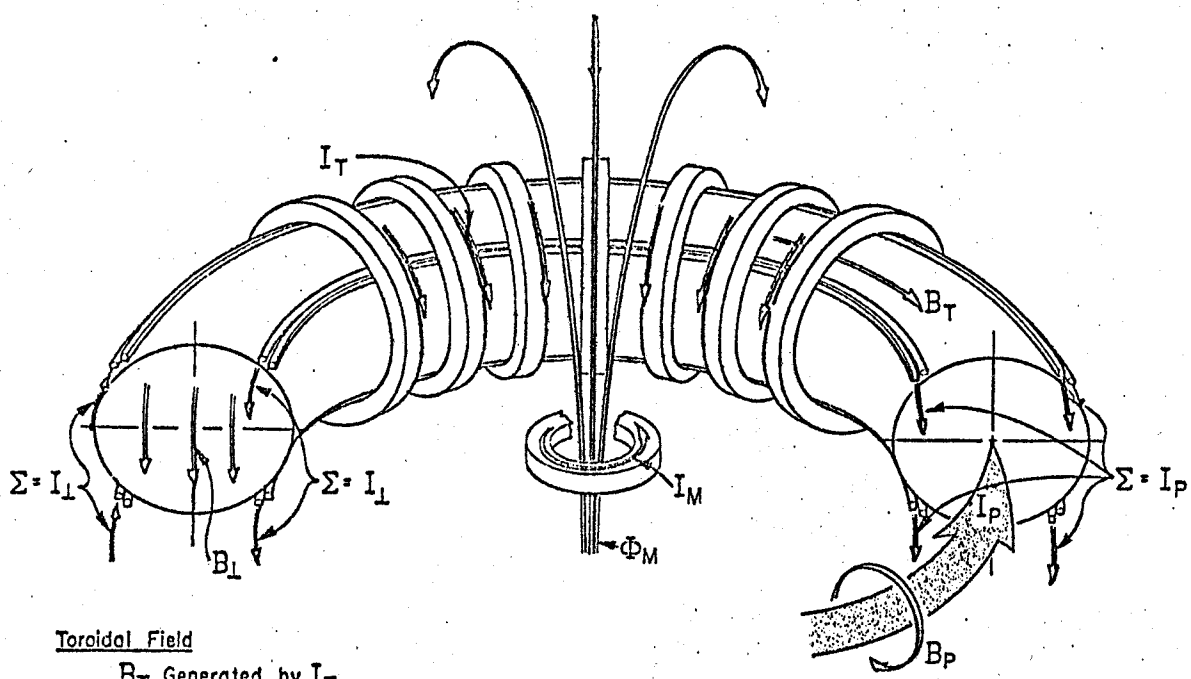

Toroidal Field

B_T Generated by I_T

Poloidal Field

B_P Generated by plasma current I_P = sum of external currents

Transverse Field

$B_\perp$ Generated by external current $I_\perp$

Magnetizing Flux

Φ_M Generated by the magnetizing current I_M

Figure 7 Principles of the Tokamak confinement scheme. See Table 5 for operating parameters.

Parameter	Value
plasma radius	2 to 5 m
major radius of torus	10 to 13 m
plasma volume	830 to 6400 m^3
ion density (a)	3 to 5%
ion temperature (b)	10 to 30 KeV
maximum toroidal field (c)	80 to 160 kG
axial current	8 to 21 MA
fusion power density	0.7 to 2.0 MW / m^3
fusion power output	1000 to 5000 MW
fractional burnup	3 to 9%
confinement time	several to tens of sec
burn time	hundreds to thousands of sec
current rise (reversal) time	10 to 100 sec
purge and reload time	30 to 60 sec
auxiliary heating power	10 to 100 MW
fuel feed rate	2 to 4 10^{22} / sec
neutron wall-loading	1 to 4 MW / m^2

(a) the ion density consists of equal amounts of deuterium and tritium
(b) the electron and ion temperatures are essentially the same
(c) this maximum in field strength occurs in the coil winding

Table 5 Operating parameters for the Tokamak reactor

THE LASER-PELLET REACTOR

This type of reactor employs inertial confinement by laser light. Theory suggests that symmetrical illumination would lead to high pellet compression ratios (ratio of compressed core density to normal solid density). In this design, the fusion reaction in the pellets occurs as follows. A precursor to the main laser wave front vaporizes and then ionizes the surface of the pellet. After this, the main front arrives and heats the remaining core centre which causes fusion reactions to begin right at the centre of the pellet core. The alphas from these reactions are attenuated rapidly in the highly dense centre and cause heating that lets the fusion reaction spread out over the remaining core. The two spherical blanket designs studied in this report had this type of reactor in mind. Figure 6[4)] lists operating parameters of this design. Note the high fusion power output which necessitates protecting the first wall by long cycle times or other means. One other means is to use a 'wetted-wall' concept where the first wall is porous to the coolant flowing on the outer side (probably liquid lithium). The thin layer of lithium would protect the first wall from X-rays and pellet debris.* The layout of this design is given in Fig. 6[4)]. Note the blowdown chamber required for spent plasma removal. This chamber would be small enough that blanket neutronics would not be seriously affected.

---

* *However, large numbers of alpha particles from the lithium breeding reactions would be created that would deposit high amounts of heat in the first wall due to the rapid attenuation of the alphas.*

LITHIUM CONSIDERATIONS

The fuel cycle which will be studied in this report is a deuterium-lithium cycle; that is, deuterium and lithium are the primary fuels. Tritium can be bred within a blanket surrounding the reaction chamber by one of two reactions:

$$Li^6 + n(slow) \rightarrow T + {}^4He$$

$$Li^7 + n(fast) \rightarrow T + {}^4He + n - 2.5 \text{ MeV}.$$

In addition, the lithium is an effective moderator and biological shield. For this reason, the designs in this report use an outer, relatively small, 'mopping up' region composed of lithium plus structure. While effectively stopping most of the low energy flux, this region does provide some tritium breeding and might prove to be a necessary region for making tritium breeding greater than 1 in some designs.

Graphs of relevant Li^6 and Li^7 cross sections are given in Fig. 1. Since the lithium is also assumed to be the first wall coolant in this report, it must compete with parasitic absorption reactions in the structural materials. The $Li^7(n,n'\alpha)T$ has an energy threshold at approximately 2.5 MeV and therefore competes with neutron downscattering processes such as elastic scattering, inelastic scattering and (n,2n), (n,3n) reactions. ((n,3n) reactions were not considered in this report since the processing code SUPERTOG available here did not take them into account. The $Li^6(n,\alpha)T$ reaction becomes 1/v below approximately

0.3 MeV and so lithium, enriched in Li^6, might be used in the final 'mop-up' layer.

There is a problem with the magnetic confinement schemes outlined earlier as regards pure lithium as a coolant. The area around the first wall has high power densities with these schemes and natural lithium has a high electromagnetic conductivity. This means that pumping in this region is a problem. A compound called Flibe[3)] made of Be, F, and Lithium has been suggested to counter this problem. It does not have the same high e-m conductivity. However, breeding rates have been reported as significantly less using this compound. Studies however, on just this pumping problem, report that these losses can be overcome with proper placement of the coolant channels and other means and so natural lithium should not be dismissed as a coolant on these grounds alone.

BLANKET MATERIALS

This section will deal briefly with various wall-coolants, first wall materials and neutron multipliers.

WALL COOLANTS

Liquid lithium is the primary choice because of its tritium breeding capabilities. Although very corrosive, it can be contained at high temperatures by pure iron, Nb or Mo. A big disadvantage is its high electrical conductivity. However, e-m resistance to Li flow decreases away from the first wall where power densities are highest so proper designing might make Li usable throughout the blanket.

Water is a good coolant and a good neutron moderator. Its low critical temperature and high vapour pressure imply low blanket temperatures. Thick stainless steel tubing (or another similar material such as Zr-2) would be needed to contain it making moderation high in a water cooled region (see Neutronics Calculations). Another problem is the exchange of H and T after diffusion through tube walls in, say, a region where tritium was being bred.

FIRST WALL

This is a highly important structure as a wall for the blanket, for heat transfer and to a far lesser extent, as a neutron multiplier. It needs to have high thermal conductivity and a low vapour pressure at temperatures around 1000 degrees Kelvin (since metal atoms

vaporized into the plasma can cause severe energy losses by Brehmstrallung in the magnetically confined plasmas). Resistance to corrosion as well as a low neutron capture cross-section are other important desired properties.

Refractory metals pretty well fill the bill. They have better high temperature properties than any other materials. Tungsten, Mo and, to a lesser extent, Nb have good (n,2n) cross-sections for 14-MeV neutrons. With proper designing, the (n,2n) multiplication can outweigh the capture in the first wall (see figs. 8 and 9 for findings of this report). Disadvantages of these metals is their brittleness at room temperature and hence fabrication difficulties.

Other first wall materials are stainless steel, nickel, graphite and other special compounds.*

NEUTRON MULTIPLIERS

To create a greater supply of breeding neutrons, it has been suggested that fissile material placed near to the first wall be used (materials such as U^{238} or Pu^{239} to utilize the high energy flux). One of the spherical designs in this report (design number 2) uses a CANDU fuel bundle with $U^{238}O_2$ pellets next to the first wall. Other reports have suggested thorium or uranium metal as well as carbides such as UC or ThC so that extra structural support would be obtained.

---

* *INOR-8 was developed to resist fluoride corrosion.*

NEUTRONICS CALCULATIONS

The basis of these studies was to study the effect in blankets of D_2O cooled CANDU fuel bundles with ThO_2 fuel elements. The elements, overall bundle design and specifications are given in Fig. 8[11].

Three infinite cylindrical blanket designs were studied. These designs varied by position and number of fuel bundles in the cylindrical shell blanket. ANISN also has an option for finite geometry corrections and so a particular finite design was chosen and run for comparison. This finite model is listed in Fig. 9. Time studies were run on the third infinite cylinder design and on two spherical designs. Basic blanket configurations are given in Fig. 10. Number densities used in all designs are given in Table 6. These designs do not include a right hand biological shield. The effect of this was approximated by an energy independent albedo of 0.32.

An important aspect of the blanket is that it produces enough tritium (greater than ∿1.15 per unit neutron source) to sustain the fusion reaction. Lithium breeding rates are shown for the five designs in Figs. 11-14.* A summary of the breeding rates in the relevant zones by design is given in Table 7. The thermalizing effect of the $U^{238}O_2$ bundle in SD1 and SD2 as well as the ThO_2 bundle in CD1** have a

---

* *In these figures, as for all other reactions, the reaction rate is based on assuming a steady production of one 14.1 MeV neutron per second per unit length of plasma in the cylindrical systems and one 14.1 MeV neutron per second in the plasma of the spherical systems.*

** *Spherical design 1, spherical design 2 and cylindrical design 1.*

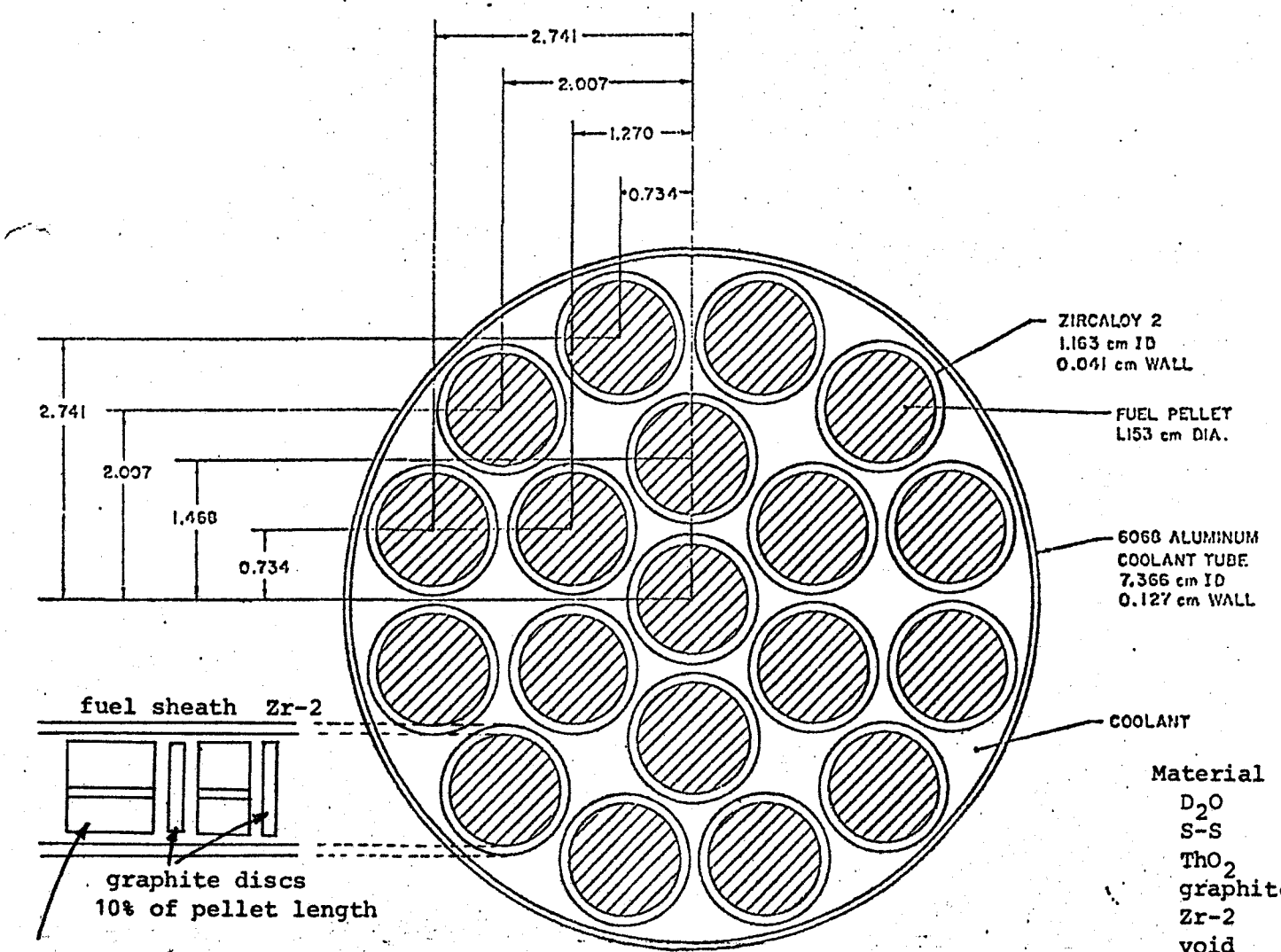

Material	V/0 in bundle
D_2O	42.7
S-S	6.55
ThO_2	37.96
graphite	4.0
Zr-2	6.46
void	2.3

Figure 8 Details of a 19-element ThO_2 fuel rod. Coolant is D_2O. Density of ThO_2 used was 9.33 gm / cm^3. Type 347 S-S was used i.e. 0.08 w/0 carbon, 18 w/0 Cr, 11 w/0 Ni, 70.92 w/0 Fe, as specified in Ref. 10.

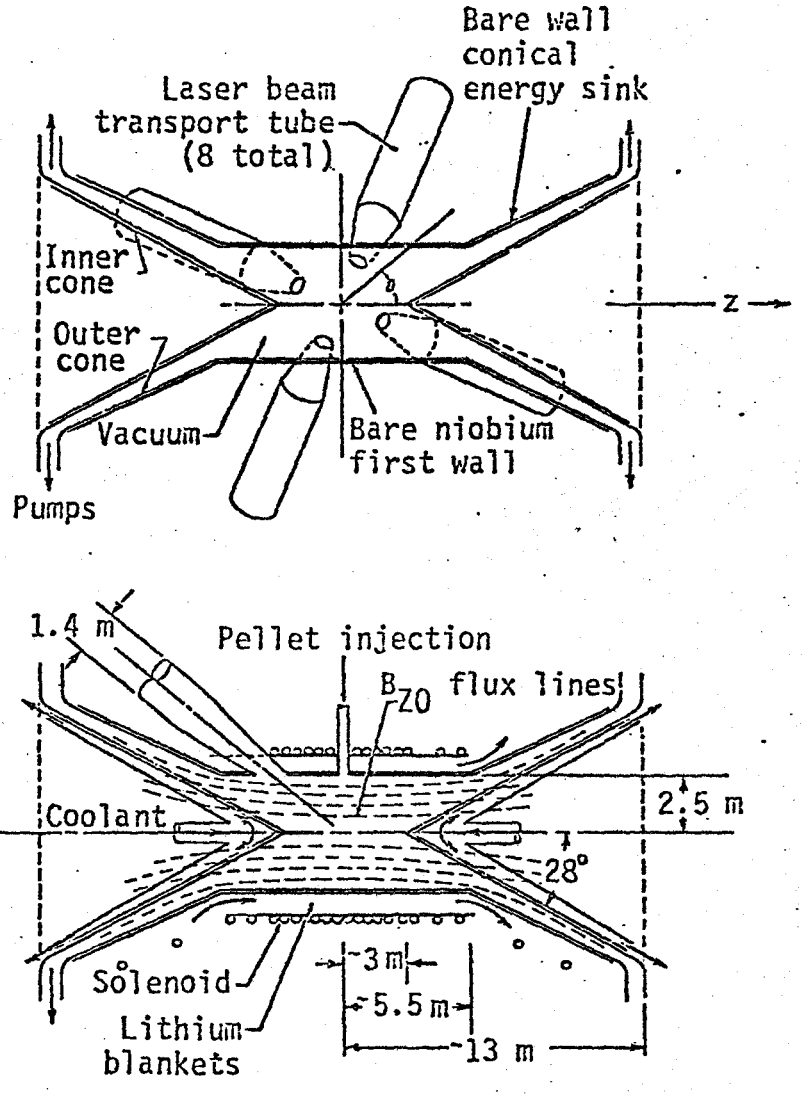

Figure 9 Possible finite cylindrical design for CD1, CD2 and CD3 specifications. See basic blanket layouts.

Cylindrical Design 1 (CD1)

Plasma	Vacuum	Nb	Nb	Th bundle	94 % Li 6 % Nb	graphite	94% Li 6% Nb

rad.	0	150	200	200.5	201	207			264	294	300
zone	1	2	3	4	5	6	7	8	9	10	
intervals	1	4	3	3	10	10	10	10	15	6	

Cylindrical Design 2 (CD2)

Plamsa	Vacuum	Nb	Nb	94 % Li 6 % Nb	Th bundle	graphite	94% Li 6% Nb

rad.	0	150	200	200.5	201			258	264	294	300
zone	1	2	3	4	5	6	7	8	9	10	11
intervals	1	4	3	3	10	10	10	16	10	15	3

Cylindrical Design 3 (CD3)

Plasma	Vacuum	Nb	Nb	94 % Li 6 % Nb	Th bundle	Th bundle	Th bundle	graphite	94% Li 6% Nb

rad.	0	150	200	200.5	201	246	252	258	264	294	300	
zone	1	2	3	4	5	6	7	8	9	10	11	12
intervals	1	4	3	3	10	10	10	10	10	10	15	4

Figure 10(a) Basic Blanket Layouts See Fig. 13(b) for remaining layouts.

Spherical Design 1 (SD1)

Plasma	Vacuum	Nb	Nb	94 % Li 6 % Nb	Th bundle	Th bundle	graphite	94% Li 6% Nb
rad. 0 2	100	100.5	101		158	164	170	185 200
zone 1	2	3	4	5 6 7	8	9	10	11
intervals 1	5	4	4	10 10 10	10	10	10	10

Spherical Design 2 (SD2)

Plasma	Vacuum	Nb	Nb	U bundle	94% Li 6% Nb	Th bundle	Th bundle	graphite	94% Li 6% Nb
rad. 0 2	100	100.5	101	107		158	164	170	185 200
zone 1	2	3	4	5	6 7 8	9	10	11	12
intervals 1	3	3	3	10	10 10 10	10	10	10	10

Figure 10(b) Basic Blanket Layouts

In the fuel bundle

Th	8.08	10^{-3} / cm^3	
O^{16}	3.03	10^{-2} / cm^3	(includes contributions from D_2O & ThO_2)
D	2.83	10^{-2} /cm^3	
C^{12}	3.18	10^{-3} / cm^3	(from stainless steel and carbon spacers)
Zr-2	2.79	10^{-3} / cm^3	

94% Li - 6% Nb region

Li^6	3.07	10^{-3} / cm^3	based on CRC Handbook compositions
Li^7	3.80	10^{-2} / cm^3	of natural lithium as 7.42 w/0 Li^6,
Nb	3.34	10^{-3} / cm^3	92.58 w/0 Li^7

First Wall

Nb	5.56	10^{-2} / cm^3

Graphite	8.03	10^{-2} / cm^3

Table 16 Number densities used in ANISN (times 10^{-24})

Figure 11(a) Cylindrical Design 1: Lithium Reaction Rates

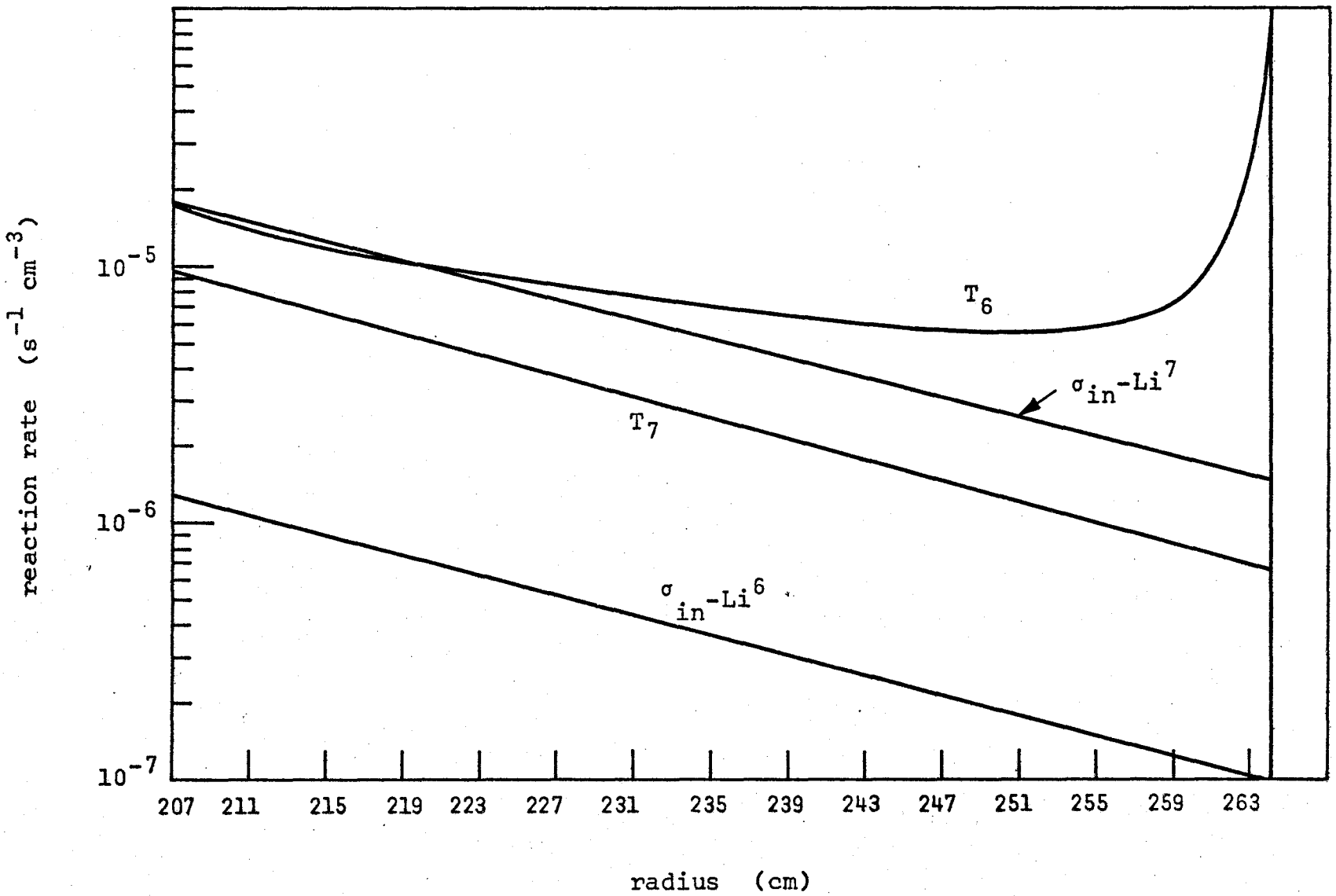

Figure 11(b) Cylindrical Design 2: Lithium Reaction Rates

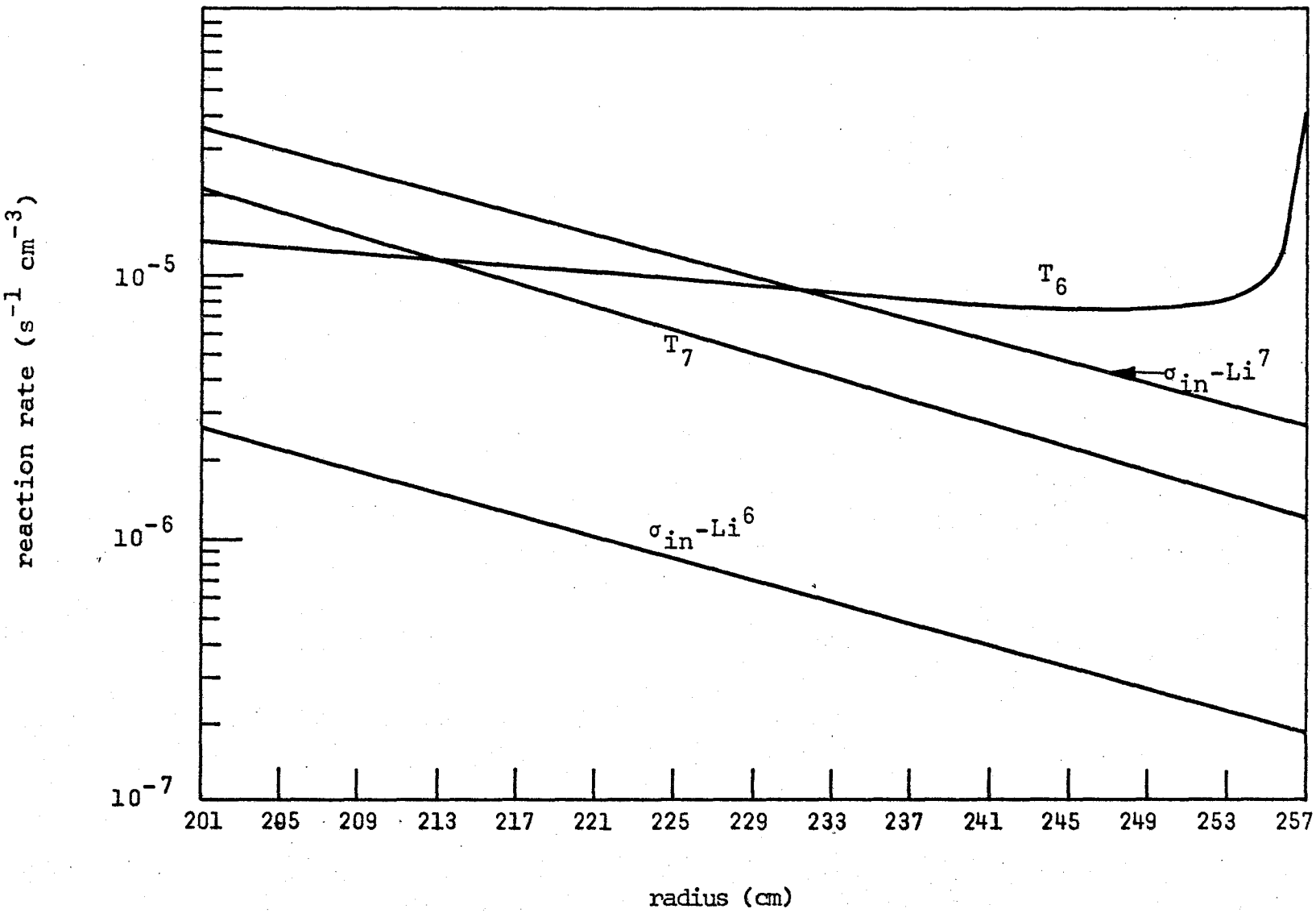

Figure 12 Cylindrical Design 3: Lithium Reaction Rates

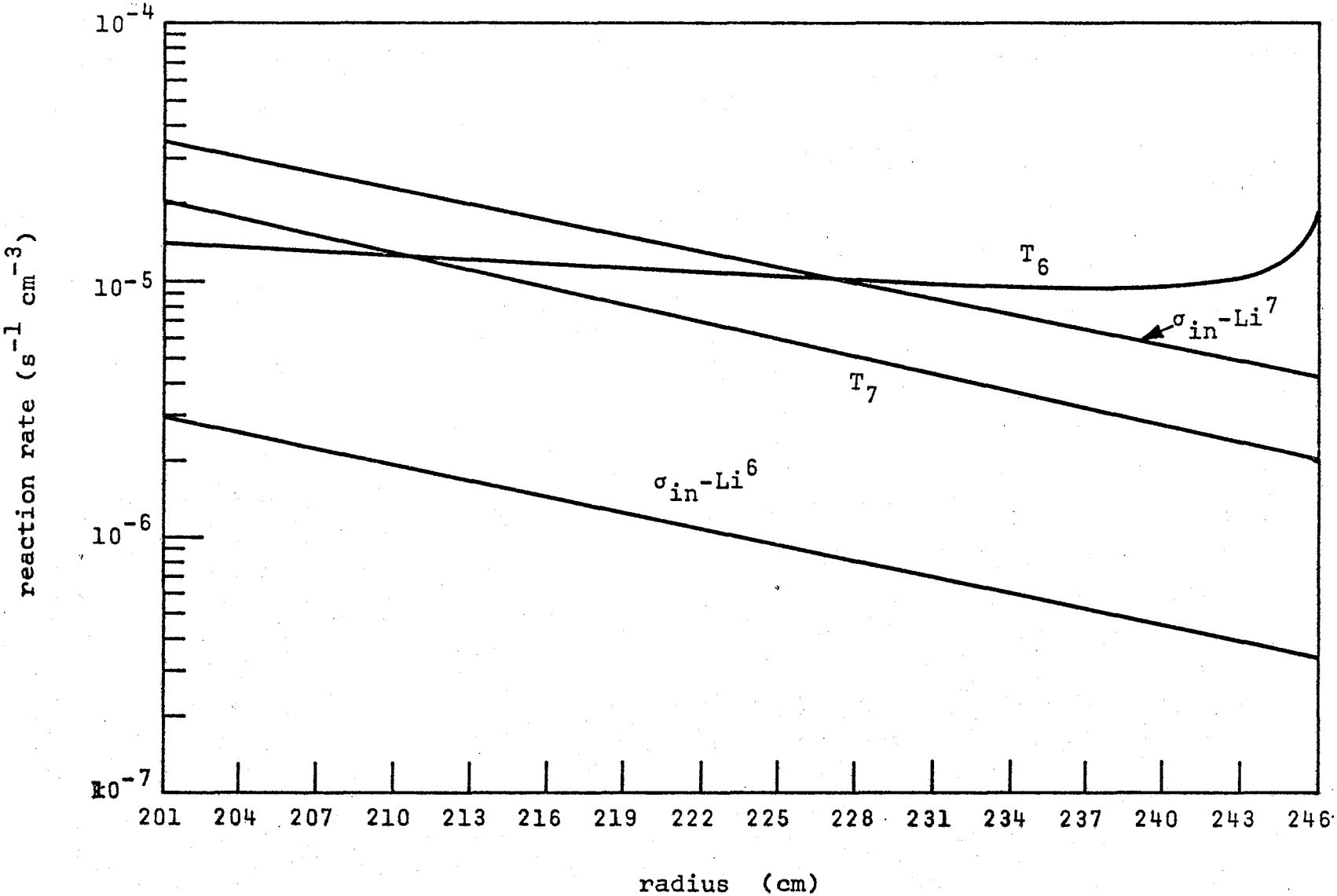

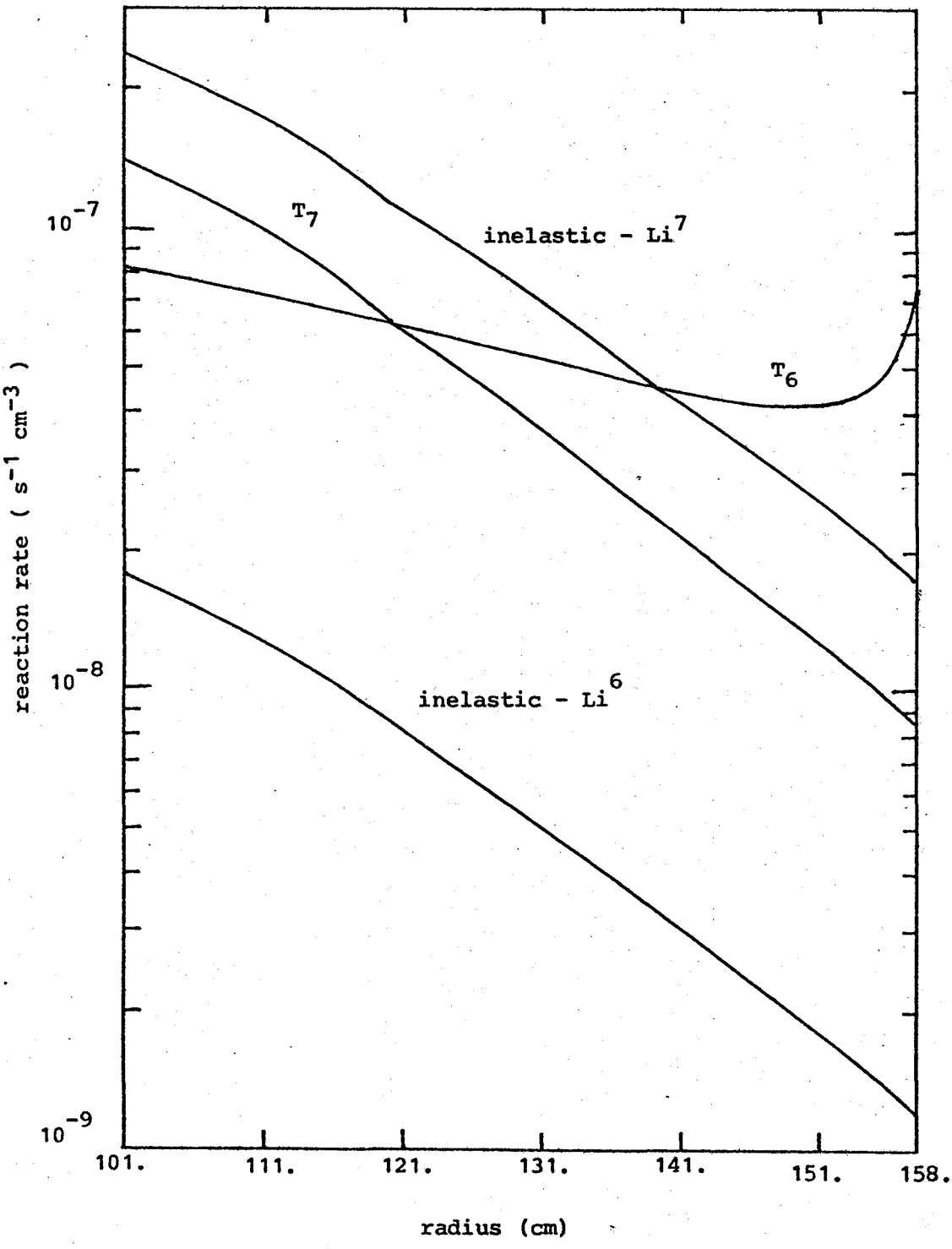

Figure 13 Lithium reaction rates in spherical design 1

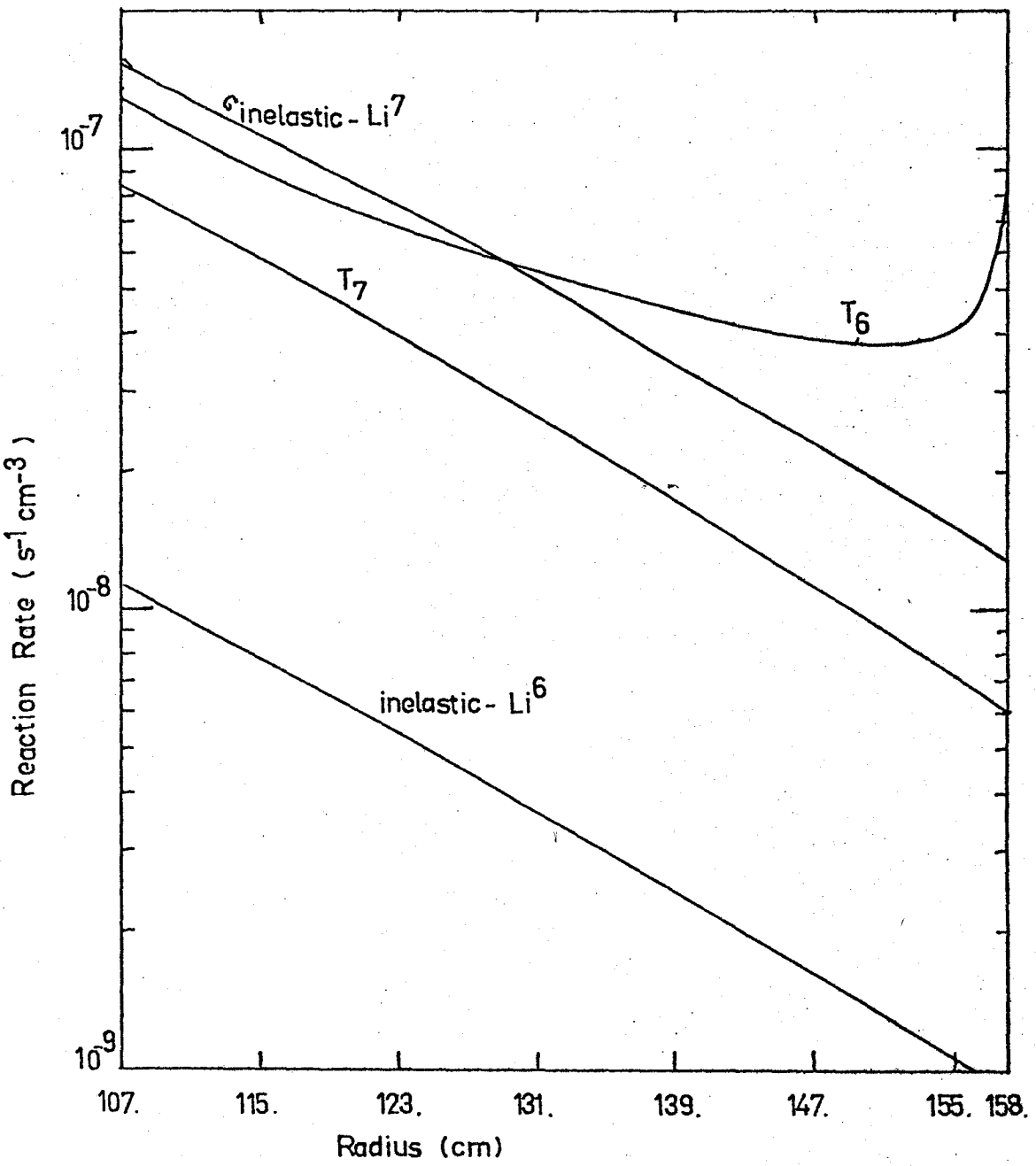

Figure 14 Lithium reaction rates for spherical design 2

CD1: reaction rates per unit 14.1 MeV neutron/s per unit plasma length

Zone	T_6	% of T	T_7	% of T	T	% of T
6	0.341	32	0.182	17	0.523	49
7	0.184	17	0.067	6	0.251	23
8	0.214	20	0.031	3	0.245	23
10	0.049	5	0.001	0.1	0.050	5
	0.788	74	0.281	26	1.069	

CD2: reaction rates per unit 14.1 MeV neutron/s per unit plasma length

Zone	T_6	% of T	T_7	% of T	T	% of T
5	0.288	21	0.336	24	0.624	45
6	0.238	17	0.143	10	0.381	27
7	0.207	15	0.063	5	0.270	19
8	0.062	4	0.004	0.3	0.066	5
11	0.056	4	0.000	0.0	0.056	4
	0.851	61	0.546	39	1.397	

CD3: reaction rates per unit 14.1 MeV neutron/s per unit plasma length

Zone	T_6	% of T	T_7	% of T	T	% of T
5	0.237	20	0.285	24	0.522	44
6	0.210	18	0.143	12	0.353	30
7	0.209	18	0.073	6	0.282	24
12	0.025	2	0.001	0.1	0.026	2
	0.681	58	0.502	42	1.183	

SD1: reaction rates per unit 14.1 MeV neutron/s

Zone	T_6	% of T	T_7	% of T	T	% of T
5	0.215	17	0.302	24	0.517	40
6	0.218	17	0.168	13	0.386	30
7	0.235	18	0.082	6	0.317	25
11	0.055	4	0.005	0.4	0.060	5
	0.723	56	0.557	44	1.280	

Table 7(a) Tritium breeding rates. See Table 6(b) for breeding rates for SD2

SD2: reaction rates per unit 14.1 MeV neutron/s

Zone	T_6	% of T	T_7	% of T	T	% of T
6	0.265	26	0.171	17	0.436	42
7	0.202	20	0.097	9	0.299	29
8	0.196	19	0.050	5	0.246	24
12	0.043	4	0.003	0.3	0.046	4
	0.706	69	0.321	31	1.027	

Table 7(b) Tritium breeding rates for spherical design 2

dominant effect on the breeding rates. It can be seen from Table 6 that although T_6 is much higher in the area immediately to the right of the bundle, the subsequent areas are much lower. Thus, while the bundle does a good job of thermalizing, it also absorbs a large amount of the neutrons. Figures 18-19 amply demonstrate this. These are the flux maps. In particular, a comparison of CD1 and CD2 as well as SD1 and SD2 is in order. It can be seen in, say, the map for CD1 that the group fluxes of largest magnitude, groups 1 and 22 and hence all the upper group fluxes are reduced by a factor of approximately 0.7 in the 94%Li - 6%Nb region of the blanket. However, the much lower in magnitude low energy fluxes are comparatively quite a bit higher in magnitude in CD1 as for example, the group 76 130 eV flux. The thermalizing effect of the bundle can be put to good use however, on the right hand side of the main 94%Li - 6%Nb region. In this case, the thermalization plus absorption effects mean higher Li^6 breeding rates to the immediate left of the bundle as well as an effective shield for neutrons escaping the system. This is further evidenced by the fact that adding extra bundles lowers the breeding rate but not to the extent that the breeding volume has been reduced. Cylindrical design 3 has 3 bundles next to the graphite region while CD2 has 1. The drop in breeding rates is .85 or 15% while the corresponding drop in available breeding volume is .77 or 23%.* It can be seen on any of the lithium reaction rate graphs how sharply increasing T_6 is

---

** It must be noted that in CD1, CD2 the bundle thickness is somewhat misleading and inaccurate. The 6 cm thickness was first used to describe a stacking like this 0000 0000 . Hence, two or more bundles will each have an effective thickness of about 6 cm. The actual bundle diameter is 7.62 cm so calculations using a single bundle will have slightly higher breeding rates as well as other differences as a result.*

Figure 15 Flux Spectra: Cylindrical Design 1

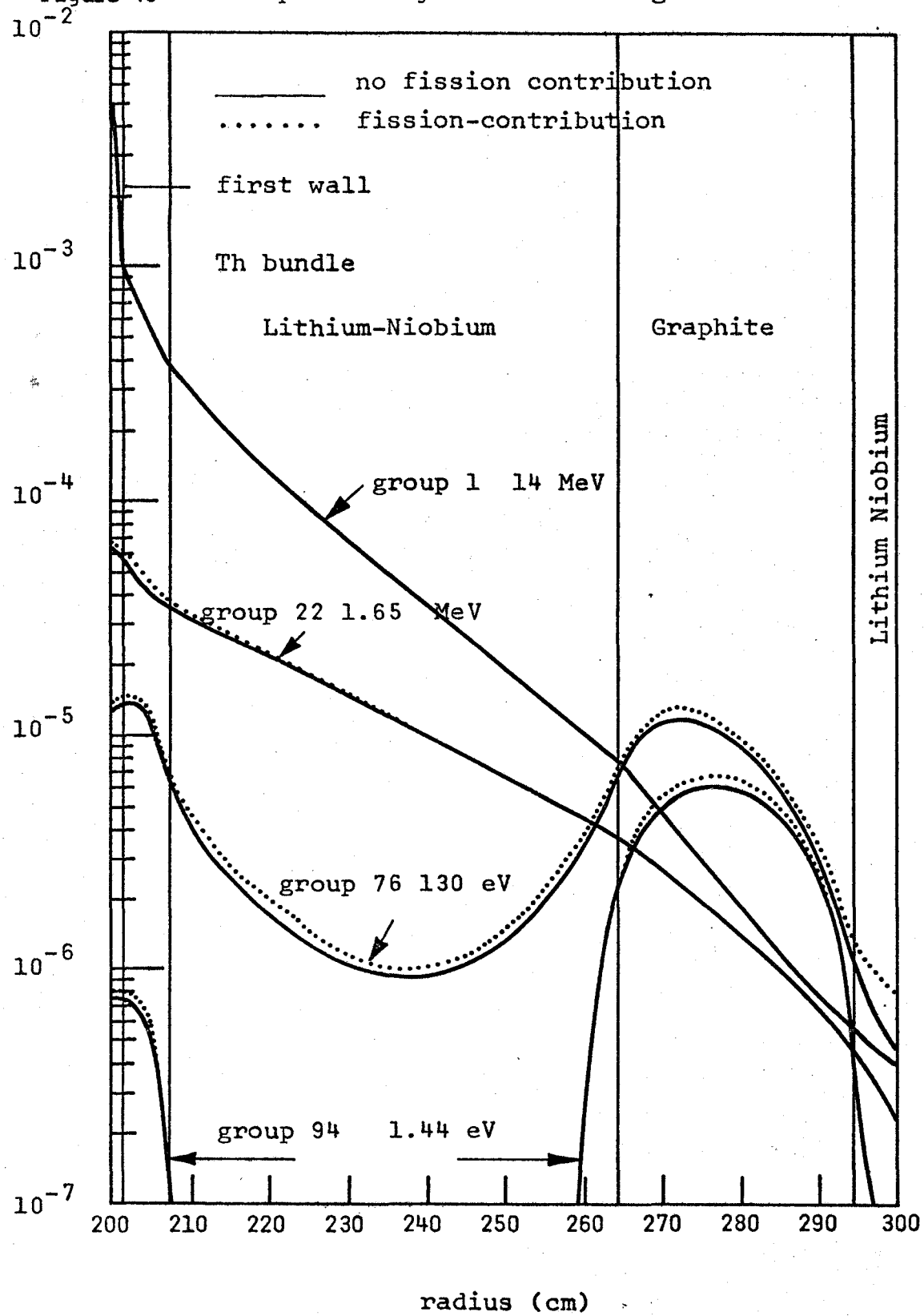

Figure 16 Flux Spectra: Cylindrical Design 2

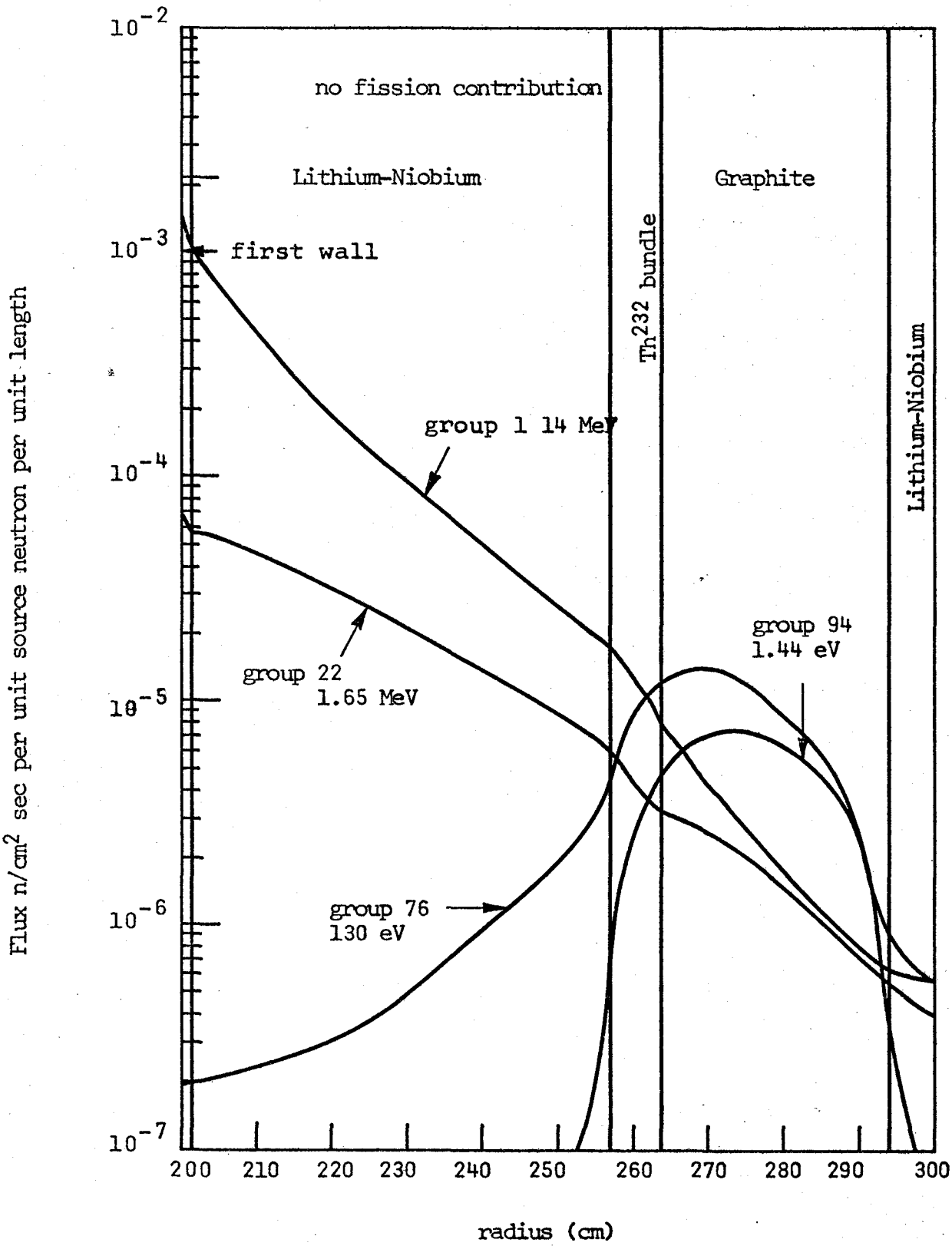

Figure 17 Flux Spectra: Cylindrical Design 3

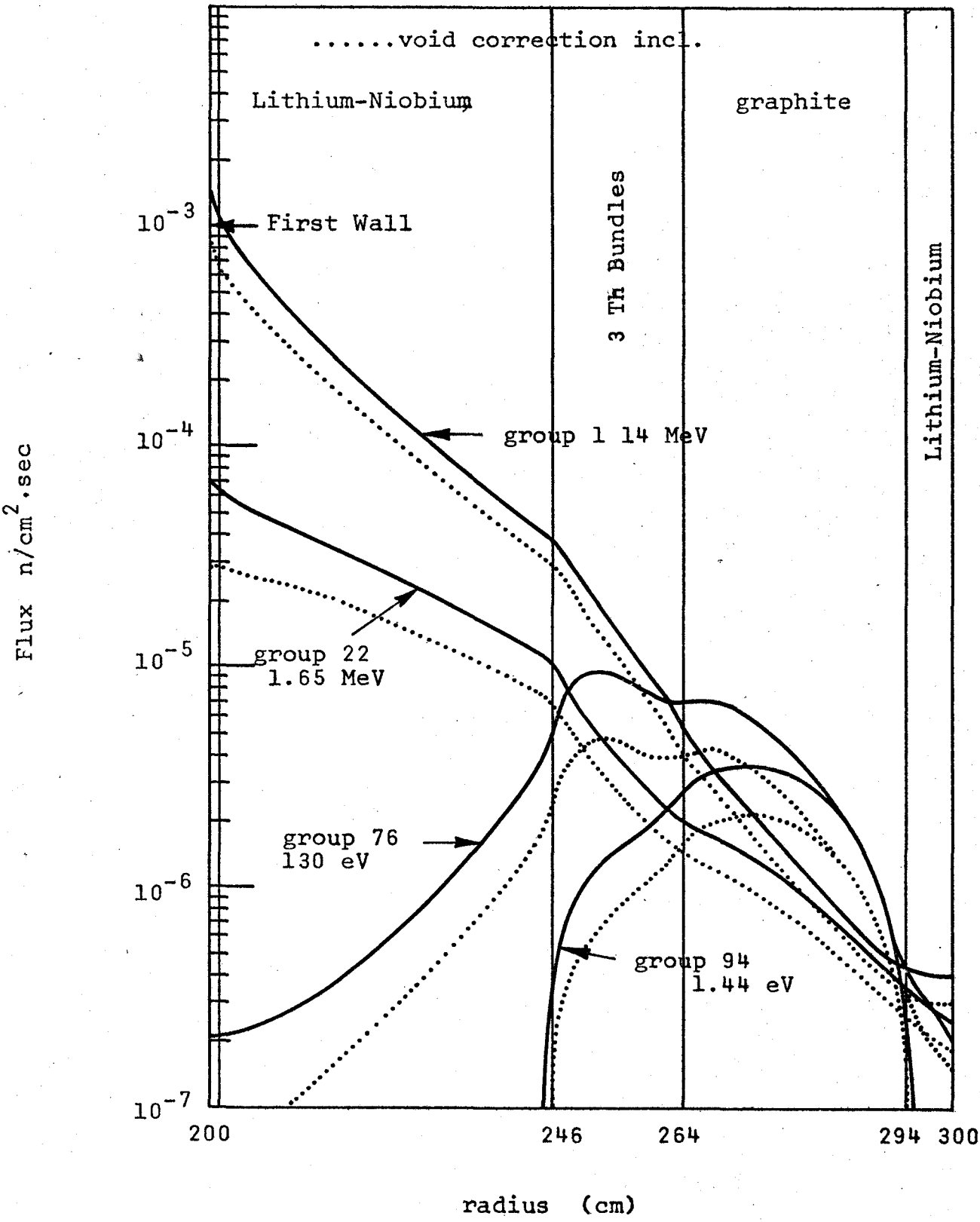

Figure 18 Flux Spectra: Spherical Design 1

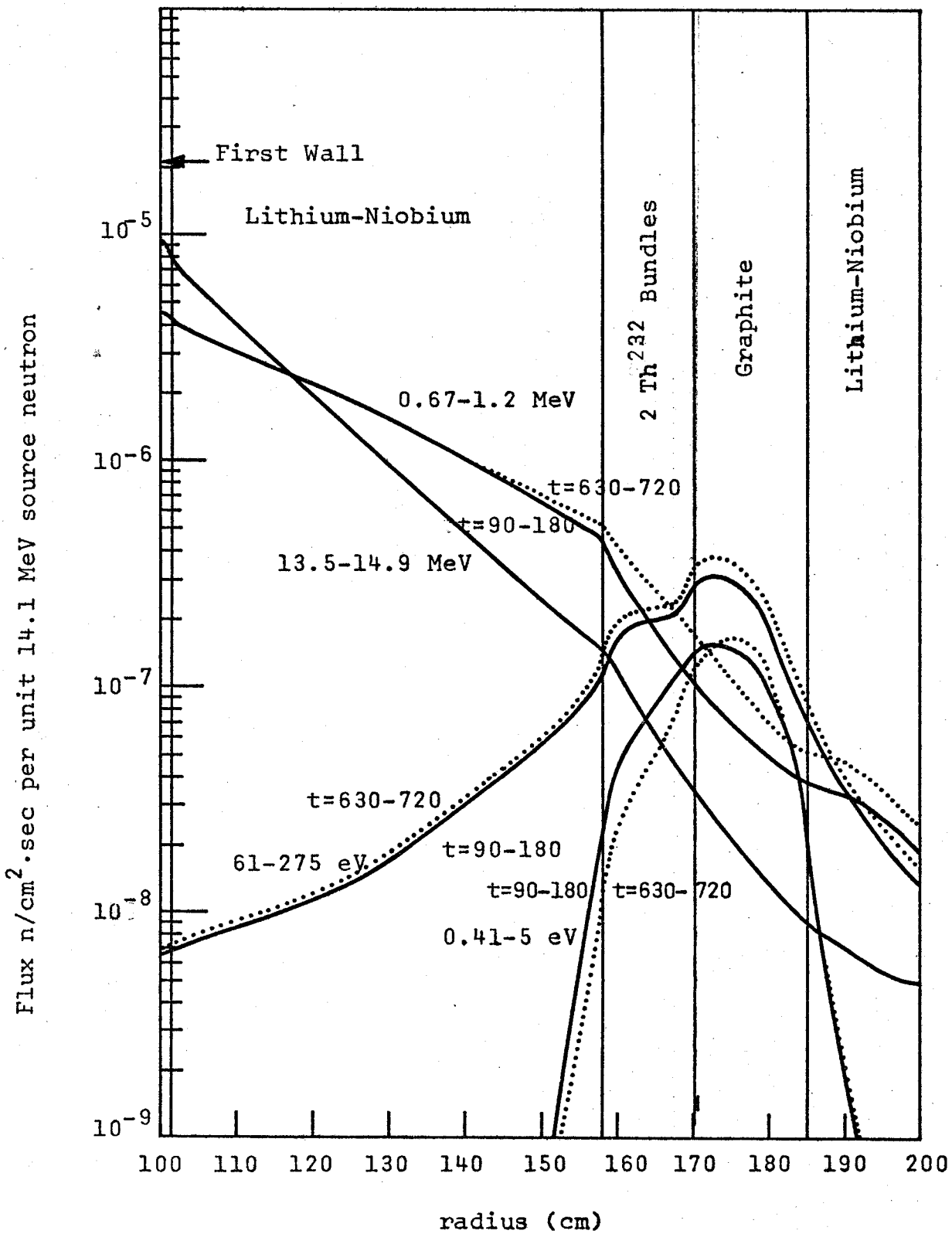

Figure 19 Flux Spectra: Spherical Design 2

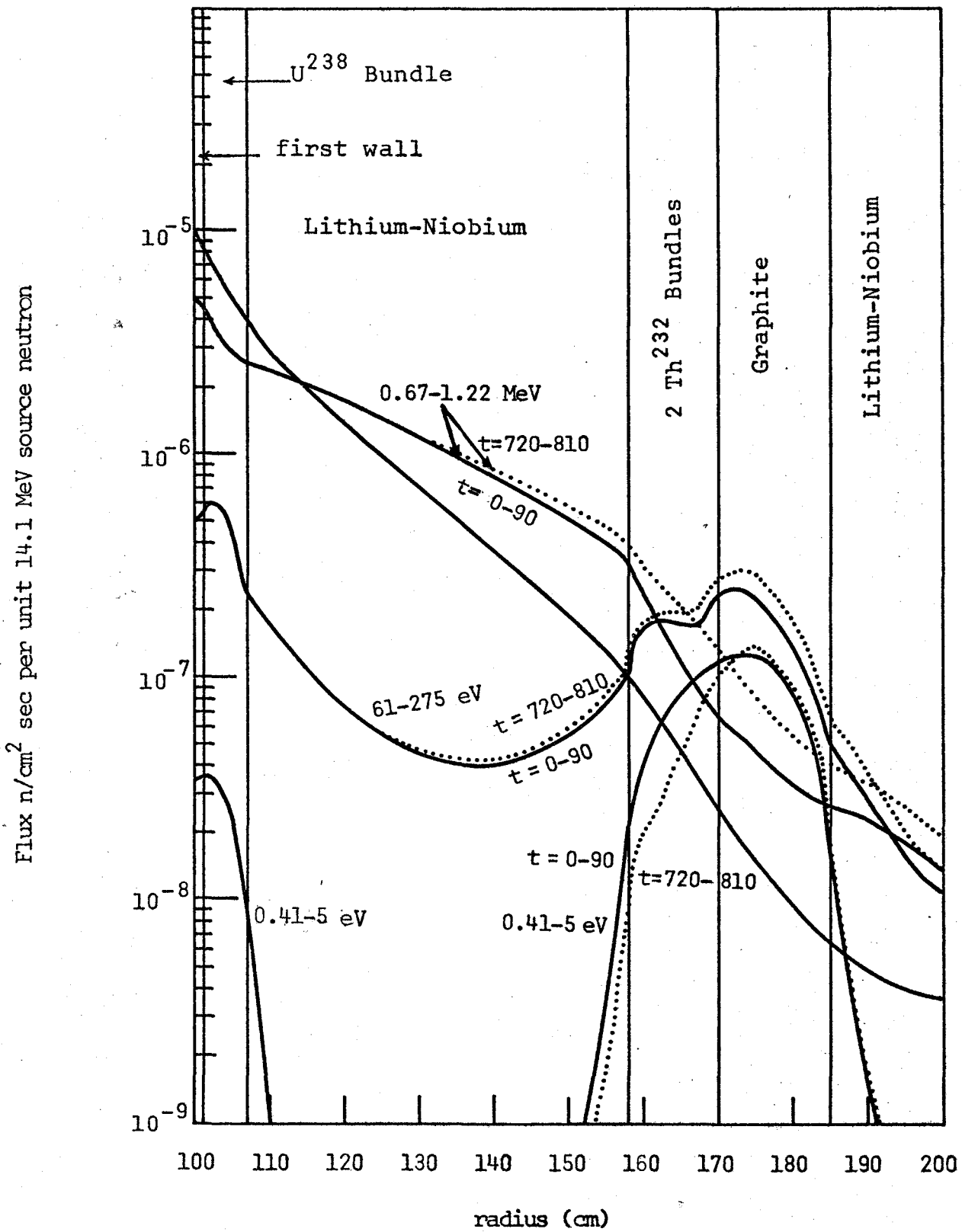

near to a moderating region on the right (graphite). This displays the 1/v variation of $Li^6(n,\alpha)T$ cross section at lower energies. Having bundles on the right instead of the left of the main breeding region benefits T_7 because of its dependence on high energy neutrons. Full evidence of this is seen in Table 6. The addition of the $U^{238}O_2$ bundle in SD2 causes a 42% drop in T_7. The addition of two extra bundles in CD3 from CD2 causes T_7 to drop by 8%.

It should be the case that part of the graphite region can be effectively replaced by bundles. This might be done in cases when the effect of a bundle near the first wall is desired for then the tritium breeding rate could be boosted by creating more breeding volume while retaining the same moderating effects similar to the graphite. In a blanket not designed for energy multiplication, the additional thermal neutrons in the bundles would cause unwanted fissioning at the expense of breeding U^{233}*. This effect can be seen in the thorium reaction rate curves given in Figs. 21-23. In the graph of CD1 Th reaction rates, (n,γ) is definitely less than absorption chiefly because of the higher fission rate. However, in CD2, the curves of absorption and (n,γ) are virtually identical meaning higher breeding efficiency. The addition of more bundles in CD3 does not change CD2 results in this regard a lot, but the fission rate is understandably higher while the average absorption and (n,γ) rates are lower and more separated. The relative magnitude of the (n,3n) reaction should be noted in Fig. 26.

---

* See Fig. 20 for a plot of U^{233}(n,fission) as a function of time.

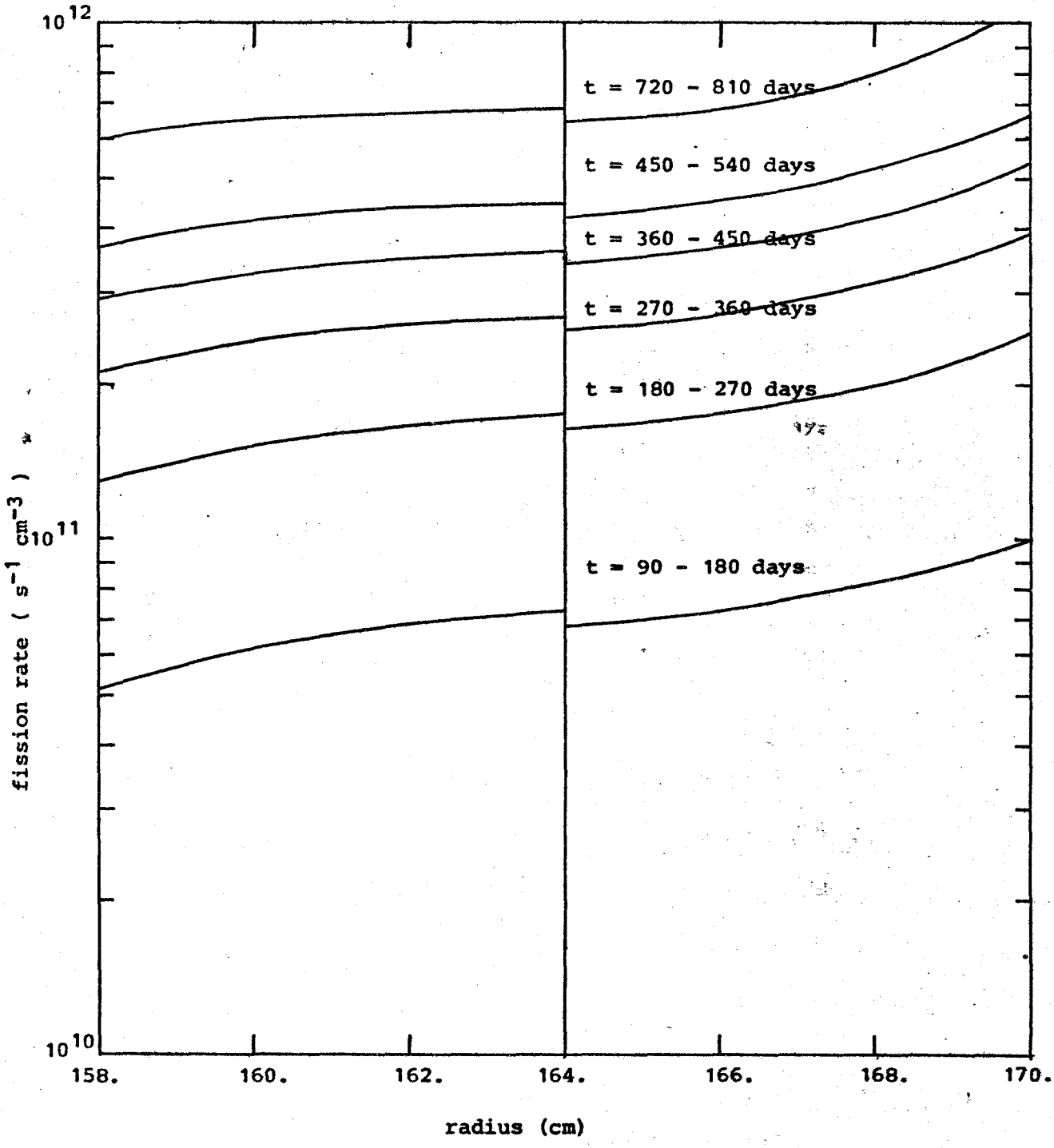

Figure 20 U^{233} fission rate in spherical design 2 . Source is 6.28 10^{19} n/s .

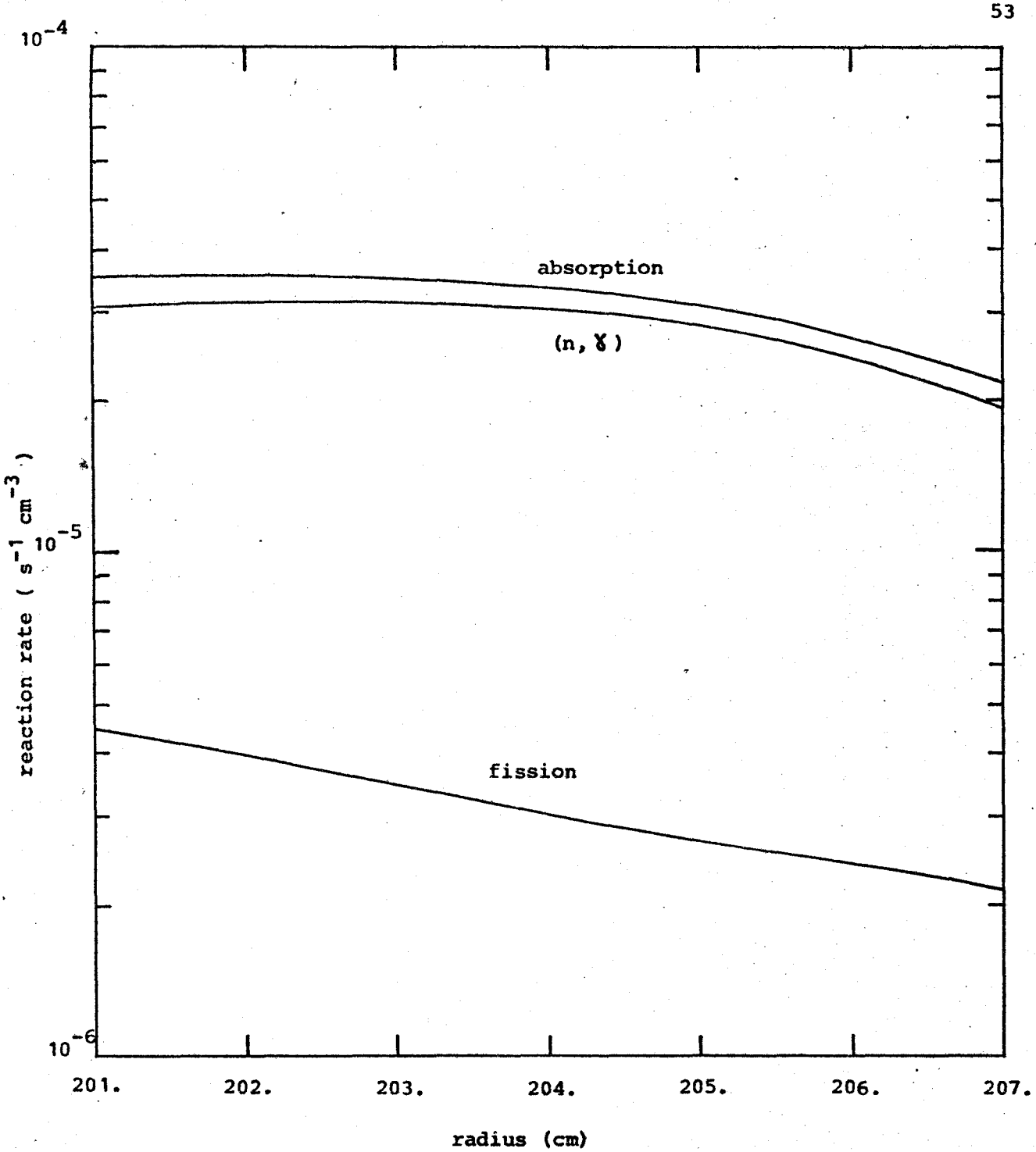

Figure 21 Th^{232} reaction rates in cylindrical design 1

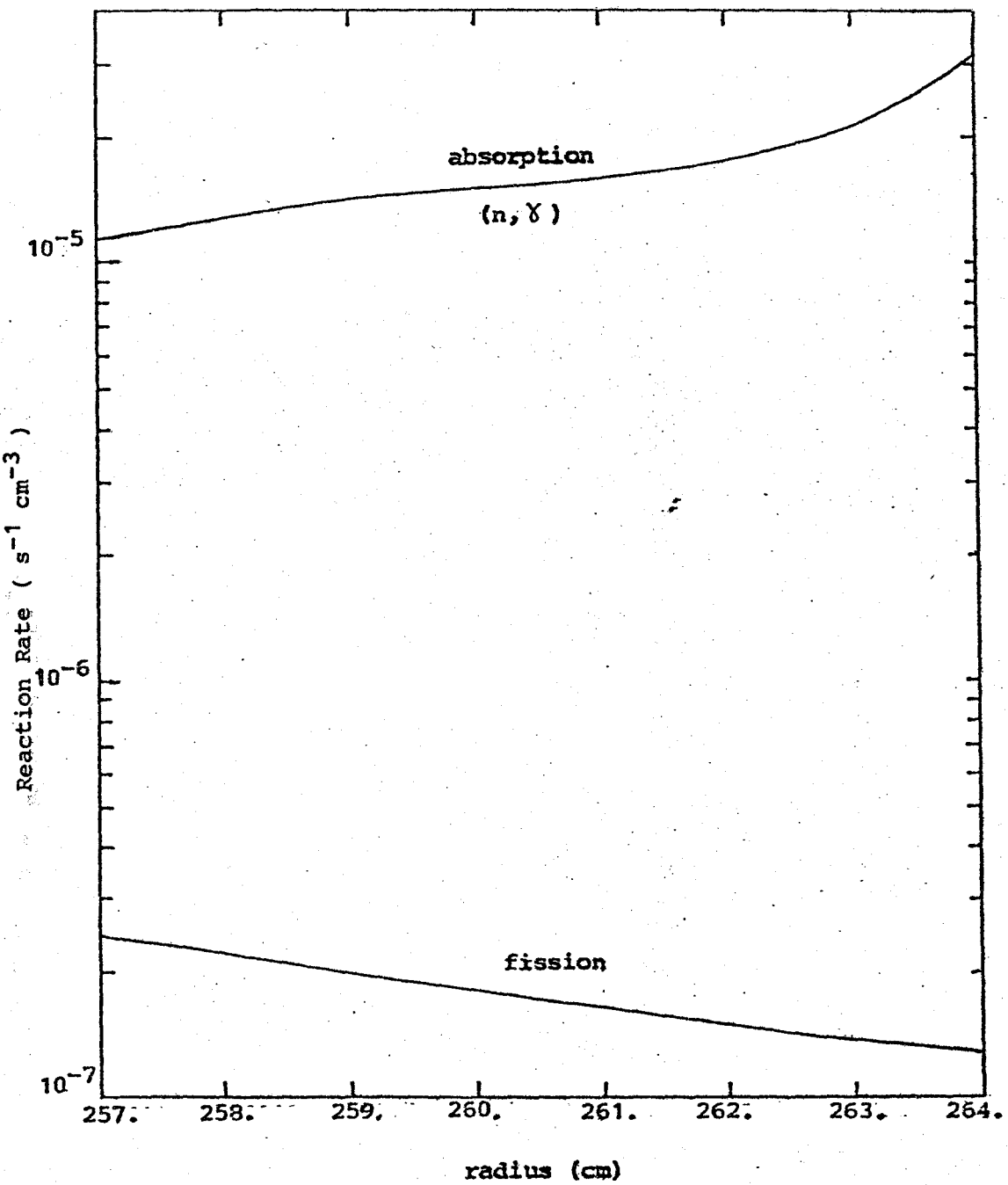

Figure 22 Thorium reaction rates in cylindrical design 2

Figure 23 Cylindrical Design 3: Thorium Reaction Rates in the Bundles

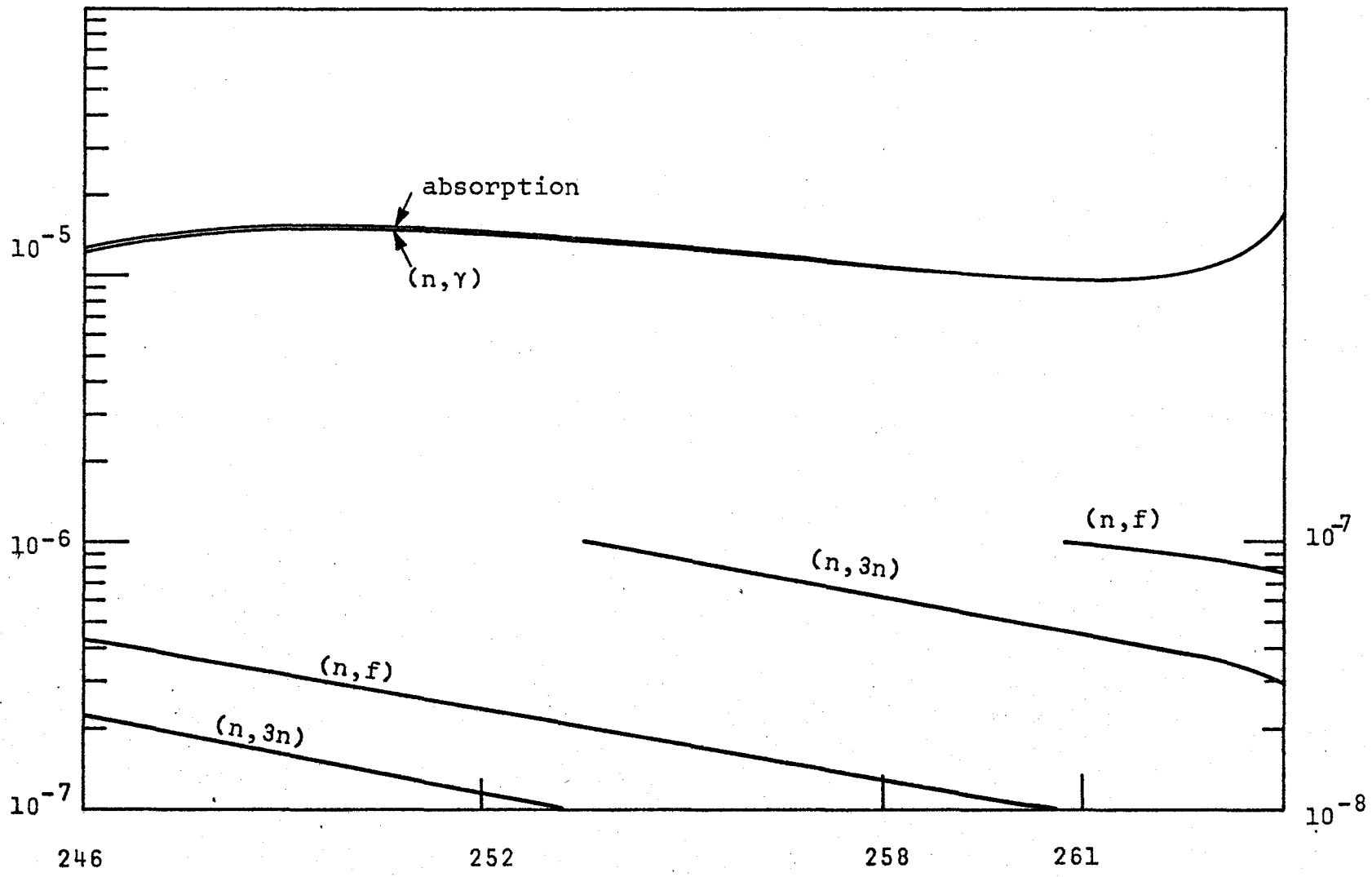

Unfortunately, it did not enter explicitly into the ANISN calculations of the flux. With the bundle positioned as in CD1, the effect should be very significant. Perhaps one of the reasons the CANDU fuel bundle did not turn out to be a good neutron multiplier is that this effect was not taken into account.

First wall reaction rates follow this same pattern. Figures 24,25&26show the niobium reaction rates in CD1,CD2& CD3. (n,2n) is a desirable neutronic characteristic in a first wall and the wall should not remove a large portion of the flux. The presence of the Th bundle next to the first wall causes the absorption to raise significantly until the wall actually becomes a net remover of neutrons for part of its length. Note that the (n,2n) reaction rate does not change perceptibly with this thermalization. Thus, absorption and (n,2n) are not competing reactions in niobium in this case since most of the extra absorption comes from absorbing the backscattered lower energy neutrons from the bundle. See also Tables 8, 9 and 10 showing the spectrum at the first wall for CD3, SD1 and SD2. Note the higher percentages in the lower keV ranges in SD2 due to inelastic collisions in the U^{238}.

Table 11 shows the effect of a finite geometry (buckling correction) and void correction (both are options with ANISN) on CD3. Listed are the discouraging breeding rates as well. The finite cylinder lengths were patterned after a design in a paper by Maniscalco, the design being shown in Fig. 12.

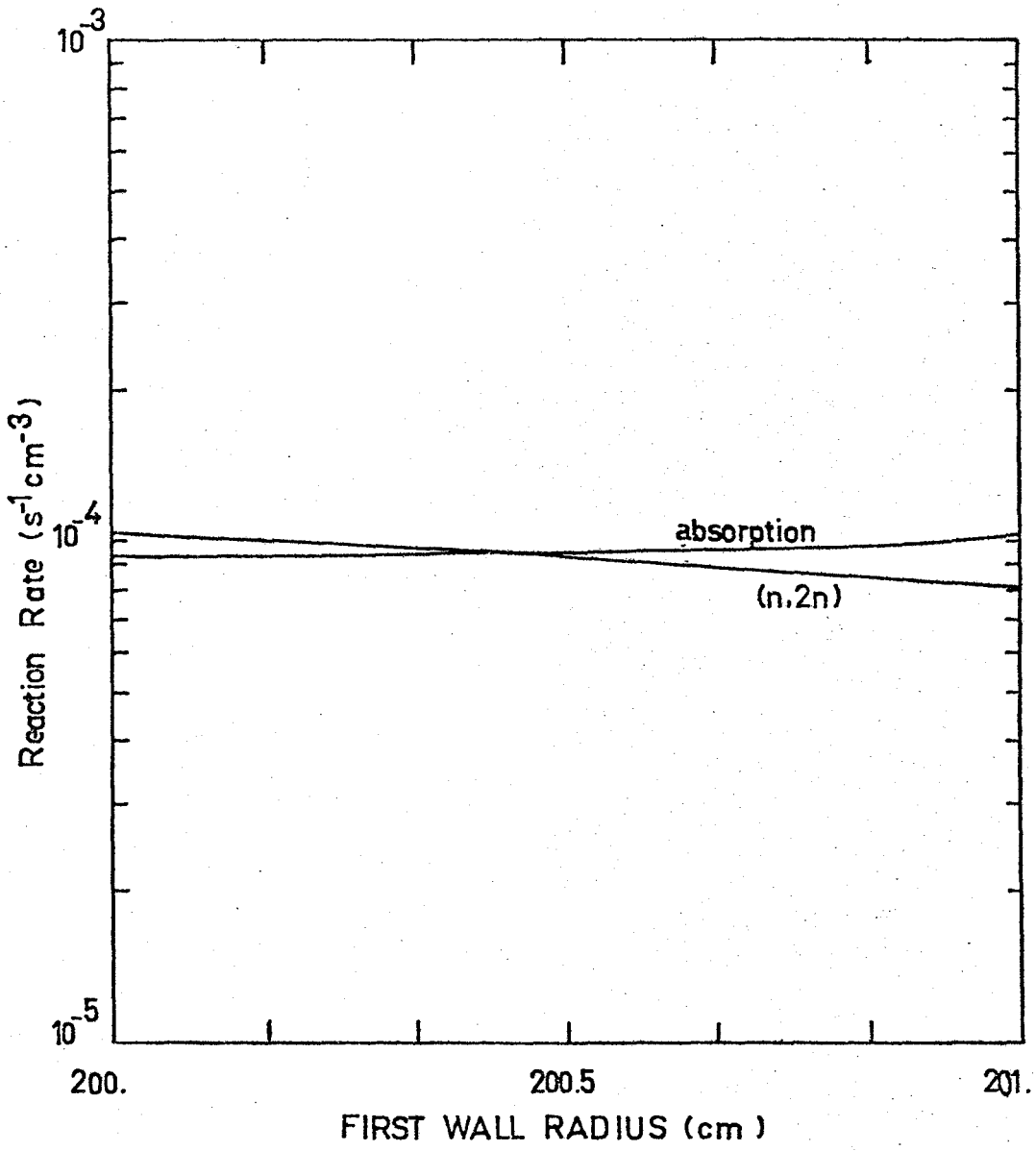

FIG.24 CYLINDRICAL DESIGN 1: NIOBIUM REACTION RATES

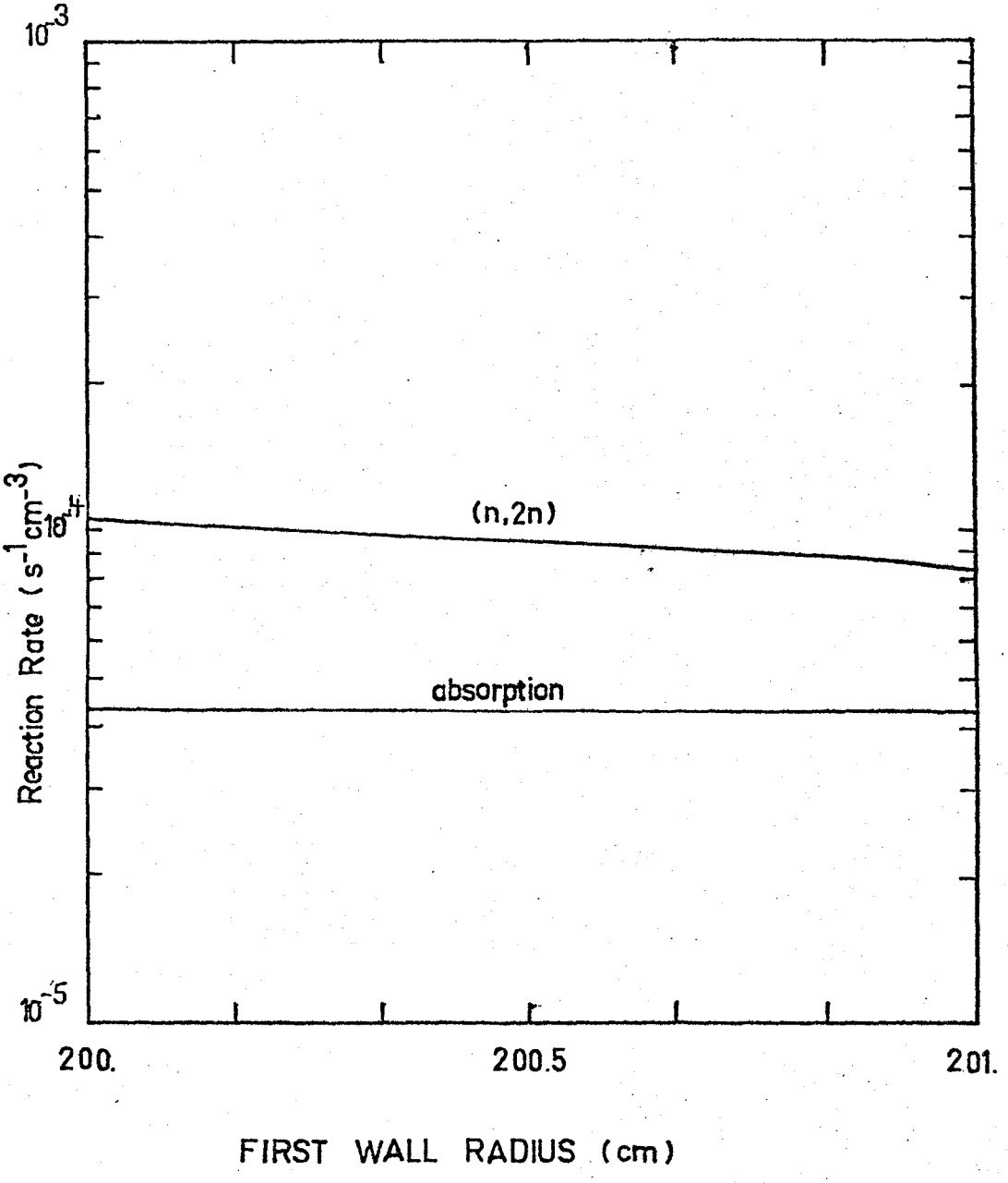

FIG.25 Cylindrical Design 2 : Niobium Reaction Rates

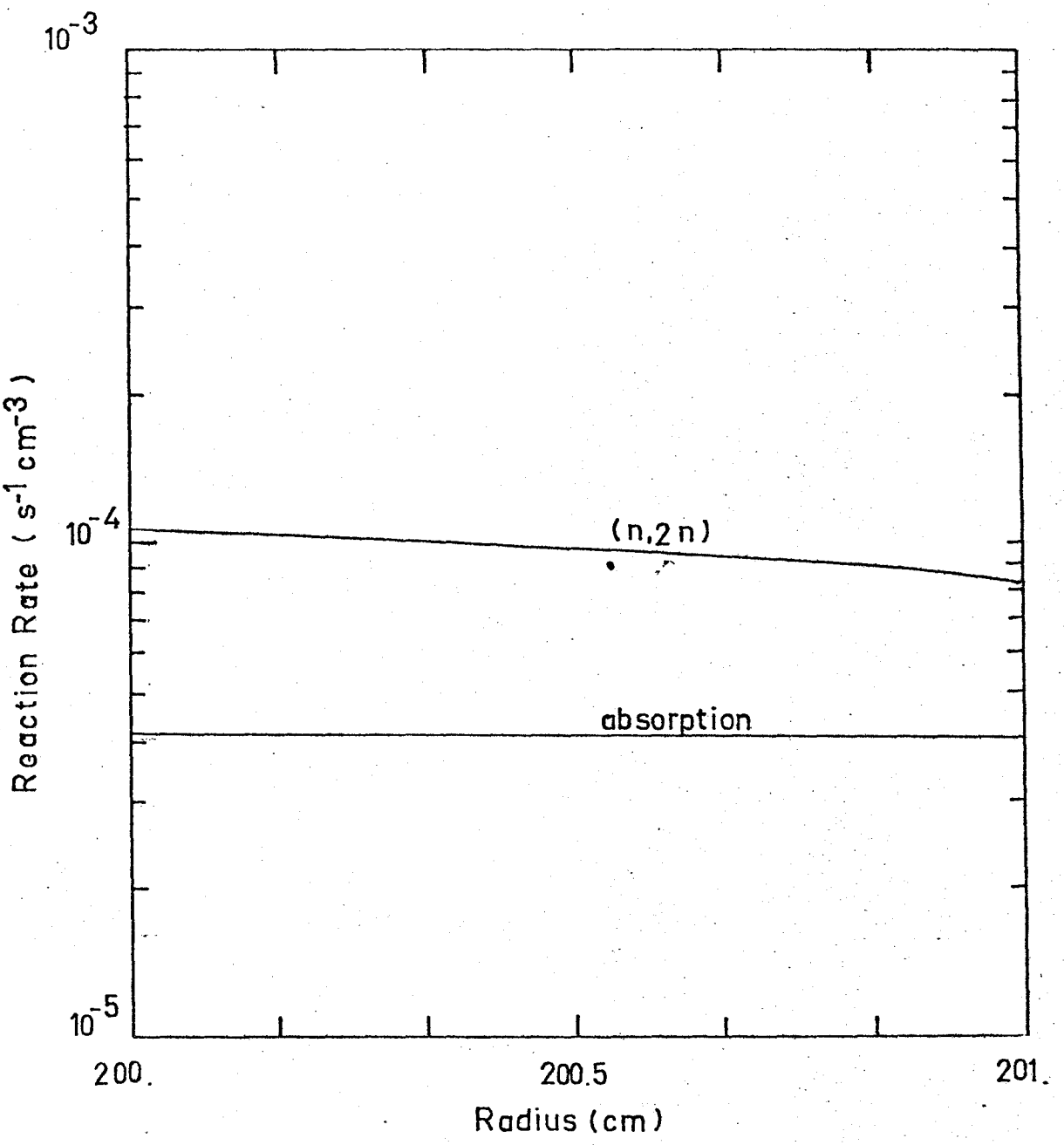

Figure 26 Niobium reaction rates for cylindrical design 3

Groups	% of Flux	Energy Range
1	37.01	13.5 - 14.9 MeV
2	3.00	7.4 - 13.5
3	2.08	4.1 - 7.4
4	2.68	2.2 - 4.1
5	4.62	1.2 - 2.2
6	7.32	0.67 - 1.2
7	9.32	369 - 672 KeV
8	5.08	202 - 369
9	9.56	111 - 202
10	13.09	25 - 111
11	4.77	5.5 - 25
12	1.30	1.2 - 5.5
13	0.16	0.28 - 1.2
14	0.01	61 - 275 eV
15	0.000	5.0 - 61
16	0.000	0.41 - 5.0
17	0.000	thermal

Table 8 Flux spectrum at the first wall for spherical design 1

Groups	% of Flux	Energy Range
1	16.54	13.5 - 14.9 MeV
2	1.98	7.4 - 13.5
3	2.01	4.1 - 7.4
4	3.56	2.2 - 4.1
5	5.71	1.2 - 2.2
6	8.14	0.67 - 1.2
7	8.21	369 - 672 KeV
8	7.83	202 - 369
9	7.61	111 - 202
10	17.27	25 - 111
11	11.39	5.5 - 25
12	6.08	1.2 - 5.5
13	2.42	0.28 - 1.2
14	0.84	61 - 275 eV
15	0.31	5.0 - 61
16	0.06	0.41 - 5.0
17	0.02	thermal

Table 9 Flux spectrum at the first wall for spherical design 2

Groups	% of Flux	Energy Range
1	21.74	13.5 - 14.9 MeV
2	4.22	7.4 - 13.5
3	2.22	4.1 - 7.4
4	3.07	2.2 - 4.1
5	5.79	1.2 - 2.2
6	9.34	0.67 - 1.2
7	11.56	369 - 672 KeV
8	6.23	202 - 369
9	11.34	111 - 202
10	16.36	25 - 111
11	6.16	5.5 - 25
12	1.72	1.2 - 5.5
13	0.23	0.28 - 1.2
14	0.02	61 - 275 eV
15	0.00	5.0 - 61
16	0.00	0.41 - 5.0
17	0.00	thermal

Table 10 Flux spectrum at the first wall for the infinite cylinder

Groups	% of Flux	Energy Range
1	35.28	13.5 - 14.9 MeV
2	5.20	7.4 - 13.5
3	2.74	4.1 - 7.4
4	3.61	2.2 - 4.1
5	6.46	1.2 - 2.2
6	9.31	0.67 - 1.2
7	10.03	369 - 672 KeV
8	4.70	202 - 369
9	7.98	111 - 202
10	10.18	25 - 111
11	3.43	5.5 - 25
12	0.92	1.2 - 5.5
13	0.13	0.28 - 1.2
14	0.02	61 - 275 eV
15	0.001	5.0 - 61
16	0.000	0.41 - 5.0
17	0.000	thermal

Zone	T_6	% of T	T_7	% of T	T	% of T
5	0.0795	18	0.0907	21	0.1702	39
6	0.0847	19	0.0484	11	0.1331	30
7	0.1123	26	0.0100	2	0.1223	28
12	0.0141	3	0.0004	0.1	0.0145	0.3
	0.2906	66	0.1495	34	0.4401	

Table 11 Flux spectrum at the first wall and breeding rates for the finite cylinder calculation. See also Table 6 for comparative breeding rates.

TIME STUDIES

Isotope changes with respect to time were studied for the two spherical designs as well as for CD3. A complete decay chain involving nuclei around Th^{232} is shown in Fig. 27. However, many of these isotopes are not significantly built up over the time steps used in this report (two to three years) and so, to make the study more practical, the following decay chain was studied:

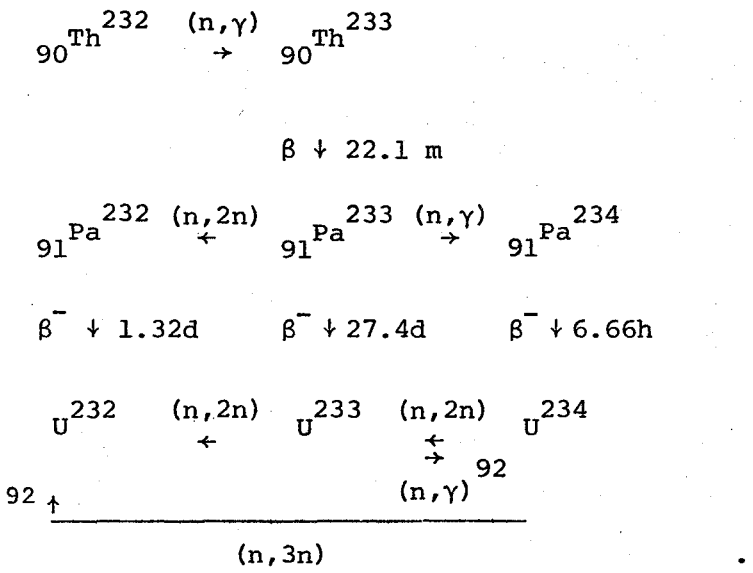

Differential equations were set up and solved analytically to follow the behaviour of Th^{232}, Pa^{233}, U^{233}, and U^{234}.

If $Th^{32}(r,t)$ denotes the concentration of Th^{232} at time t, position r in the blanket, similarly for $Pa^{33}(r,t)$, $U^{34}(r,t)$, and $U^{33}(r,t)$,

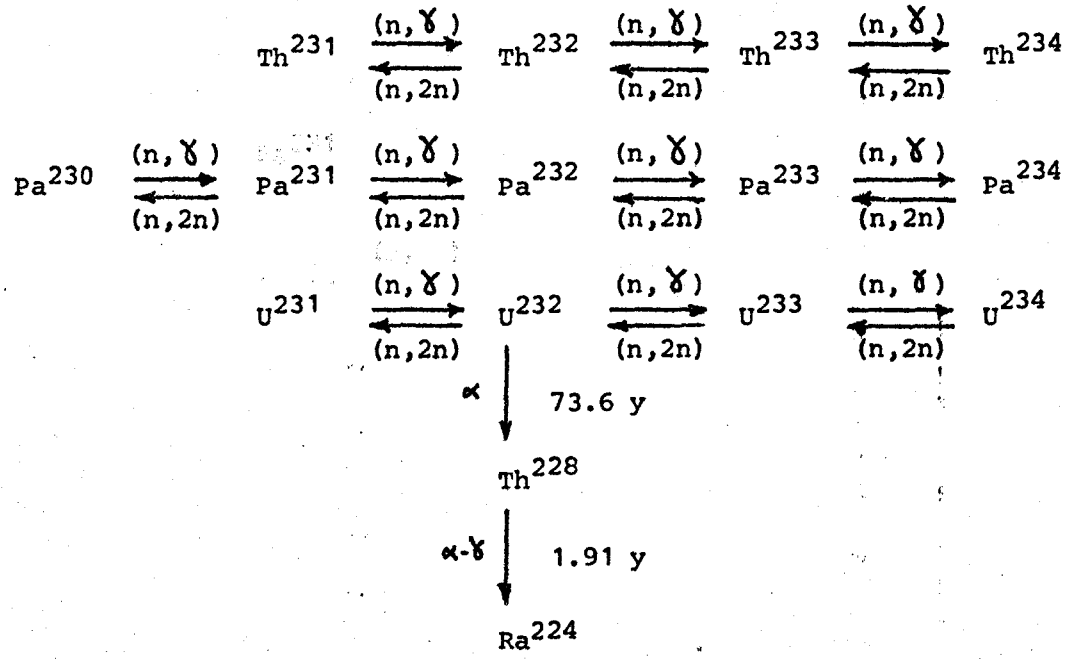

Figure 27 Decay Chain Around Th^{232}

$$\frac{d}{dt} Th^{32}(r,t) = -\int_0^\infty (\sigma^{Th}_{n,\gamma}(E) + \sigma^{Th}_{n,2n}(E) + \sigma^{Th}_{n,3n}(E) + \sigma^{Th}_{f}(E))\phi(r,E,t_0)Th^{32}(r,t)dE \quad *$$

$$\frac{d}{dt} Pa^{33}(r,t) = Th^{32}(r,t) \int_0^\infty \sigma^{Th}_{n,\gamma}(E)\phi(r,E,t_0)dE - Pa^{33}(r,t) \cdot \int_0^\infty (\sigma^{Pa^{33}}_{n,2n}(E) +$$

$$\sigma^{Pa^{33}}_{n,3n}(E) + \sigma^{Pa^{33}}_{n,\gamma}(E) + \sigma^{Pa^{33}}_{f}(E))\phi(r,E,t_0)dE + \frac{1}{\tau_{Pa^{33}}}$$

$$\frac{d}{dt} U^{34}(r,t) = Pa^{33}(r,t) \int_0^\infty \sigma^{Pa^{33}}_{n,\gamma}(E)\phi(r,E,t_0)dE$$

$$- U^{34}(r,t) \int_0^\infty (\sigma^{U^{34}}_{n,2n}(E) + \sigma^{U^{34}}_{n,3n}(E) + \sigma^{U^{34}}_{f}(E) + \sigma^{U^{34}}_{n,\gamma}(E))\phi(r,E,t_0)dE$$

$$+ U^{33}(r,t) \int_0^\infty \sigma^{U^{33}}_{n,}(E)\phi(r,E,t_0)dE$$

$$\frac{d}{dt} U^{33}(r,t) = \frac{Pa^{33}(r,t)}{\tau_{Pa^{33}}} \quad ** + U^{34}(r,t) \int_0^\infty \sigma^{U^{34}}_{n,2n}\phi(r,E,t_0)dE$$

$$- U^{33}(r,t) \int_0^\infty (\sigma^{U^{33}}_{n,2n}(E) + \sigma^{U^{33}}_{n,3n}(E) + \sigma^{U^{33}}_{f}(E) + \sigma^{U^{33}}_{n,\gamma}(E))\phi(r,E,t_0)dE.$$

Note that in order to make a meaningful time study of the nuclide concentrations, values of neutron fluxes actually present in the blanket should be used. The values used in the calculations were based on total neutron source strengths of 4.55×10^{16} n/s per unit length[6] for the cylindrical design and 6.28×10^{19} n/s[6] for the spherical designs. Short lived β-decays of Th^{233} and Pa^{234} were considered instantaneous in the equations above.

---

* *The 't_0' in the above equations reflects the fact that the flux $\phi(r,E,t)$ is assumed constant over a time step t_0 to t_1.*

** $\tau_{Pa^{33}} \equiv$ *mean lifetime of* Pa^{233} *= 39.53 days.*

Figures 28-35 show the distribution of these isotopes in the bundles for SD1 and SD2. The discontinuities at the interface of the bundles are a result of having to volume average the concentration (by interval volume) over each bundle to run ANISN and hence the average concentration for each bundle is different. Also readily noticeable is the higher concentrations in SD1 of all isotopes due to the larger fluxes present.

All of the isotope concentrations increase as radius increases due to the decrease in removal by (n,2n), (n,3n), (n,f) and the thermalizing effect of the bundle and graphite. Shapes of the concentration curves are accentuated in SD2 (notice U^{234}) because of the longer times needed to build up equivalent inventories in the bundles. The Pa^{233} curves are comparatively flat since its source is Th^{232} which stays essentially constant over the bundles and since a large part of the removal of this isotope is by β-decay which is not a function of radius (see $Pa^{33}(r,t)$ eqt^{n}. above). This flatness in the Pa^{233} curve also contributes to the overall flatness of the U^{233} curve for the same reason.* The curve is flatter in SD1 primarily because removal by (n,γ) is not so prevalent (see figs. 1-4 for cross-section plots). On the other hand, Pa^{233} contributes to U^{234} buildup only through an (n,γ) reaction** which is preominantly a lower energy reaction. Thus, the contribution from Pa^{233} also leads to a flattening of the curve in SD2. The larger variation in the U^{234} curve in SD1 is due to increased dependence on $U^{233}(n,\gamma)$ for its existence.***

---

* *It must be remembered that these plots use a logarithmic scale for the ordinate and so flatness is accentuated. For a better idea of shapes, see figs. 36 and 37.*

** *The mean lives of Th^{233} and Pa^{234} were considered short enough for the time steps used that production of Pa^{233} was assumed to be by $Th^{232}(n,\gamma)$ and production of U^{234} was contributed to by $Pa^{233}(n,\gamma)$. See decay chains above.*

*** *U^{233} concentration varies much more through the bundles than does Pa^{233} concentration.*

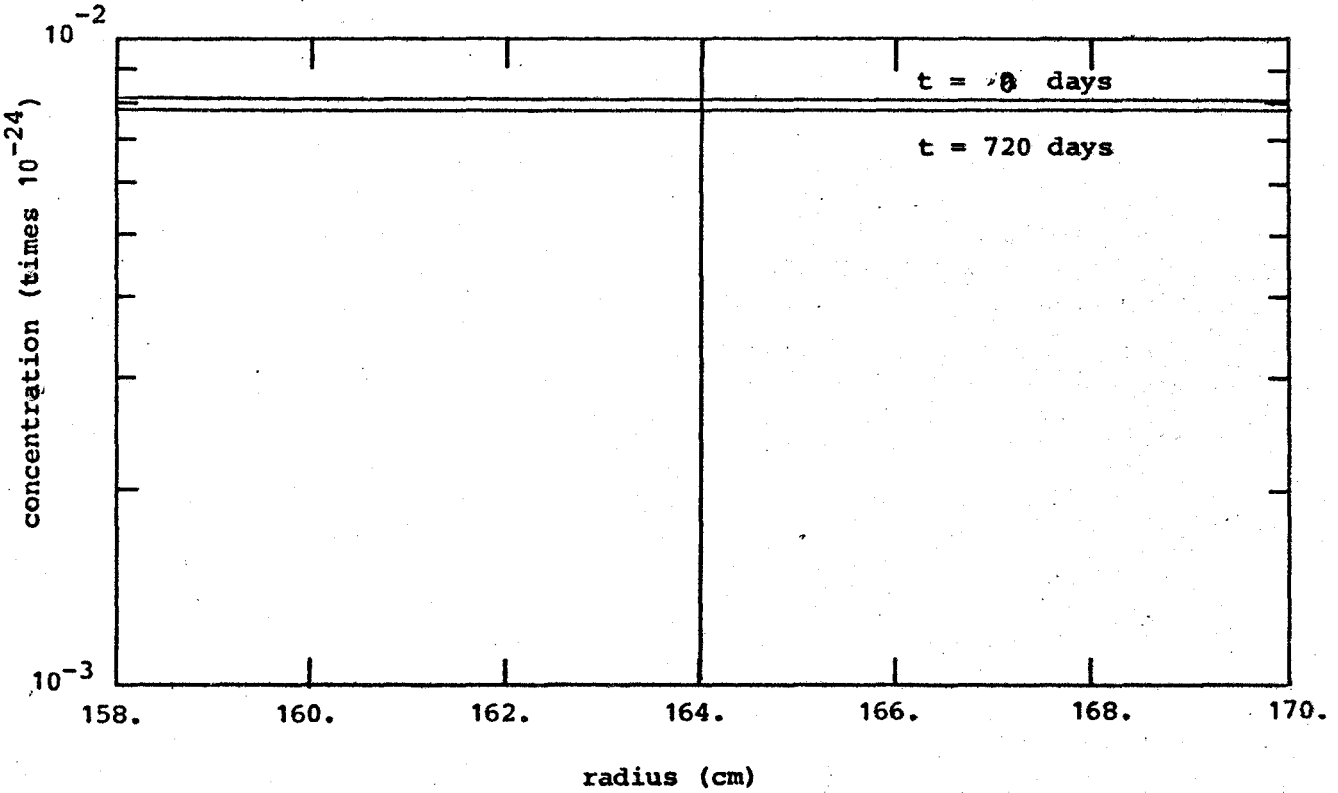

Figure 28 Th^{232} distribution in the bundles in spherical design 1

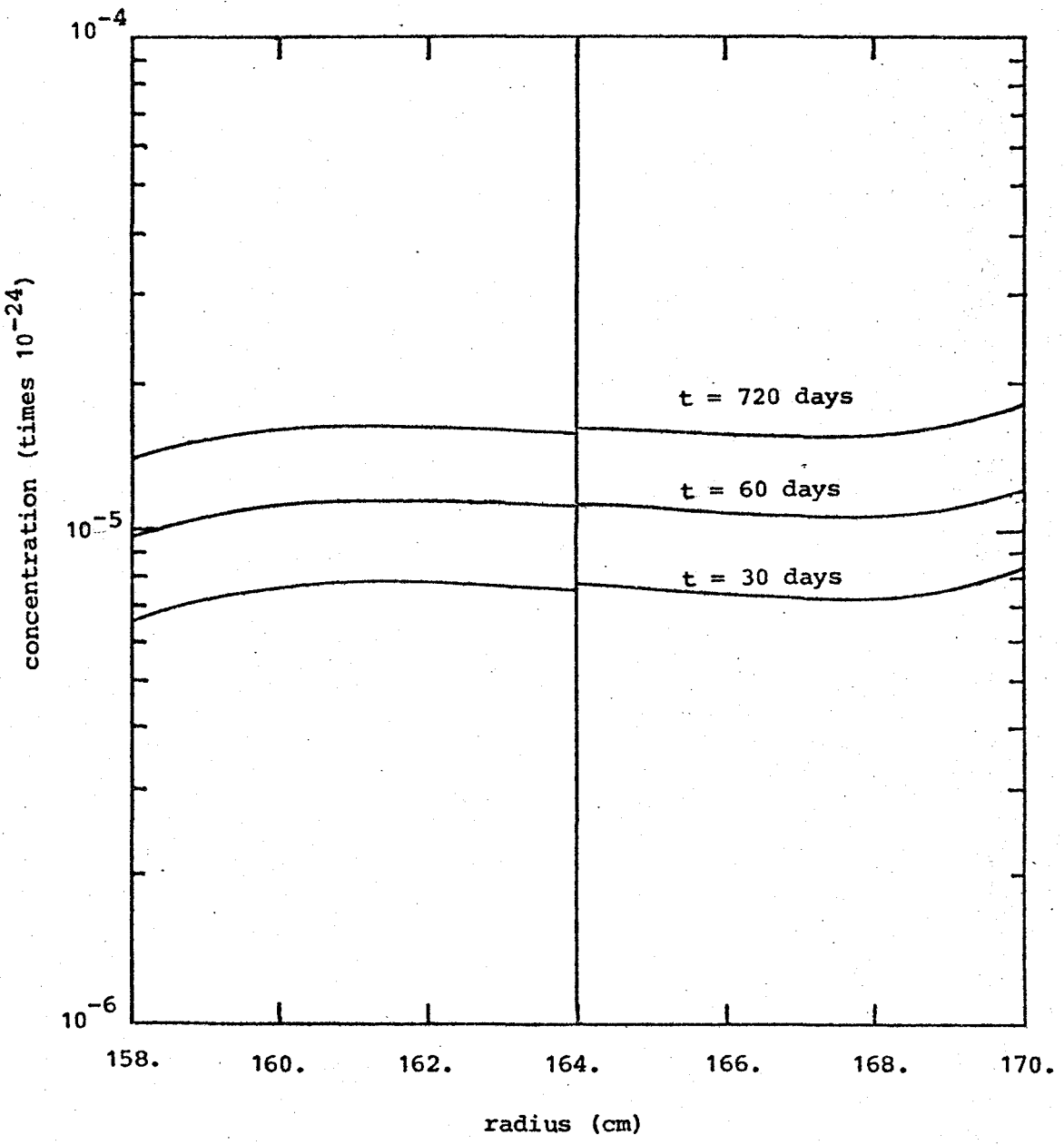

Figure 29 Pa^{233} distribution in the bundles in spherical design 1

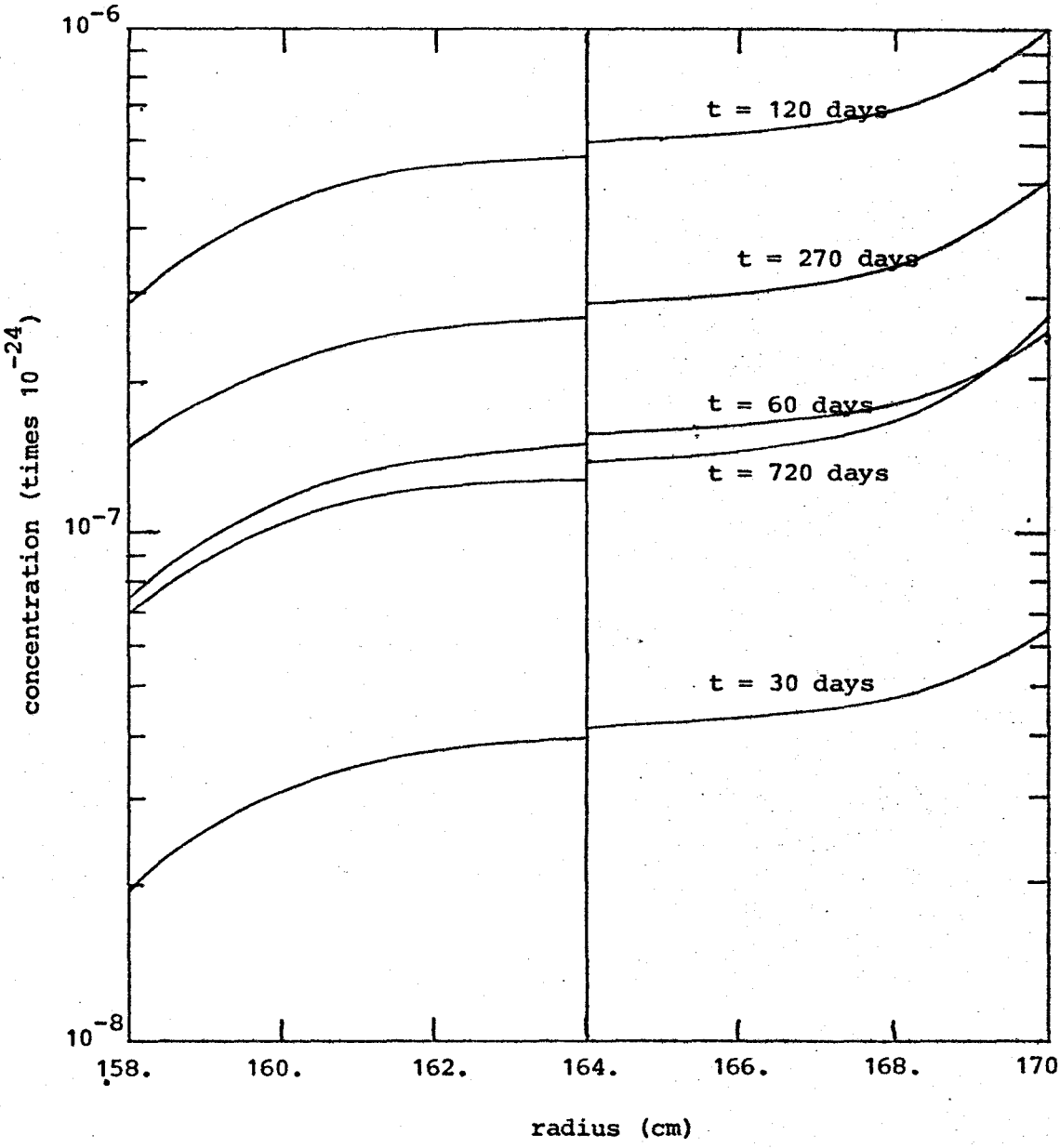

Figure 30 U^{234} distribution in the bundles in spherical design1

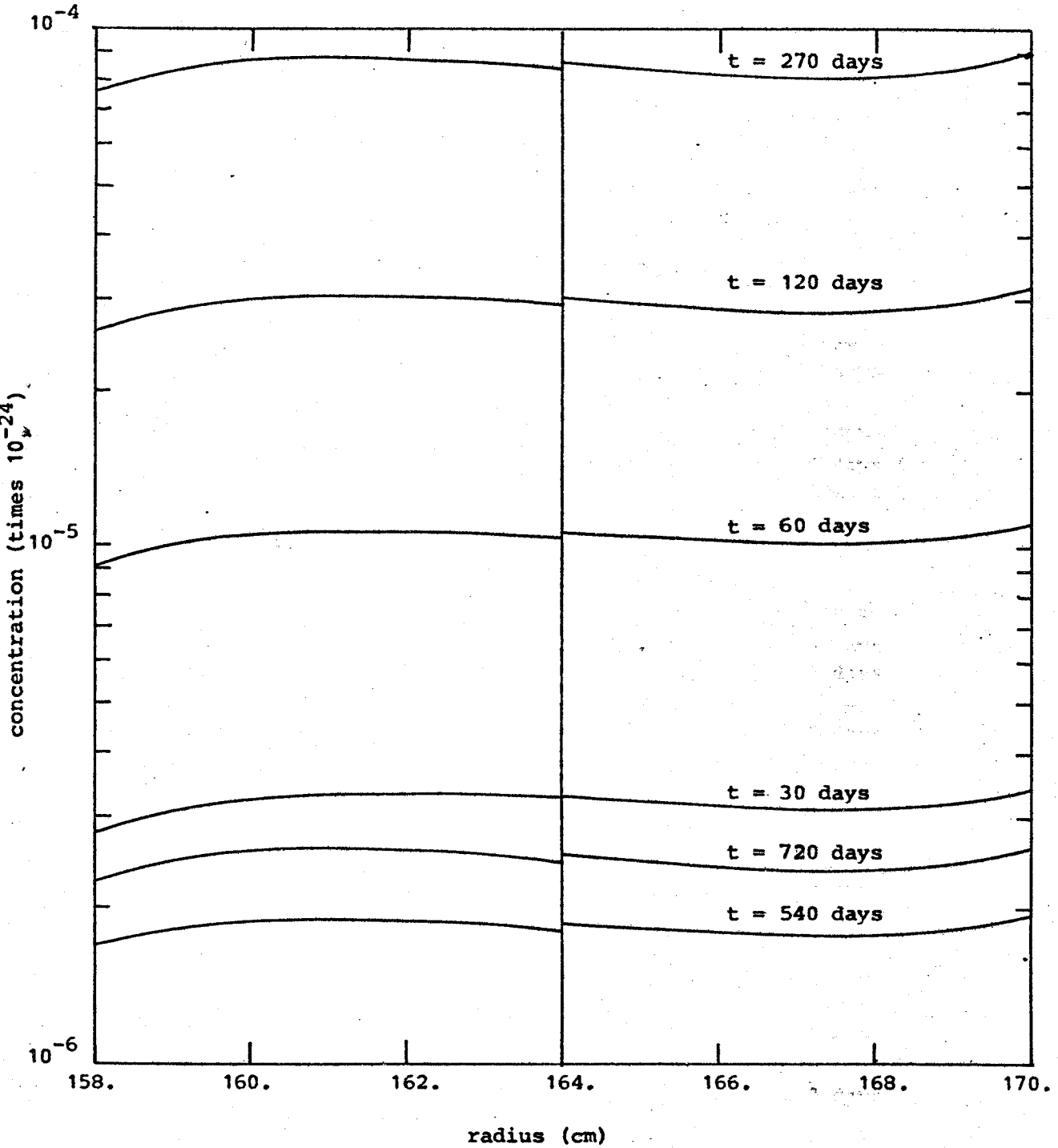

Figure 31 U^{233} distribution in the bundles of spherical design 1

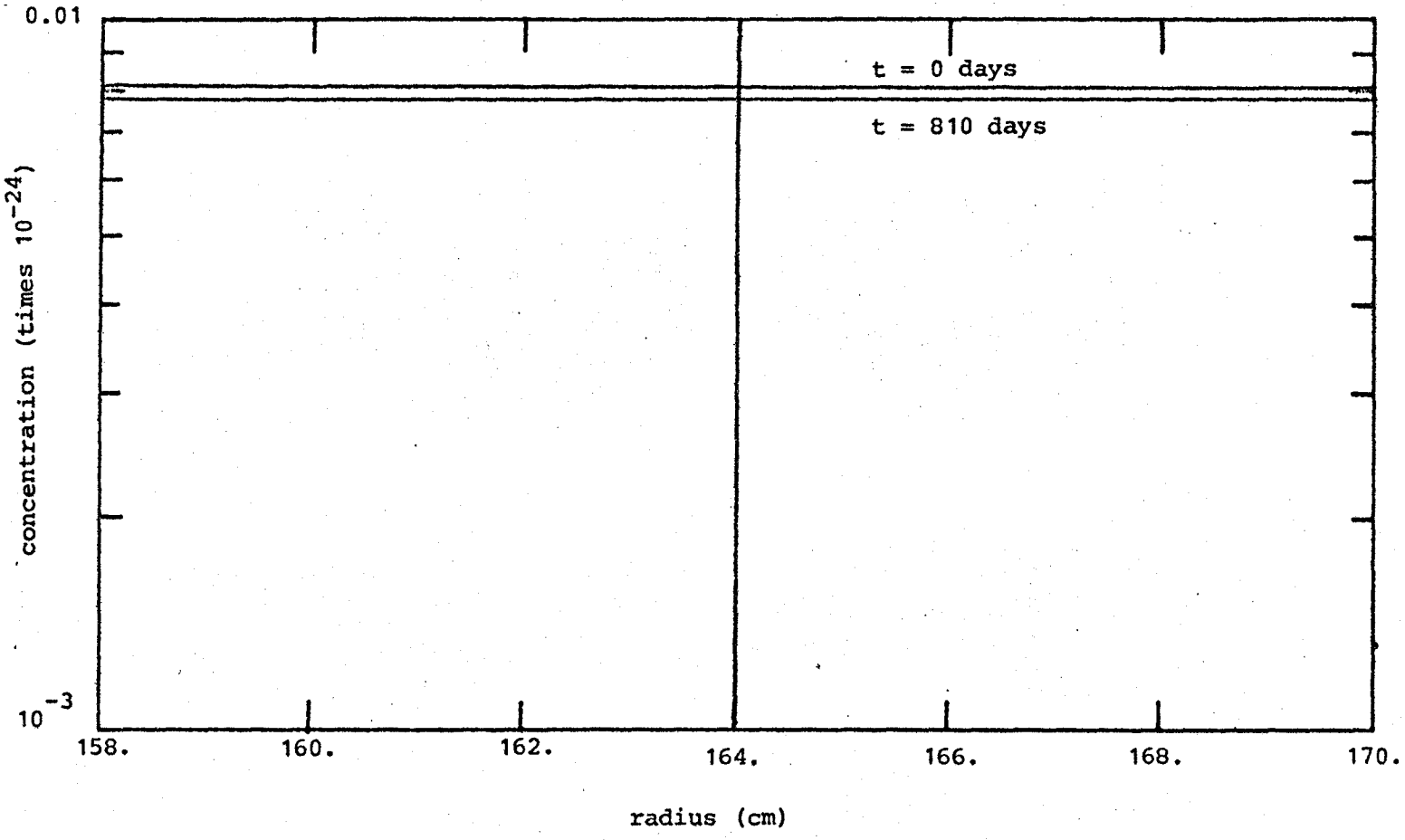

Figure 32 Th^{232} distribution in the bundles in spherical design 2

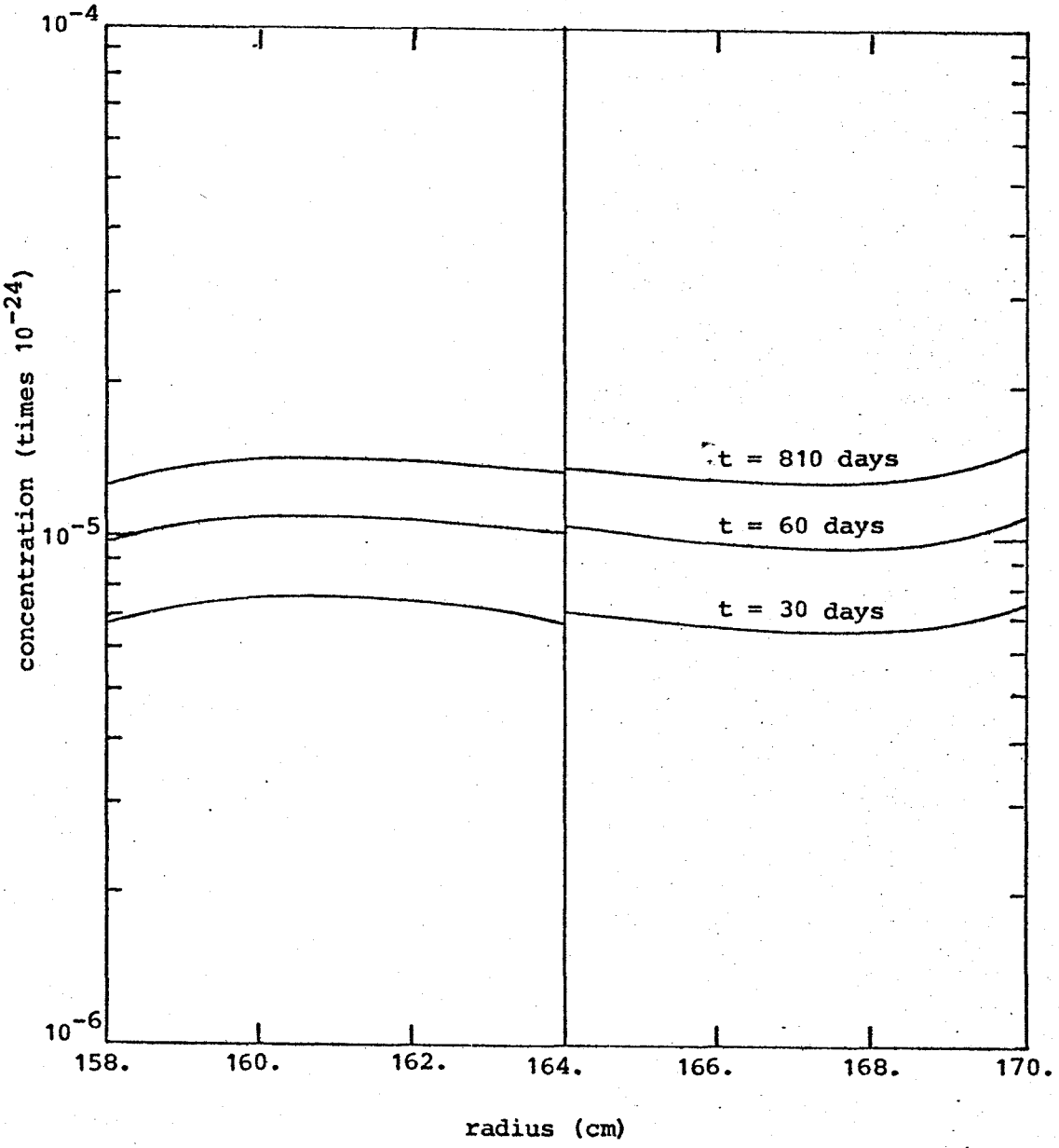

Figure 33 Pa^{233} distribution in the bundles in spherical design 2

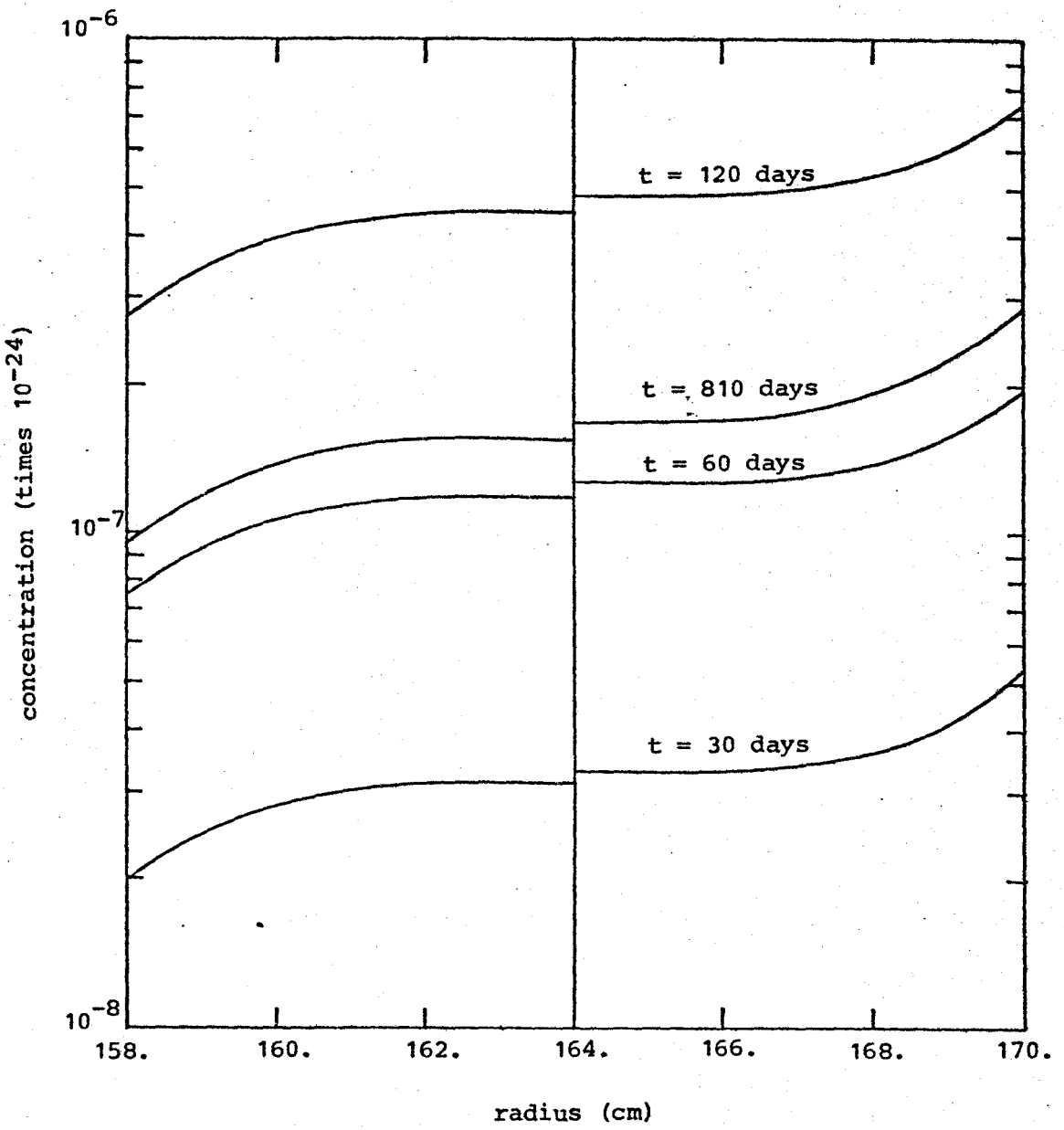

Figure 34 U^{234} distribution in the bundles in spherical design 2

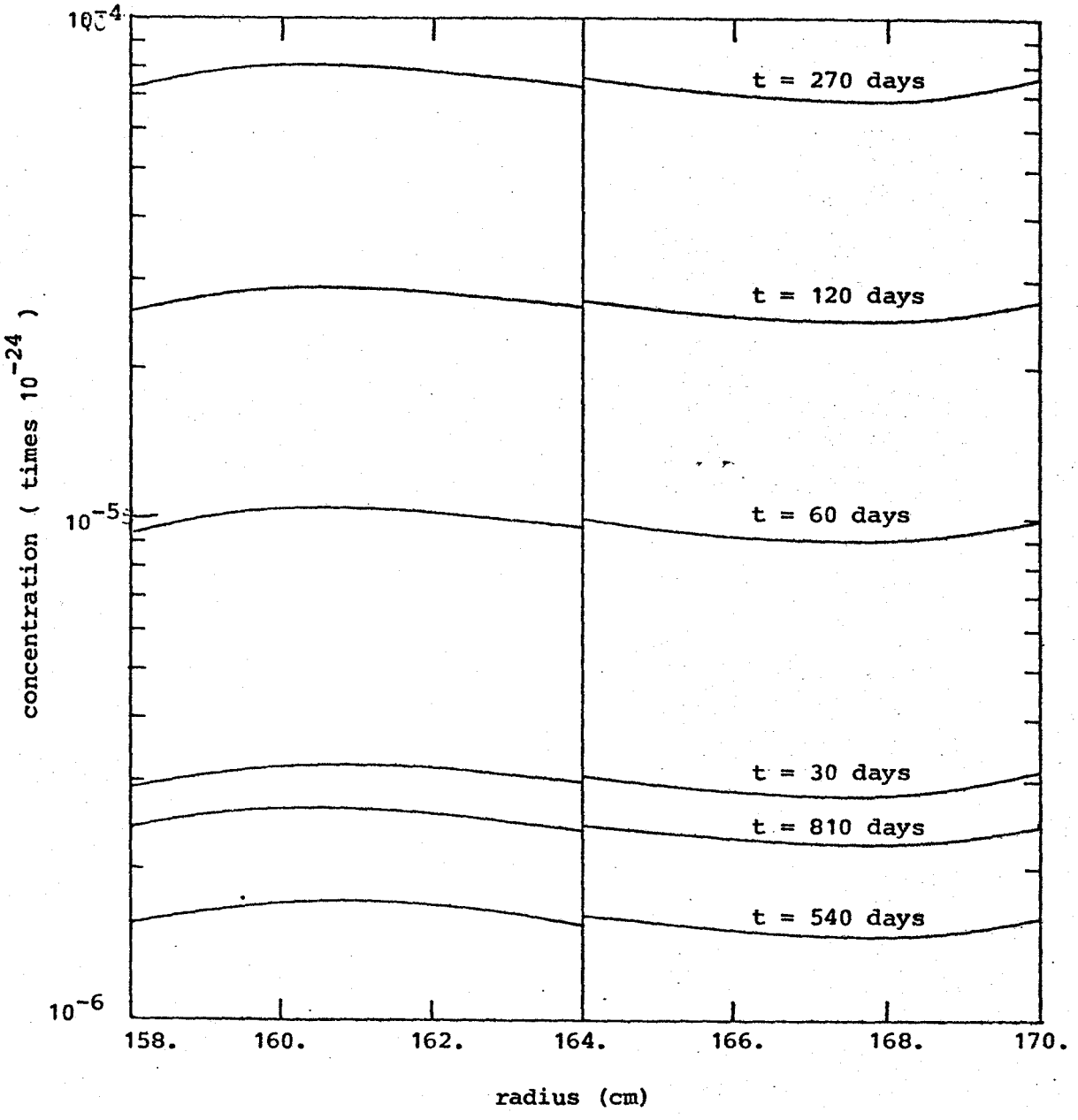

Figure 35 U^{233} distribution in the bundles in spherical design 2

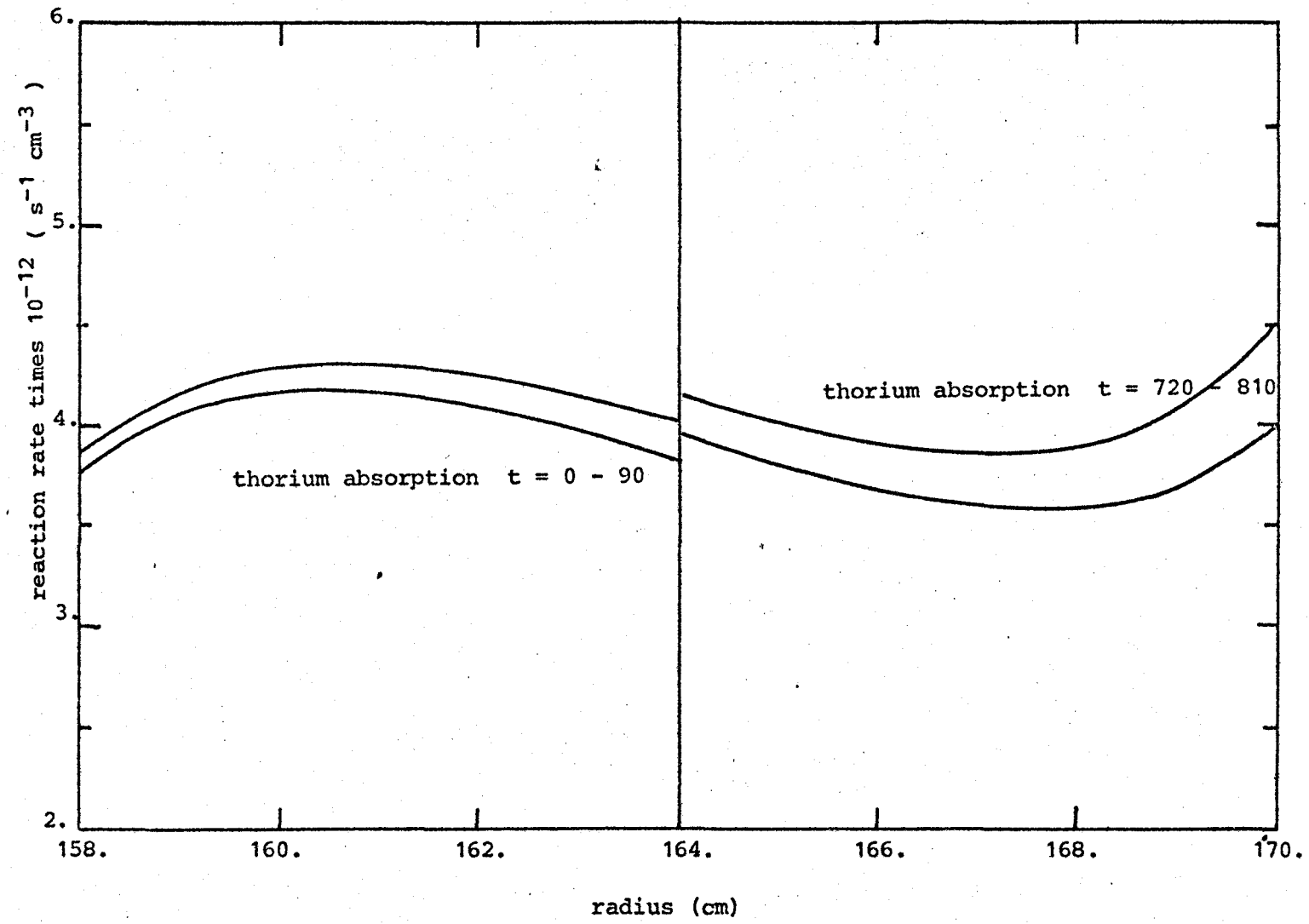

Figure 36 Th^{232} absorption in the bundles in spherical design 2

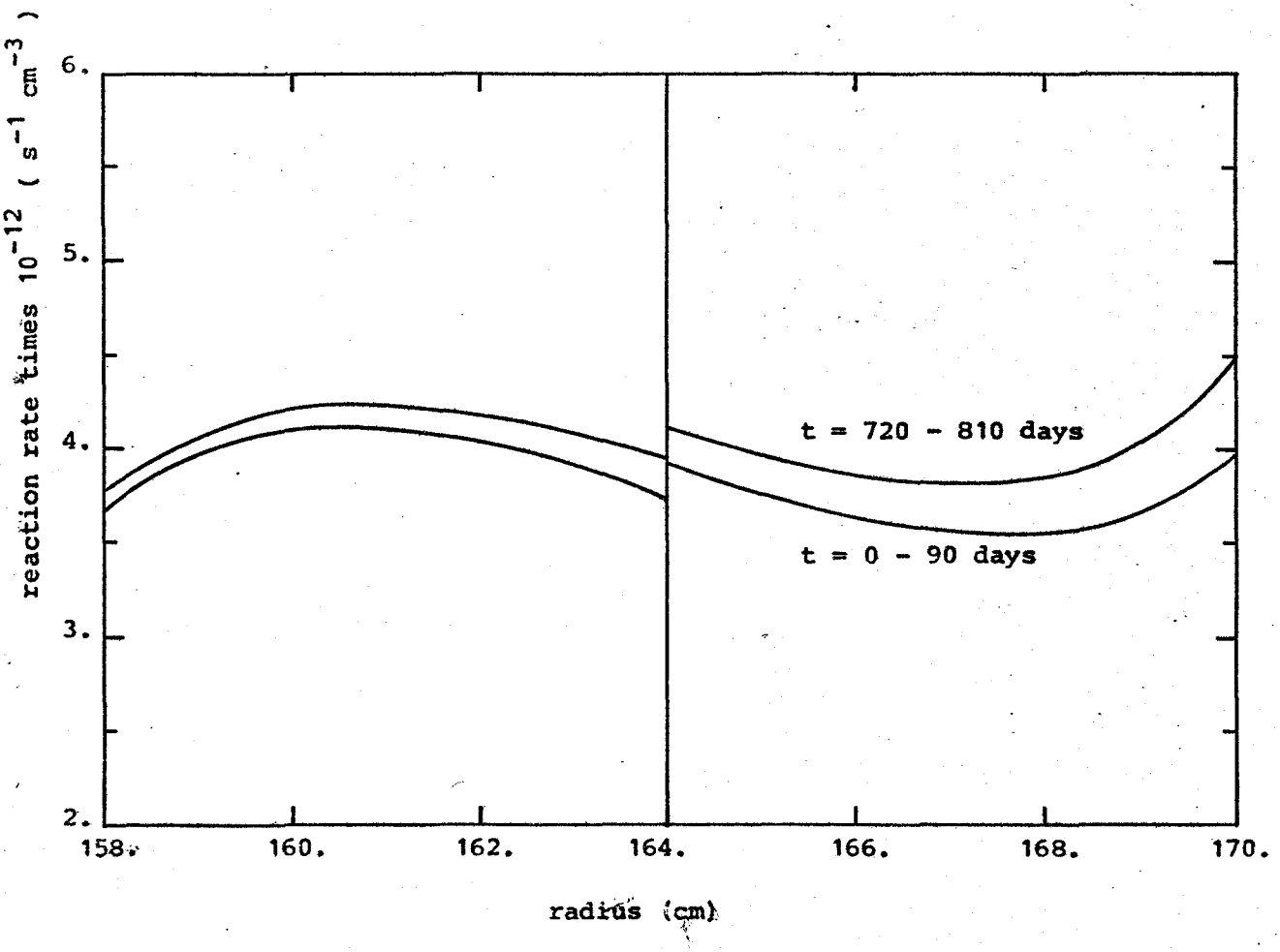

Figure 37 Th^{232} (n,γ) in the bundles in spherical design 2

The higher overall energy of the spectrum in SD1 has the disadvantage of contributing to U^{232} production via $Pa^{233}(n,2n)Pa^{232} \xrightarrow{\beta^-} U^{232}$ as well as the $U^{233}(n,2n)$ reaction. The $U^{233}(n,2n)$ reaction rate is given in Fig. 38.* As expected, the design with the extra U^{238} bundle yields less U^{232}. Differences of these two reaction rates between SD1 and SD2 are approximately 20% in the first bundle and approximately 25% in the second bundle. (A measure of the effect that the $U^{238}O_2$ bundle has on the total system is to compare the total absorption for the systems as calculated by ANISN. For a unit 14.1 MeV neutron source, SD1 absorbs 1.37 neutrons while SD2 absorbs 1.71 neutrons with a difference of 20%. Differences such as these are significant when dealing with the radioactive isotope U^{232}. These calculations were made with the U^{233} concentration approximately 3% of the initial Th concentration.)

Comparison of the times for U^{233} concentration to reach approximately 3% of initial Th concentration is given in Tables 12,13,14 for CD3, SD1 and SD2 respectively. The values for CD3 are for an infinite cylinder and the source chosen was probably not representative of a typical source for this configuration.** The source used in the SD1 and SD2 calculations was 6.28×10^{19} n/sec. This was obtained from a paper by Booth[5]. A value for a pellet design of approximately the same dimensions was given by Steiner as 4.2×10^{19} n/sec which is a 33% difference. These differences mean that figures obtained in this report are only ball park figures and good only for studying overall behaviour rather than specific magnitudes. Times for U^{233} concentration to reach approximately 3% of initial Th concentration were 720 and 810 days for SD1 and SD2 respectively. The difference is 11%.*** U^{233}, U^{234} and Pa^{233} production for the system is given in Figs. 39-41.

* *Because of the overall higher concentration of U^{233} with time, this will be the main contributor to U^{232}* buildup.

** The source was based on reference designs given in ref. 6.

*** Difference in overall absorption for the two systems was 20%.

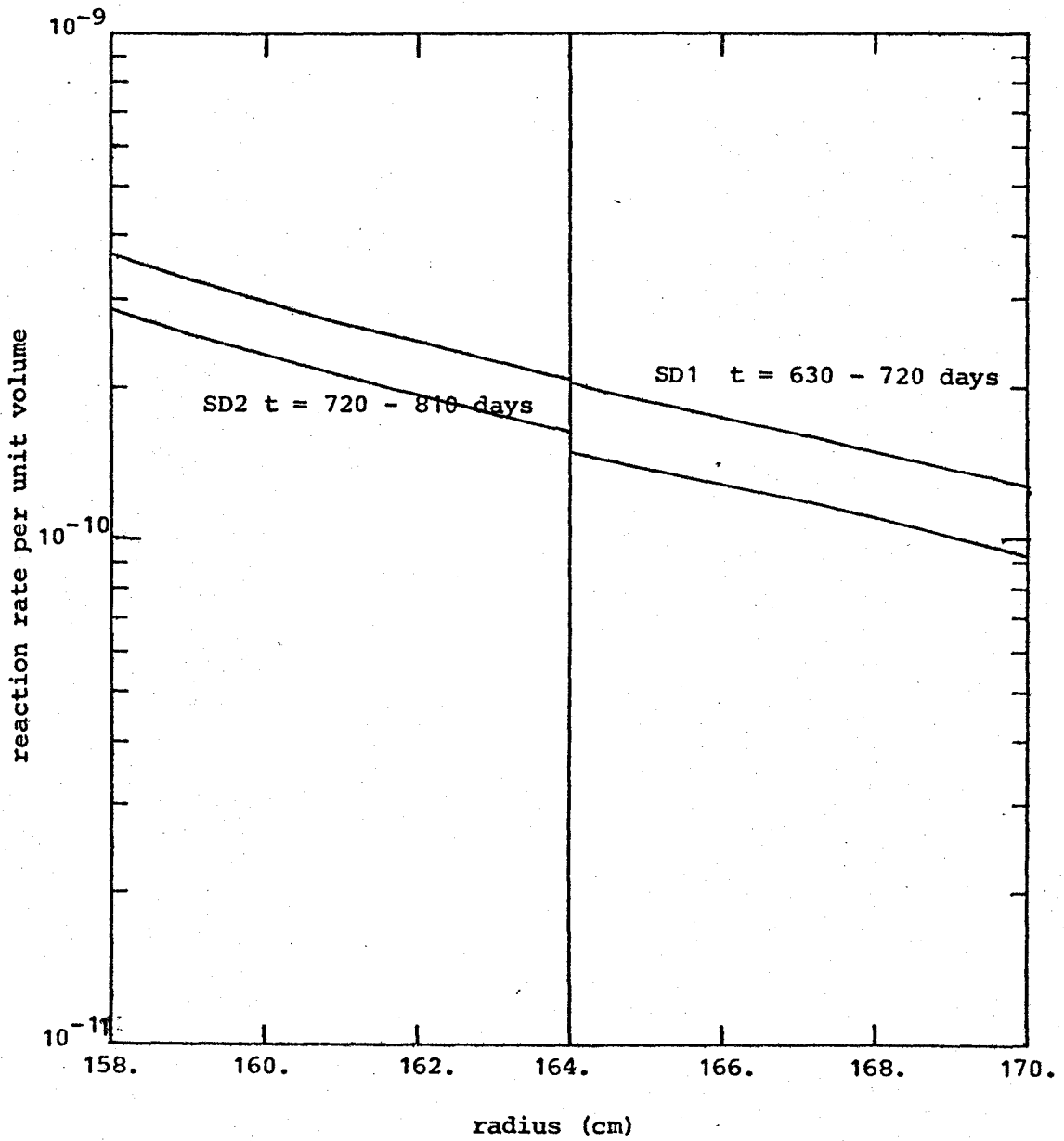

Figure 38 Comparison of $U^{233}(n,2n)U^{232}$ in SD1 and SD2

Time	Th^{232}	Pa^{233}	U^{234}	U^{233}	% Loss
0	100.	0.	0.	0.	0.
360	99.75	0.03	0.001	0.20	0.02
720	99.50	0.03	0.005	0.43	0.04
1080	99.25	0.03	0.01	0.67	0.05
1440 (3.94 yrs)	98.99	0.03	0.02	0.90	0.07

source = 4.55 10^{16} n / cm - s (LFTF, Maniscalco [6])

Table 12 Percentage of initial thorium inventory for infinite cylinder design 3.

Time (days)	Th^{232}	Pa^{233}	U^{234}	U^{233}	% Loss
0	100.	0.	0.	0.	0.
90	99.57	0.16	0.004	0.240	0.026
180	99.11	0.19	0.02	0.63	0.06
270	98.64	0.19	0.03	1.05	0.09
360	98.16	0.19	0.06	1.46	0.13
450	97.68	0.19	0.09	1.87	0.17
540	97.20	0.20	0.13	2.27	0.21
630	96.72	0.20	0.17	2.67	0.24
720 (1.97 yrs)	96.23	0.20	0.22	3.07	0.29

source = $6.28\ 10^{19}$ n/s (Booth [3], Steiner [4])

Table 13 Percentage of initial thorium inventory in spherical design 1

Time (days)	Th^{232}	Pa^{233}	U^{234}	U^{233}	% Loss
0	100.	0.	0.	0.	0.
90	99.61	0.14	0.003	0.22	0.02
180	99.22	0.16	0.01	0.57	0.05
270	98.82	0.16	0.03	0.92	0.07
360	98.43	0.16	0.05	1.28	0.09
450	98.02	0.16	0.07	1.63	0.12
540	97.61	0.17	0.10	1.98	0.15
630	97.21	0.17	0.13	2.32	0.18
720	96.80	0.17	0.16	2.67	0.21
810 (2.2 yrs)	96.38	0.17	0.20	3.00	0.25

source = 6.28 10^{19} n/s (Booth), Steiner [4])

Table 14 Percentage of initial thorium inventory in spherical design 2

Figure 39 Cylindrical Design 3: Isotope Inventories

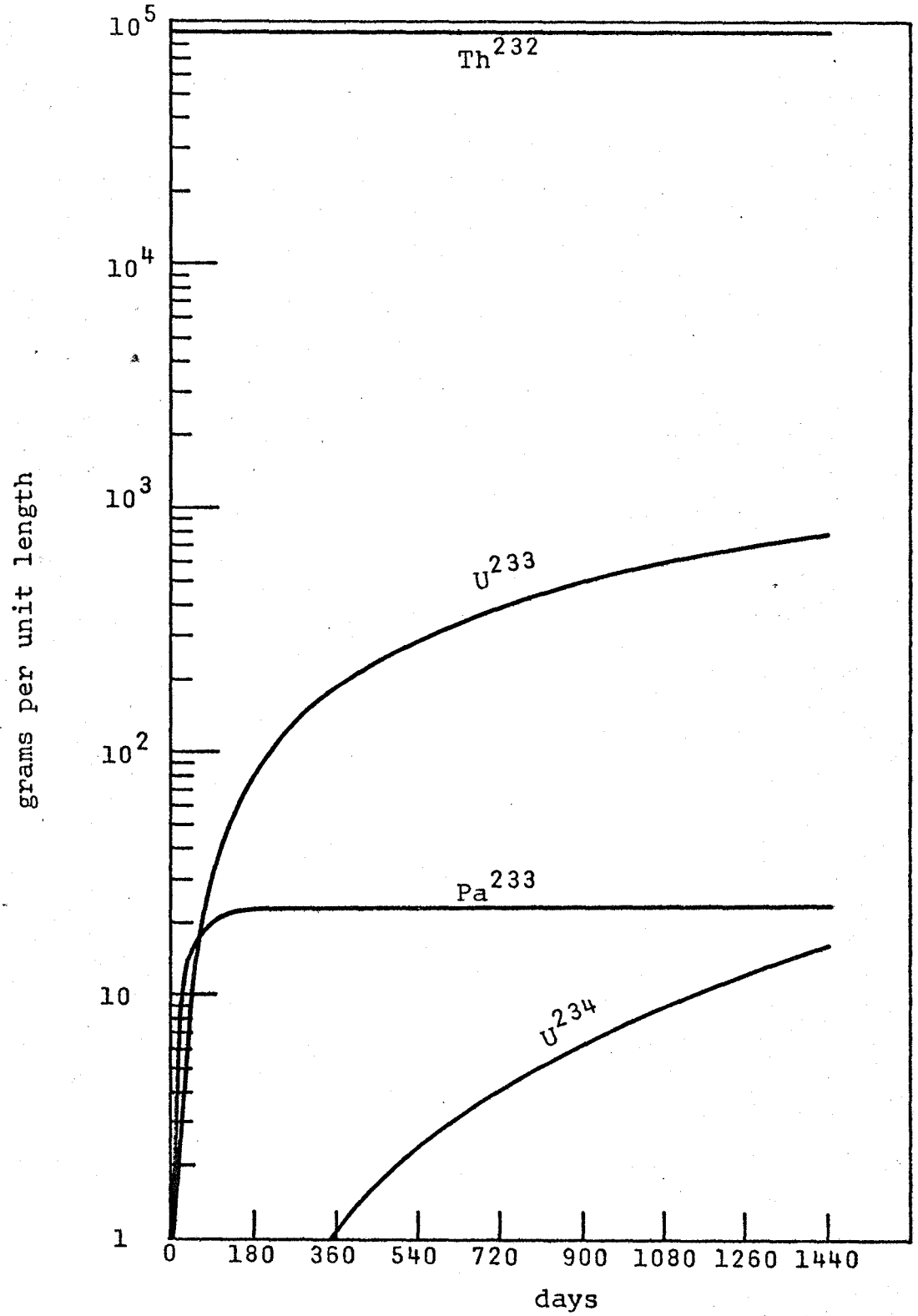

Figure 40 Spherical Design 1: Isotope Inventories

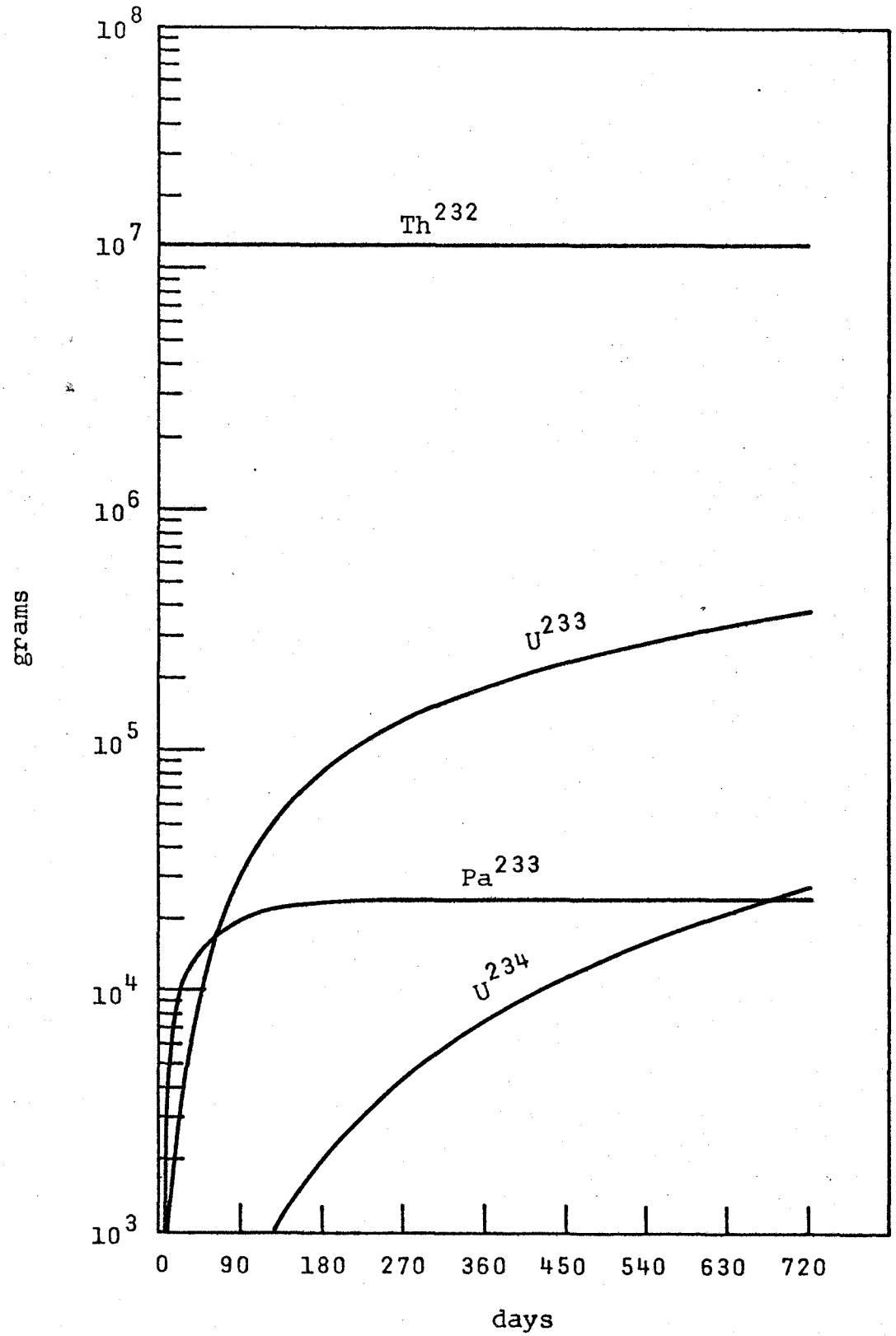

Figure 41 Spherical Design 2: Isotope Inventories

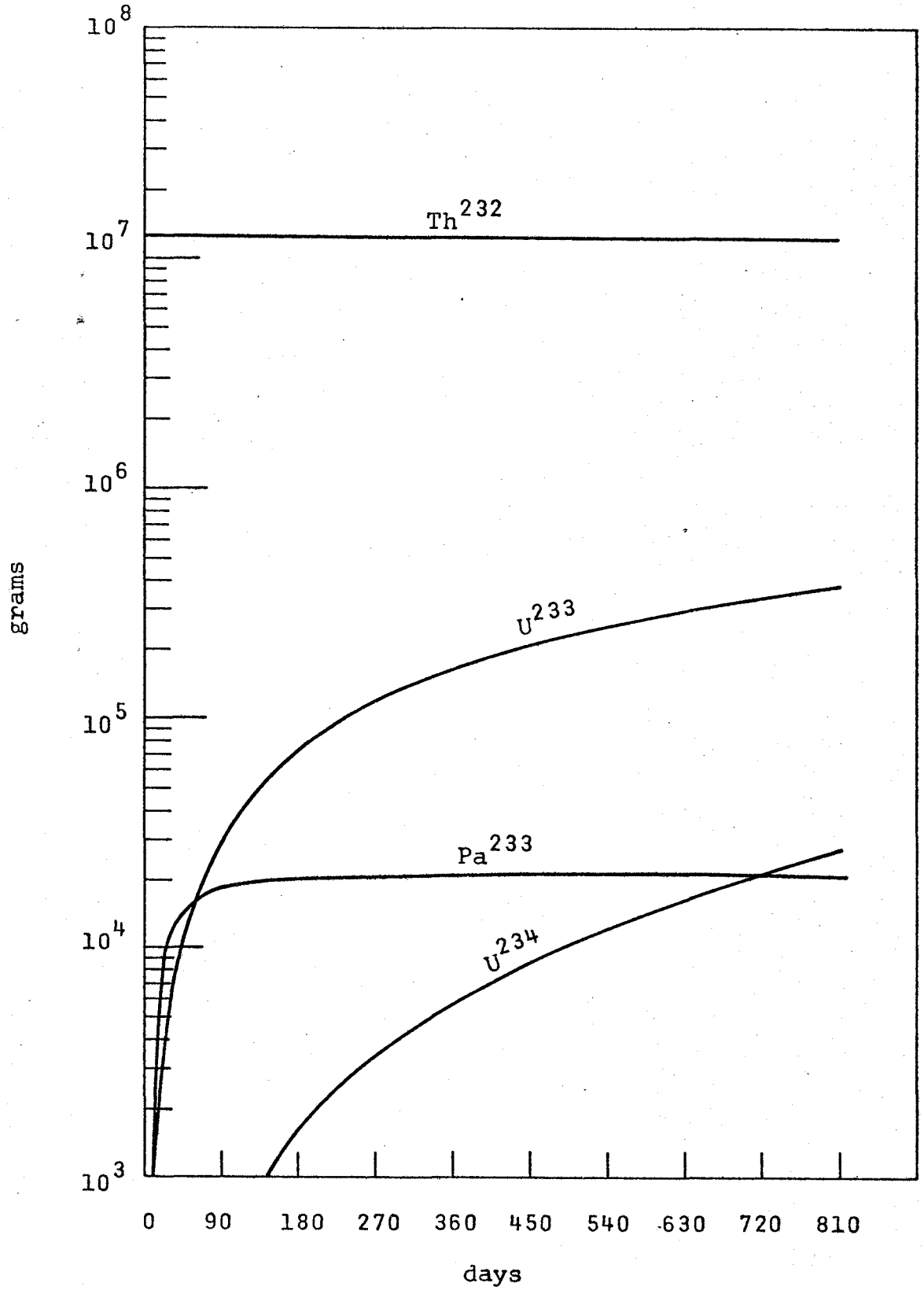

CONCLUSION

Basic aspects of blanket designs have been examined. Neutronics calculations of various designs and a simple time study to look at U^{233} breeding as well give an indication of U^{232} buildup was carried out. The analysis used was brief and the figures obtained are only expected to be ball-park figures.

It was shown that the CANDU 19 element fuel bundle studied in this report with D_2O coolant has a thermalizing as well as absorbing influence on the blanket as a whole. However, this is not necessarily bad. Placing a bundle with $U^{238}O_2$ pellets next to the first wall means approximately 11% more time for U^{233} concentration to reach the 3% level but the overall rate of production of U^{232} is approximately 20% less due to the increased thermalization and absorption.

This higher absorption affected the tritium breeding rate. With the $U^{238}O_2$ bundle, the breeding rate was calculated as approximately 1.05 per unit source neutron. This could be increased by moving the bundles into regions occupied by graphite in these designs thereby making more volume available for tritium breeding.

If the fluxes do turn out to be of the magnitudes used in this report, the CANDU fuel bundle with D_2O cooling could keep tritium breeding at acceptable levels while minimizing the U^{232} production. Studies with different coolants and materials in this bundle should be made but probably not before more accurate design characteristics of fusion reactors are known. The use of D_2O as a coolant and hence use of the CANDU fuel bundle in a form studied in this report is, to some extent, questionable

because of the expected exchange of deuterium with tritium after tritium diffusion into the bundle. This could have a significant effect on overall tritium production but the magnitude of such an effect is unknown. Following a suggestion in the Lavergne[1)] article, using techniques listed in ref. 7, the bundles could be irradiated in a region that is separated by a tritium barrier from the lithium. The bundles also might be cooled by high pressure helium as suggested in ref. 7 in order to separate the tritium that will unavoidably leak into this area.

It may be possible to use different types of coolants in different parts of the blanket as assumed in this study. With no fuel bundle near the first wall, liquid Li might be used there and then D_2O coolant in the bundles further out in the blanket. Studies should also be made of using helium in the bundles for cooling since tritium removal from the bundle could be accomplished at the same time.

It is apparent from the finite cylinder calculations that great care and effort will need to be taken to minimize neutron losses.

APPENDIX

ANGULAR QUADRATURE WEIGHTS FOR USE IN DISCRETE ORDINATES CALCULATIONS: CYLINDRICAL GEOMETRY

One of the terms in the transport equation involves the integration over all directions of a function of a direction vector $\underset{\sim}{\Omega}$. Doing this numerically involves a double integration for which the numerical theory is not very advanced. While sets of weights and points exist, generally they are not suitable for the integration to be performed here since they involve biasing with respect to direction to some extent. The actual term in the transport equation that needs evaluating is the following term within the brackets:

$$\int_{v'}\int_{t'}\left[\int_{\underset{\sim}{\Omega}'}\psi(\underset{\sim}{r},v'\underset{\sim}{\Omega}',t')\sigma(v'\underset{\sim}{\Omega}',t'\rightarrow v\underset{\sim}{\Omega},t)d\underset{\sim}{\Omega}'\right]dt'dv'.$$

As such, it represents the source S as discussed in the section in Discrete Ordinates. Thus, contributions from all directions to the source should contain no biasing whatsoever and it is with this in mind that the direction cosines and quadrature weights are developed here. Biased sets can be derived* for special cases but this appendix deals only with a completely symmetric set.

Quadrature weights, w_m, used in the angular integration can be looked at as area elements on the unit sphere with integration over all directions being integration over the unit sphere. Let μ_ℓ, η_ℓ, ξ_ℓ be the direction cosines of the unit vector $\underset{\sim}{\Omega}_\ell$; where '$\ell$' stands for a discrete

---

* *see LA-3186, p.16.*

direction. It is reasonable to require that $\{\mu_\ell\}$, $\{\eta_\ell\}$, $\{\xi_\ell\}$ be rearrangements of some basic set $\{\mu_m\}$; otherwise, one would obtain different numerical solutions depending upon the unit sphere orientations at different points of the space mesh. Thus, invariance with respect to 90° axis rotations and reflections about an axis, axes and the origon is required. Therefore, only one octant of a unit sphere need be considered. Also required, then, are (1) rotational invariance of $\frac{2\pi k}{3}$, k = 1,2 since an octant on the sphere has 3 sides and, (2) inversion invariance about the spherical arcs connecting the midpoints and vertices.

an octant

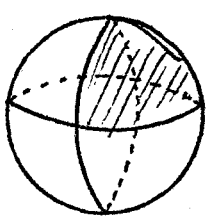

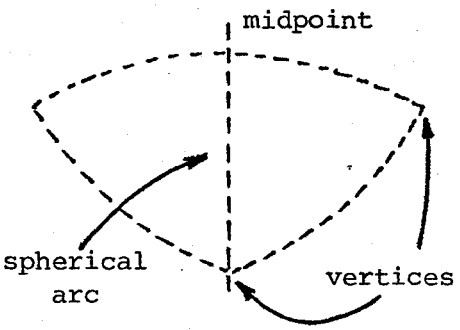

The integration desired can be written as

$$N(R) = \int_{\underset{\sim}{\Omega}} N(R,\underset{\sim}{\Omega})\, d\underset{\sim}{\Omega} = \sum_s p_s\, N(R, \underset{\sim}{\Omega}_s)$$

where p_s now is a certain area on the surface of the unit sphere associated with $\underset{\sim}{\Omega}_s$. If $N(R,\underset{\sim}{\Omega})$ is a unit function, $\sum_s p_s = 1$ where the p_s then are in units of 4π. Since the directions $\underset{\sim}{\Omega}_s$ can be represented by a single cosine set $\{\mu_m\}$ (that is, only one direction cosine need be split into discrete points or levels), all that is needed are level weights w_m with $w_m = \sum_s p_{sm}$; $\{p_{sm}\}_{m \text{ fixed}}$ being all areas on the unit sphere associated with the cosine μ_m. For S_6, an octant looks like

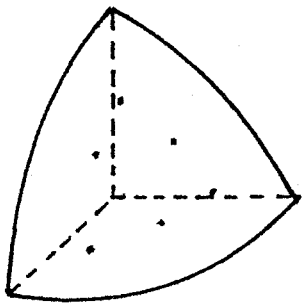

and for S_8,

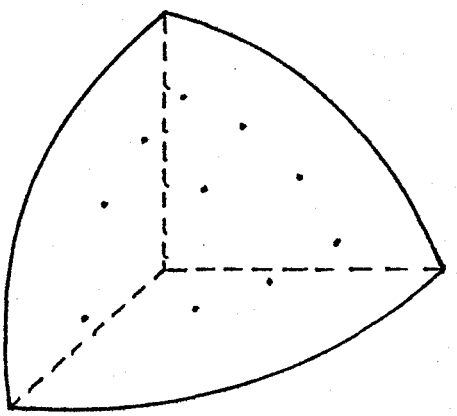

Let (μ_i,μ_j,μ_k) represent one of these points. Then i+j+k = N/2+2 in an S_N calculation*. Also, because this is a unit sphere, $\mu_i^2+\mu_j^2+\mu_k^2 = 1$. Since i+j = N/2+2-k, letting $k \rightarrow k+1$** gives

$$\mu_i^2 + \mu_{j-1}^2 + \mu_{k+1}^2 = 1$$

and

$$\mu_{i-1}^2 + \mu_j^2 + \mu_{k+1}^2 = 1.$$

Subtracting gives

$$\mu_i^2 - \mu_{i-1}^2 = \mu_j^2 - \mu_{j-1}^2$$

so that

$$\mu_m^2 = \mu_1^2 + (m-1)\Delta, \; m = 1,2,\ldots \frac{N}{2}.$$

Substituting this into $\mu_i^2 + \mu_j^2 + \mu_k^2 = 1$ gives $\Delta = \frac{2}{N-2}(1-3\mu_1^2)$. Finally matching integration of even powers of μ gives the remaining conditions (odd powers are properly integrated because of symmetry about μ=0).***

---

* *N, then, is the number of points of the basic set* $\{\mu_m\}$ *in (-1,+1).*

** *and hence i or j must be adjusted in order that* $i+j+K = \frac{N}{2}+2$ *still holds.*

*** *other recipes in LA-2595 and LA-3186.*

Example S_6

The conditions are

$$\mu_2^2 = 1/2(1-\mu_1^2)$$

$$\mu_3^2 = \mu_1^2 + (1-3\mu_1^2)$$

$$w_1 + w_2 + w_3 = 1/2$$

$$2(w_1\mu_1^2 + w_2\mu_2^2 + w_3\mu_3^2) = 1/3$$

$$2(w_1\mu_1^4 + w_2\mu_2^4 + w_3\mu_3^4) = 1/5$$

and

$$2(w_1\mu_1^6 + w_2\mu_2^6 + w_3\mu_3^6) = 1/7.$$

This is satisfied by

	μ_i	w_i
1	.2666355	.2547297
2	.6815076	.1572071
3	.9261808	.0880631
		$\sum_i w_i = .4999999$

(1)

Note that this corresponds to an integration over only half of the sphere. (The full set would include the negative μ_i also).

In cylindrical coordinates, two direction parameters are needed; say ξ and ϕ where ϕ is defined by

$$\mu = \sqrt{1-\xi^2}\,\sin\phi \text{ and}$$

$$\eta = \sqrt{1-\xi^2}\,\cos\phi \text{ and } \xi = \cos\theta.^*$$

---

* *see reference* 8.

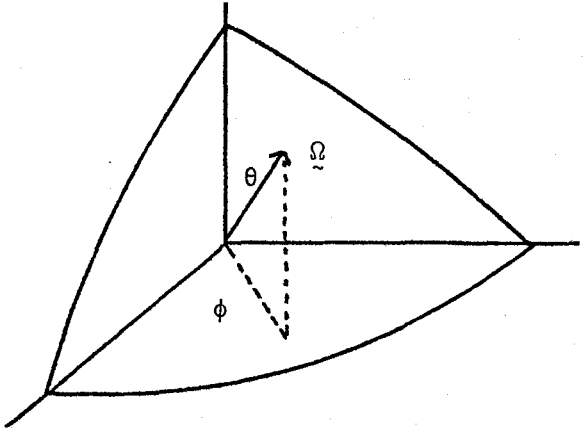

If $\mu = -\sqrt{1-\xi^2}$, $\phi = -\frac{\pi}{2} \pmod{2\pi}$ and this is taken as an initial reference direction in the cell.* Since N/2 separate sets of cosines are needed in cylindrical geometry**, one set is assigned to each ξ level. Therefore, weights and cosines for S_6 are (using the values from (1) above),***

	μ_i	ω_i	ξ level
1	-.3770795	(=- $\sqrt{1-\xi_3^2}$) 0.0	ξ_3 = .9261808
2	-.2666355	.0880631	"
3	+.2666355	.0880631	"
4	-.7318110	(=- $\sqrt{1-\xi^2}$) 0.0	ξ_2 = .6815076
5	-.6815076	.0786035	"
6	-.2666355	.0786035	"
7	+.2666355	.0786035	.6815076
8	+.6815076	"	"
9	-.9637974	0.0	ξ_1 = .2666355
10	-.9261808	.0880632	"
11	-.6815076	.0786035	"
12	-.2666355	.0880632	"
13	+.2666355	.0880632	"
14	+.6815076	.0786035	"
15	+.9261808	.0880632	"

---

* *See reference* 8.

** *Since cylindrical coordinates use only 1 angular variable, a separate set is needed for each ξ (or direction cosine in the z direction) value.*

*** *The values for the ξ levels are just the cosines from (1). The sum of all weights at a ξ level should sum to twice the corresponding weight in (1) since these weights are for integration over the total sphere. Notice that the μ_i (between the initial values) are all from the same set in (1).*

REFERENCES

1. LaVergne, G., Robinson, J.E., Martel, J.G., "On the Matching of Fusion Breeders to Heavy Water Reactors", Nucl. Tech. 26(1975)12.

2. Kushneriuk, S.A., Wong, P.Y., "Bench-Mark Neutronic Calculations for Fusion-Reactor Blankets", unpublished report.

3. Steiner, D., "The Nuclear Performance of Fusion Reactor Blankets", Nucl. App. & Tech., 9(1970)83.

4. Steiner, D., "The Technological Requirements for Power by Fusion", Nucl. Sci. & Eng. 58, #2 (1975)107.

5. Booth, L.A. (compiler), "Central Station Power Generation by Laser-Driven Fusion", LA4858-MS, Vol. 1.

6. Maniscalco, J.A., Hovingh, J., Buntzen, R.R., "A Development Scenario for Laser Fusion", preprint UCRL-76980.

7. Wistwall, R.H. Jr., Wirsing, E., "Removal of Tritium from Solid CTR Blanket Material", Am. Nucl. Soc. Trans. 19(1974)20.

8. Carlson, B.G., Lathrop, K.D., "Computing Methods in Reactor Physics", Chapter 3, Gordon & Breahch, 1968.

9. "CRC Handbook of Chemistry and Physics - 49th edition", Pub. by The Chemical Rubber Co., 1968.

10. Glasstone, S., "Principles of Nuclear Reactor Engineering", D. Van Nostrand Company Inc., 1955.

11. Okazaki, A., "Lattice Measurements with 19-Element Rods of ThO_2-$U^{235}O_2$ in Heavy Water Moderator - Part II", Atomic Energy of Canada Limited Report (AECL-2779).